SINTERING AND CHARACTERISATION OF NANO-SIZED YTTRIA-STABILISED ZIRCONIA

Prepared by

Muhammad Hasanuzzaman, B.Sc. (Eng)

A Thesis Submitted for the fulfillment of the requirements for the Degree of Masters of Engineering (M.Eng)

Supervised by

Dr. Abdul-Ghani Olabi

School of Mechanical and Manufacturing Engineering
Dublin City University

August 2006

DECLARATION

I hereby certify that this material, which I now submit for assessment on the programme of study leading to the award of Master of Engineering is entirely my own work and has not been taken from the work of others save to the extent that such work has been cited and acknowledged within the text of my work.

Signed:  ID No.: 53126505

Date: 26.09.2006

ACKNOWLEDGEMENTS

It is a pleasure to thank the many people who made this thesis possible.

I would like to express my sincere thanks and gratitude to my project supervisor Dr. Abdul-Ghani Olabi, without his continuous help and advice this work would not be possible. I am also very much grateful to Professor M. S. J Hashmi for giving me the opportunity and facilities to carry out my study.

I am indebted to Dr. Aran Rafferty and Dr. Tim Prescott for their assistance in technical support, especially Dr. Aran Rafferty, he provided encouragement, sound advice, good teaching, good company, and lots of good ideas. I would have been lost without him.

I would like to thank Chris Crouch, Michael May, Liam Domican, Keith Hickey and all other staffs of the school of Mechanical and Manufacturing Engineering.

I wish to thank my elder brother Abu Raihan Rashid (Harun), my best friend and mentor Dr.Qasim Murtaza, my entire family and all my friends, for helping me get through the difficult times, and for all the emotional support, comradeship, entertainment, and caring they provided.

Lastly, and most importantly, I wish to thank my parents, Mohammad Isa and Syeda Raihana Begum. They bore me, raised me, supported me, taught me, and loved me. To them I dedicate this thesis.

SINTERING AND CHARACTERISATION OF NANO-SIZED YTTRIA-STABILISED ZIRCONIA

By

Muhammad Hasanuzzaman

Abstract

A study has been conducted on the pressure-less sintering of the ZrO_2- Y_2O_3 system that contains 3 mol% Y_2O_3, and the effect that the temperature / time relationship has on the properties of the final product. Experiments were performed on two types of commercially available, nano-sized, ZrO_2 - 3mol% Y_2O_3 (3Y-TZP) powders. An unstabilised zirconia powder was also investigated for comparison purposes. Particle size analysis of these powder yield particle sizes ranging from 1.29 μm to 1.78 μm, suggesting that the particles are heavily prone to agglomeration in water. BET specific surface area analysis showed the powders to be nano-sized as determined using equivalent spherical diameter theory. The density of the powders was measured using helium gas pycnometry. DTA/TGA analysis indicates that binder burnout occurs on heating in the range 300-440°C. Shrinkage and densification rate characteristics of the powders during sintering was investigated using dilatometry. One of the powders demonstrated full shrinkage during isothermal sintering; the other did not. The point of maximum densification rate differed by approximately 100°C for these powders. A dramatic expansion associated with the tetragonal to monoclinic transformation on cooling from 1400°C is observed by dilatometry for unstabilised zirconia powder sample but not for stabilised powder samples. This indicates that the sintered samples retain in tetragonal phase on cooling to room temperature. Pressureless conventional sintering and two-step sintering were used to sinter pressed discs. The density of discs which were sintered across a temperature range of 1350°C to 1550°C varies between 5.72 g/cm^3 and 6.03 g/cm^3, corresponding to 97.40% and 99.10% of theoretical density respectively. Density as high as 98.85% of theoretical was recorded for two-step sintering applying holding time of 16 h. Vickers hardness values increased with increasing sintering temperature. Fracture toughness measurements were carried out. X-ray diffraction analysis confirmed that sintered discs were fully tetragonal. Microstructural analysis of sintered samples was conducted to assess microstructural changes with respect to sintering temperature.

TABLE OF CONTENTS

CHAPTER THREE EXPERIMENTAL TECHNIQUES

CHAPTER FOUR RESULTS AND DISCUSSION

APPENDIX C

APPENDIX D

APPENDIX E

APPENDIX F

LIST OF FIGURES

LIST OF TABLES

CHAPTER ONE

INTRODUCTION

CHAPTER ONE
INTRODUCTION

1.0 Introduction

Yttria-stabilised, zirconia-based ceramics can yield sintered parts with excellent mechanical properties. This material has found uses in cutting and wear resistant applications due to its reliable and outstanding hardness and toughness. Refractory and chemical durability properties have broadened its potential to include high temperature chemistry and ceramic biomaterial applications [1,2,3,4].

Zirconia (ZrO_2) has three crystalline forms: monoclinic (m), tetragonal (t) and cubic (c). Pure zirconia is monoclinic at room temperature and this phase is stable up to 1170°C. Above this temperature it transforms into tetragonal. The tetragonal phase is stable up to 2370°C, above which it transforms into a cubic phase. Un-stabilised zirconia undergoes a non-containable volume expansion (3-4%) tetragonal to monoclinic ($t \rightarrow m$) phase transformation during cooling in a temperature range of about 100°C below 1070°C [1,5]. This transformation is generally catastrophic, resulting in cracked parts. It is well known that additions of small quantities of stabilising oxides such as Y_2O_3, CeO, CaO, MgO during manufacture result in co-precipitated "partially stabilised" zirconia. Thus, on cooling the $t \rightarrow m$ phase transformation is prevented and a purely metastable tetragonal phase is retained at room temperature. As tetragonal zirconia possesses high strength, high toughness and good wear resistance over a wide temperature range, a key aim in zirconia research is to exploit the transformability of tetragonal ZrO_2 phase at room temperature [6]. The fraction of t-phase retained at room temperature is dependent on the size of the grains, on stabiliser content, on environmental conditions and on the degree of constraint exerted on the grains by the matrix [7,8,9,10,11]. Yttria (Y_2O_3) is the most commonly used stabiliser [12]. In the zirconia-yttria system, tetragonal-only phase ceramics can be obtained, commonly known as tetragonal zirconia polycrystals (TZP). Y-TZP materials, containing approximately 2-3% mol Y_2O_3, are completely constituted by tetragonal grains with sizes of the order of hundreds of nanometres [1].

The metastability of the tetragonal phase means that high toughness can be achieved during transformation toughening, tetragonal grains are transformed into monoclinic grains by stresses e.g. an advancing crack accompanied by a volume expansion. This expansion leads to compressive stresses ahead of the crack tip which in turn leads to blunting of the crack tip and slows the progress of the crack [1,13,14].

Much work has been carried out recently by Vleugels et al [15,16,17], into TZP ceramics. This work has questioned the quantity of yttria required to achieve optimum properties, including fracture toughness. In one paper, Basu et al [18] investigated a simple but innovative route based on the mixing and hot pressing (under identical conditions) of TZ-3Y zirconia powders with varying yttria content (3 and 0 mol%). The experimental results clearly revealed that the fracture toughness of yttria-stabilised tetragonal zirconia polycrystalline (Y-TZP) ceramics could be tailored by careful mixing of co-precipitated and yttria-free zirconia starting powders. They found that the indentation fracture toughness of Y-TZP ceramics could be tailored from 2 to 10 $MPam^{1/2}$ by the controlled addition of monoclinic zirconia particles to 3 mol% Y_2O_3 co-precipitated zirconia powder. Hot pressed TZPs with an overall yttria content of 2 mol% exhibited an excellent indentation toughness (10 $MPam^{1/2}$) combined with a high flexural strength (around 1250 MPa). This was a dramatic improvement on the original 3 mol% powder which showed a fracture toughness of approximately 2.5 $MPam^{1/2}$ and a flexural strength of around 1000 MPa. Basu et al [2], in his another study, used thermo-mechanical analysis to investigate the thermal hysteresis behaviour of the powder mixture based 2Y-TZP's. The results showed that these materials were prone to reversible tetragonal (t) to monoclinic (m) transformation, also known as low temperature degradation phenomenon, but that the effect was almost negligible for the unmodified 3Y-TZP powder.

Lawson [19] studied environmental degradation of zirconia ceramics and claims that partially stabilised zirconia is susceptible to various environments such as humid air, water vapour and other aqueous fluids over a temperature range of 65-500°C, but in aqueous solutions the effect is more catastrophic at lower temperatures and in shorter times. A key area of interest is thus the development of ageing resistant zirconia ceramics with good mechanical properties.

Some authors have reported fully dense sintered ceramics, after hot pressing for 1 hr at 1450°C [18]. However, other authors have investigated the possibility of using two-step sintering to achieve high densities and fine grain sizes. In two step sintering the sample is first heated at a higher temperature, where the pores between the aggregate and agglomerates are eliminated and a fast grain growth is observed, then cooled at a lower temperature with longer dwelling time until it is fully dense without further grain growth [20,21,22]. Lee [23] used rate-controlled; two step sintering to sinter 3mol% Y_2O_3 stabilised zirconia. Bending strengths of two-step sintered samples were four times greater than those of samples sintered using conventional sintering. Lee attributed this to denser microstructures and finer grain size. Laberty-Robert et al [24] synthesized nanocrystalline YSZ powders and found that a high density (>98% D_{th}) with fine average grain size (5μm) could be achieved by using two-step sintering.

1.1 Research objectives

The main objectives of this research are:

1. Characterisation of as-received, nano-sized commercial 3Y-TZP powders and optimization of sintering to achieve high density, high toughness ceramic, suitable for use in homogenising machine as a valve seat and other applications where it required combination of strength, toughness, and chemical inertness.

2. To compare results obtained from two 3Y-TZP powders obtained from separate suppliers.

3. To investigate the mechanical properties of sintered parts.

1.2 Research plan

The experimental steps employed to realise the research objectives are:

1. Powder particle size measurement.

2. Thermal analysis of the powders.

3. Dilatometric analysis.

4. Density measurement

    a) Measuring the green density by geometric volume measurement (vernier calipers) method.

    b) Measuring the density after sintering using two methods; geometric volume measurement (vernier calipers) method and Archimedes method.

5. Using two-step sintering in an attempt to achieve higher densities with reduced grain size.

6. Evaluation of the following mechanical properties: Vickers hardness, fracture toughness and Young's Modulus.

7. Examination of the microstructure using SEM and optical microscopy.

8. Phase-study before and after sintering by using XRD.

1.3 Structure of thesis

A literature review of related research is elaborated on in Chapter 2. In Chapter 3, experimental procedures are described. Results and discussion are detailed in Chapter 4. Finally, the conclusions and proposed future work are outlined in Chapter 5.

CHAPTER TWO
LITERATURE REVIEW

CHAPTER TWO
LITERATURE REVIEW

2.0 Introduction

Zirconia is extensively used in manufacturing parts, blades, solid electrolytes, etc [1,2,3,4]. Its refractory properties and chemical durability make it suitable in high temperature chemistry and ceramic biomaterial applications. Yttria-stabilised zirconia can undergo transformation toughening which makes it a candidate for use as a homogenizer valve capable of withstanding high pressures. The following sections describe zirconia's different properties and uses:

2.1 Yttria-stabilised zirconia ceramics
2.2 Tetragonal zirconia polycrystals (TZP)
2.3 Toughening mechanism
2.4 Properties of 3 mol% Y-TZP
2.5 Applications of zirconia ceramics
2.6 Material processing and properties
2.7 3Y-TZP sintering profile

2.1 Yttria stabilised zirconia

Zirconium oxide (ZrO_2) is a polymorph which has three crystalline forms: monoclinic (m), tetragonal (t) and cubic (c). Pure zirconia is monoclinic at room temperature and this phase is stable up to 1170°C. Above this temperature it transforms into tetragonal. The tetragonal phase is stable up to 2370°C, above which it transforms into a cubic phase. Its physical properties as well as crystallographic data are presented in Table 2.1.

Un-stabilised zirconia undergoes a non-containable volume expansion (3-4%) tetragonal to monoclinic (t→ m) phase transformation during cooling in a temperature range of about 100°C below 1070°C [1,5]. This transformation is generally catastrophic and results in cracked parts. Additions of small quantities of stabilising oxides such as Y_2O_3, CeO, CaO, MgO during manufacture result in co-precipitated "partially stabilised" zirconia. Therefore, on cooling the t → m phase

transformation is prevented and a purely metastable tetragonal phase is retained at room temperature. Since tetragonal zirconia possesses high strength, high toughness and good wear resistance over a wide temperature range, one of the major aims in zirconia research is to exploit the transformability of tetragonal ZrO_2 phase at room temperature [6]. The fraction of t-phase retained at room temperature is dependent on the size of the grains, on stabiliser content, on environmental conditions and on the degree of constraint exerted on the grains by the matrix [7,8,9,10,11]. The most commonly used stabiliser is yttria (Y_2O_3) [12].

Table 2.1 Physical and crystallographic properties of zirconia [1,25]

Property	*value*
Polymorphism, °C	
Monoclinic to tetragonal	1000-1170
Tetragonal to cubic	2370
Cubic to liquid	2680
Crystallography, monoclinic	
a	5.1454 Å
b	5.2075 Å
c	5.3107 Å
β	99°14'
Crystallography, tetragonal	
a	3.64 Å
c	5.27 Å
Crystallography, cubic	
a	5.065 Å
Density, g/cm^3	
Monoclinic	5.68
Tetragonal	6.10
Thermal expansion coefficient, $10^{-6}/K$	
Monoclinic	7
Tetragonal	12
Heat formation, kJ/mol	-1096.73
Boiling point, K	4548
Thermal conductivity, W/m.K	
At 100°C	1.675
At 1300°C	2.094
Hardness, Hv	1200
Fracture toughness, $MPa.m^{-1/2}$	1.54-4.07
Refractive index	2.15

ZrO_2 -toughened ceramics are basically of three types. They are:

- Tetragonal-only phase ceramics: These are generally known as tetragonal zirconia polycrystals (TZP) that contain approximately 2-3 mol% Y_2O_3 or CeO_2. They are completely constituted by tetragonal grains with sizes of the order of hundreds of nanometres [1]. Here high toughness can be achieved via stress-induced transformation toughening due to the metastable nature of the tetragonal phase.
- Partially stabilised ZrO_2 (PSZ): Here t-ZrO_2 particles are coherently precipitated within a cubic (c) stabilised ZrO_2 matrix (precipitation-toughened ceramics). A typical PSZ ceramic contains a stabiliser of MgO, CaO, or Y_2O_3 (for example, Mg-PSZ containing 8 wt% MgO has a microstructure consisting of 40 to 70 μm cubic grains containing finely dispersed precipitates of sub micron t-ZrO_2 and m-ZrO_2
- ZrO_2-toughened ceramics (ZTC): Here t- or m-ZrO_2 particles are dispersed in ceramic materials such as Al_2O_3, mullite ($3Al_2O_3{\cdot}2SiO_2$) and spinel ($MgAl_2O_4$) (dispersion-toughened ceramics). The critical ZrO_2 particle size varies with different matrices but is usually between 0.5 and 1.2 μm. The t-phase is usually strengthened by the addition of small amounts of Y_2O_3.

2.2 Tetragonal zirconia polycrystals (TZP)

Rieth et al [26] was the first to obtain ceramics at room temperature with a tetragonal only phase named TZP, using the ZrO_2-Y_2O_3 system (Fig 2.1). This research was subsequently followed up by Gupta et al [27]. Polycrystalline TZP materials are generally fabricated from co-precipated powders, i.e., ZrO_2 plus the alloying addition. These powders are in the size range of 10-200 nm. Depending on the reactive nature of powders as well as the form of the phase equilibria, firing is conducted in the range 1300 -1500°C for Y-TZP, as indicated in Fig. 2.1. The final grain size after fabrication was ~0.5-2 μm, depending on sintering temperature, hold time, and stabiliser content [5]. The critical tetragonal zirconia grain size also depended on the stabiliser content and the density of the sintered compact [5]. Fracture toughness of 2.5 to 14 MPa $m^{1/2}$ with hardness of 11 to 13.5 GPa were

obtained when sintering took place in the temperature range 1400° to 1500°C [2,13,18,28,29,30].

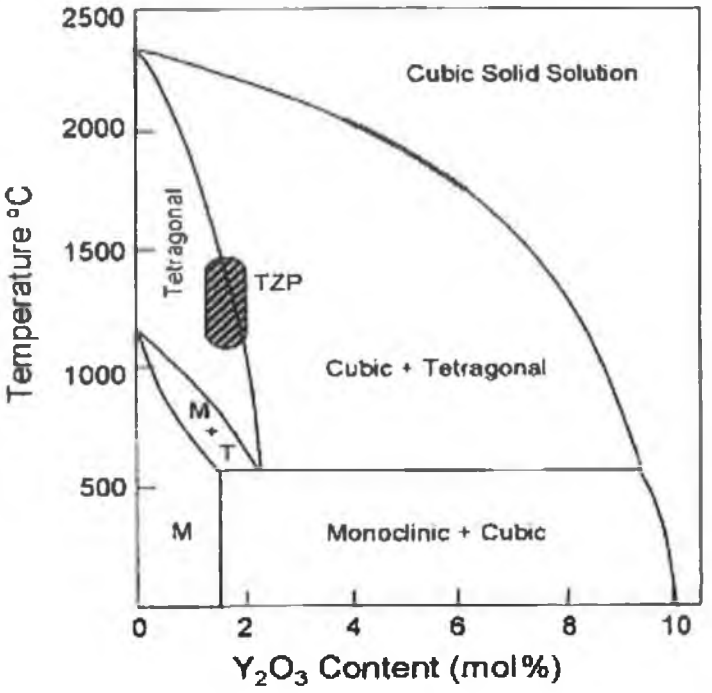

Figure 2.1. ZrO_2-Y_2O_3 phase diagram [5].

In early stages of development of TZP ceramics, high densities were difficult to achieve within a reasonable sintering time because of using low sintering temperature. To overcome the low-density problems, hot isostatic pressing (HIP) has become a popular technique to increase density without excessive grain growth [2,18,28]. More recently, high-quality powders have become available which enable densities > 98% of theoretical to be achieved at 1400°C, with a resulting grain size < 0.5 μm [11,15,16,29].

2.3 Toughening mechanism

Garvie et al [31] were the first to point out the potential for high strength and high toughness zirconia ceramics by utilizing the tetragonal monoclinic phase transformation in PSZ. They observed that tetragonal metastable precipitates finely dispersed within a cubic matrix were able to transform into monoclinic phase when a constraint was applied on them by the matrix. A great deal of research has been carried out since to devise theories and develop mathematical frameworks to explain the phenomenon. It is commonly recognized that the t-m transformation can develop

significantly improved properties via two different mechanisms a) microcracking, b) transformation toughening, apart from crack deflection which can occur in two-phase ceramics, though the mechanisms are different the concept in both cases is to increase the required energy before brittle fracture.

a) **Microcracking.** Incorporation of ZrO_2 particles in a ceramic matrix (cubic ZrO_2 or another ceramic such as Al_2O_3) induces microcracking. On cooling through the transformation temperature *($T_{t\text{-}m}$),* the volume expansion of 3 to 4% occurring in the ZrO_2 particles causes a crack to form (Fig 2.2)

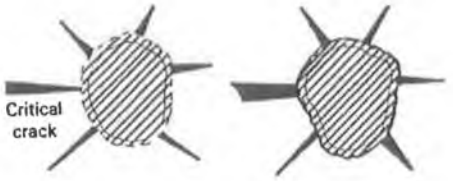

(a) (b)

Figure 2.2 The martensitic transformation that occurs in ZrO_2 (tetragonal to monoclinic at 900 to 1100°C with a 3 to 4% volume expansion, develops microcracks around the ZrO_2 particles (a). A crack propagating into the particle is deviated and becomes diverged (b), thus increasing the measured fracture resistance [32].

Tangential stresses are generated around the transformed particles which induce microcracks in the matrix. These are induced due to their ability to extend in the stress field of a propagating crack or to deflect the propagating crack can absorb or dissipate the energy of the crack, thereby increasing the toughness of the ceramic. The optimum conditions are met when the particles are large enough to transform, but small enough to cause limited microcrack development. Generally the ZrO_2 particle size can be controlled by milling time prior to sintering or aging conditions after sintering to develop the desired size range.

To get maximum toughness, the volume fraction of ZrO_2 inclusions must be at an optimum level [33]. It is to be carefully noted that the toughness will increase to a maximum above which microcracks generated by the ZrO_2 particles will interact with one another resulting in a decrease in strength.

b) Transformation toughening. Transformation-toughened ceramics owe their very large toughness to the stress-induced transformation of a metastable phase in the vicinity of a propagating crack. To understand the phenomenon, it is useful to refer to Fig. 2.3, where fine tetragonal zirconia grains are dispersed in a matrix. If these tetragonal particles are fine enough, then upon cooling from the processing temperatures, they can be constrained from transformation by the surrounding matrix and consequently can be retained in a metastable tetragonal phase. These metastable tetragonal particles can be transformed into monoclinic phase accompanied by a relatively large volume expansion (3-4%) when the constraint exerted on them by the matrix is relieved, i.e. by a crack advancing in the material. The stress field associated with expansion due to the phase transformation acts in opposition to the stress field that promotes the propagation of the crack. The energy associated with crack propagation is dissipated both in the t-m transformation and in overcoming the compressive stress due to the volume expansion, which increase both the toughness and the strength of the ceramic.

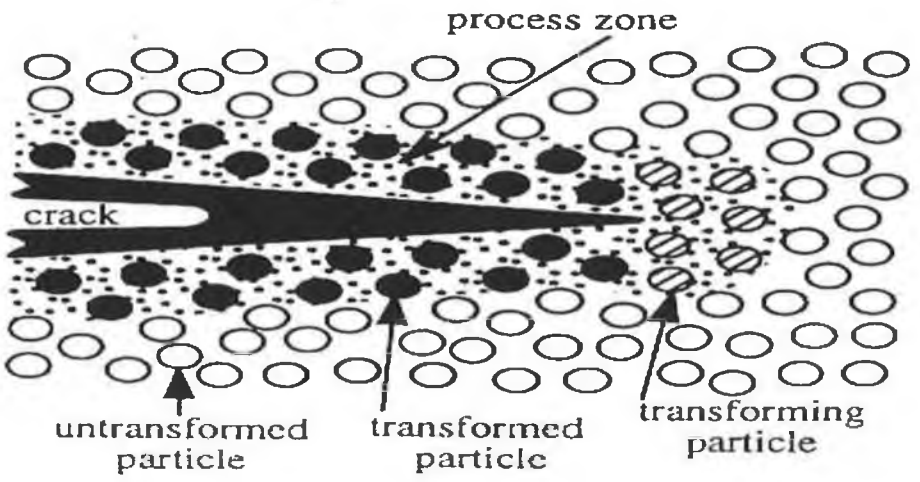

Figure.2.3 Representation of stress-induced transformation toughening process [1].

It is unfortunate that the reason transformation toughening works so well at ambient temperatures, mainly because the metastability of the tetragonal phase, is the same reason it is ineffective at elevated temperatures. Increasing the temperature reduces the driving force for transformation and consequently the extent of the transformed zone, leading to less tough materials.

2.4 Properties of TZP

TZP ceramics are supposed to have long-term stability and this property greatly depends on factors such as yttria content and grain size. In the presence of water at temperatures in the range 200 to 300°C, degradation of properties can be severe. In contrast, the Mg-PSZ commercial ceramic appears not to be as sensitive to atmospheric moisture over this temperature range. Lawson [19] investigated environmental degradation of zirconia ceramics and claimed that partially stabilised zirconia is susceptible to various environments such as humid air, water vapour and other aqueous fluids over a temperature range of 65-500°C, but in aqueous solutions the effect is more catastrophic at lower temperatures and in shorter times. So a prime area of interest is to develop an ageing-resistant zirconia ceramic with good mechanical properties. This behaviour might well be attributed to the low-volume-fraction of the transformable tetragonal phase present in or adjacent to the grain boundaries.

The exact mechanism for the degradation of properties with time has not yet been identified. It is established that the removal of elastic constraint at the grain boundaries is the cause of the phenomenon, the reason for this occurrence is still unknown. One school of thought attributes the action of water or polar liquids on the grain-boundary glassy phase as being significant [34, 35], while another suggests the removal of Y_2O_3 from solid solution in the ZrO_2 surface as being an important mechanism [36]. Kimel et al [6] established a diffusion control led leaching model which did not show any significant diffusion of hydroxide into the 3Y-TZP from the aqueous solution at room temperature. By XRD, they showed that yttrium leaching has no effect on the amount of monoclinic and tetragonal phases present in the powder in room temperature. To further determine the mechanism responsible for aqueous degradation, he also performed leaching experiments in deuterated water. Deuterium remained on the surface of the powder, indicating that hydroxide migration into the 3Y-TZP lattice is not a probable reaction in aqueous suspension at room temperature. One of the most plausible [37] explanations for gross destabilisation of the *t*- phase is that leaching of Y_2O_3 leads to subsequent transformation of the surface layers to *m*-phase and the introduction of incipient flaws [38]. Several approaches have been used to overcome this instability. These approaches vary from reducing the initial grain size and the use of additions of other

stabilising oxides or non-oxides. Sato et al [39], through the addition of 5 mol% CeO_2 to 3 mol% Y-TZP, were able to suppress any degradation in fracture toughness properties after annealing for 168 h at 100°C in water. Tsukuma et al [40] reported that 2 mol% Y-TZP is much more unstable compared to 3 mol% Y-TZP, which leads to a higher toughness and stronger degradation. Basu et al [41] carried out a comprehensive study with different commercial grades of Y-TZP powders and concluded that overall yttria content and the impurity content in the zirconia matrix were found to be important factors, whereas higher impurity and/or lower yttria content with inhomogeneous yttria distribution resulted in higher resistance against low temperature degradation. However, both of these solutions will lower the M_s (martensitic start) temperature, resulting in reduced toughness. Whalen et al [42] proposed a post sintering grinding and annealing treatment to inhibit the low temperature tetragonal to monoclinic transformation in Y-TZP ceramics. Chung et al [29] proposed a new post heat treatment to prevent low temperature degradation where the already sintered 3Y-TZP samples were further heat-treated for 2 h at either 1600° or 1700°C under flowing nitrogen gas in a furnace with graphite heating elements to form nitrogen-stabilised surface layers resulting in the grain size of the surface layer increasing to > 10 μm, whereas that of the interior remained ~ 1 μm. Moreover, the nitrified layer of the 3Y specimens had higher hardness values at same time no strength change was observed annealing at 200°C in air.

Even though the matter has not been resolved yet, this nucleation event is an important phenomenon. As soon as a monoclinic nucleus is formed, the transformation process can become self-generating in that adjacent grains can be triggered to transformation. The microcracks generated from the process can then provide ready access for the water vapor to continue the chemical attack on the TZP.

The major controlling variable for property determination is the yttria content of the zirconia. To generate significant mechanical properties, it is necessary to have a microstructure free of any monoclinic phase which would act as a flaw, and this dictates the minimum level of stabiliser added. Therefore approximately 1.8 mol% Y_2O_3 in solid solution results in a composition close to the phase boundary and in a ceramic where the metastable tetragonal is readily transformable. Consequently high values of fracture toughness can be obtained with this composition. Vleugels et al [15,16,17] has recently done some extensive research work on TZP ceramics. This

work has questioned the quantity of yttria required to achieve optimum properties, including fracture toughness. Basu et al [18] explored a simple but innovative route based on the mixing and hot pressing (under identical conditions) of TZ-3Y (Tosoh) zirconia powders with varying yttria content (0 and 3 mol%). The experimental results showed that the fracture toughness of yttria-stabilised tetragonal zirconia polycrystalline (Y-TZP) ceramics could be tailored by careful mixing of co-precipitated and yttria-free zirconia starting powders. They observed that the indentation fracture toughness of Y-TZP ceramics could be tailored from 2 to 10 $MPam^{1/2}$ by the controlled addition of monoclinic zirconia particles to 3 mol% Y_2O_3 co-precipitated zirconia powder. Hot pressed TZP's with an overall yttria content of 2 mol% showed excellent indentation toughness (10 $MPa.m^{1/2}$) combined with a high flexural strength (around 1250 MPa). This was a remarkable improvement on the original 3 mol% powder which showed a fracture toughness of approximately 2.5 $MPa.m^{1/2}$ and a flexural strength of around 1000 MPa. Exposure to moisture at 200 to 300°C enhances this process with the result that long-term exposure under these conditions produces a drastic decrease in fracture strength. Electron probe microanalysis (EPMA) analysis showed that the presence of intentionally added yttria-free ZrO_2 particles in the starting powder mixtures caused a redistribution of the yttria during sintering. Yttria from the co-precipitated grains diffused into the original monoclinic grains resulting in highly transformable tetragonal grains. This factor was accountable for the high toughness in the mixed grade 2Y-TZP's. Basu et al [2] used thermo-mechanical analysis to investigate the thermal hysteresis behaviour of the powder mixture based 2Y-TZP's. This behaviour showed that these materials were prone to reversible tetragonal (t) to monoclinic (m) transformation, also known as low temperature degradation phenomenon, but that the effect was almost negligible for the unmodified TZ-3Y powder.

In order to get a maximum in the fracture strength of TZP, the composition required is 3 mol% Y_2O_3 and this must occur when the value of, $\sqrt{\gamma}/c$, where γ is the fracture energy and c is the critical flaw length [43, 44], is optimized. If the intrinsic flaw size due to fabrication techniques was considered constant over the range 2 to 4 mol% Y_2O_3 γ is at a maximum at 2 mol% Y_2O_3, this would appear to be contradictory. To resolve this, the microstructure of 3 mol% composition where relatively large grains (~5 to 8 μm) of the cubic phase are to be found often in fairly close association with one another. A relatively thick layer of glassy phase is often

found at the cubic grain boundary. Together with the lower value of the fracture toughness for the cubic phase ($K_{Ic} \approx 2.2$ MPa.m$^{1/2}$), this points towards a change in the flaw distribution.

The bend strength decreases with temperature, the rate of decrease fairly constant up to 800°C; after that the decrease is at a lesser rate. The elastic modulus decreases with temperature. Since the flaw size distribution should remain constant, the rapid initial decrease in strength can be explained by a decrease in the fracture toughness from the room-temperature value to that at the transformation temperature. A summary of the properties of TZP is given in Table 2.2.

Table 2.2 Typical Properties of TZP [45, 46]

Property	Value
Density, g/m^3	6.05
Hardness, HV	1200
Modulus of rupture(a), MPa	900
Fracture Toughness (k_{Ic}), MPa.m$^{1/2}$	2-10
Elastic modulus, GPa	200
Thermal conductivity, W/m.K	2

2.5 Applications of zirconia ceramics

Y-TZP is suitable for the application of the materials in harsh environments under severe loading conditions since it has the combination of strength, toughness, and chemical inertness [5]. Together with the development of a surface compressively stressed layer, many novel applications in wear-resistant cutting devices are envisaged and on the way of development. The excellent mechanical properties combined with biocompatibility, wear resistance, high chemical resistance, which make the material a promising candidate for biomedical applications [47]. Research is going on the possibility of zirconia as a biological implant material to replace worn joints [48]. But the main application of this ceramic biomaterial is in the manufacturing of ball heads for total hip replacements [47, 49] (Fig 2.4 and 2.5)

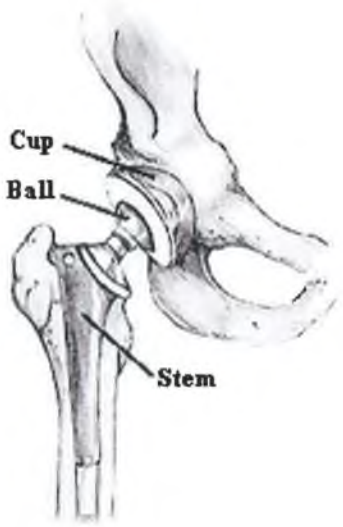

Figure 2.4 -Typical hip replacement components [50].

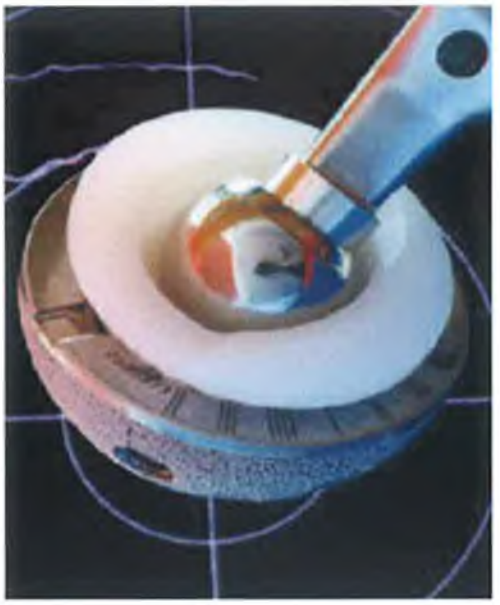

Figure 2.5 This zirconium head has been oxidized to acquire a zirconia outer layer, which was then polished. The head has a 28-mm diameter. The stem is a titanium alloy (Ti-6Al-4V) [51].

With steel like strength and ultra high hardness, Y-TZP increases the service life up to 50 times over conventional materials. It is used for cutting and slitting of industrial materials, particularly for magnetic tape, plastic film, and paper items such as cigarette filters (Fig 2.6) [52,53]. The advantages are the extra life obtained by the zirconia component allows longer runs of the machines and the resulting loss of down-time more than compensates for the higher initial cost of the component. Similarly zirconia wire-drawing dies and hot extrusion dies are proving themselves superior to conventional dies, specifically in the finishing runs where good dimensional tolerance and a high surface quality are required [52,53,54].

Figure. 2.6 Different type of Y-TZP zirconia blades [5].

Seals in valves, chemical, and slurry pumps are also made of zirconia ceramics. Lately the impellers have been fabricated with zirconia and tested. Valve seat and valve heads which need to withstand high pressure in homogenising machine also made of Y-TZP ceramics (Fig 2.7). Homogenising machines, used for producing extracts from brewer's yeast, gives the products higher food value for human consumption.

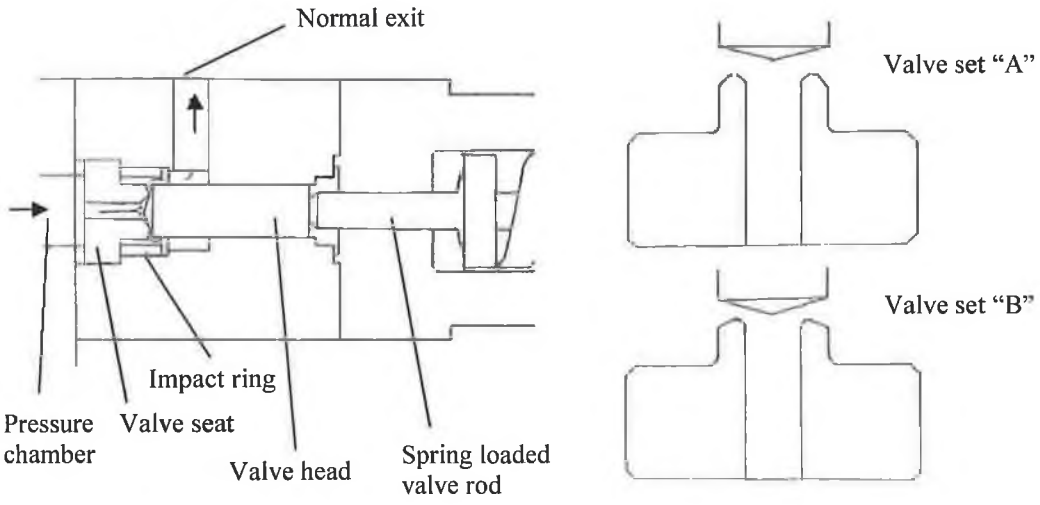

(a) Diagram of homogenizing valve (b) Different valve sets

Figure 2.7 Different Valves made of Y-TZP in homogenizing machines.

Components that require long life under low load conditions can be made effectively with zirconia. For instance, thread guides and bearing guides, dot matrix printers etc.

Zirconia has huge prospect in automotive engine parts, in particular the diesel engine. Two types of applications are envisaged. In the first the low thermal conductivity of zirconia would be used to advantage in components such as piston crowns, head face plates, and piston liners (Fig 2.8). As a result the heat loss from the combustion chamber would be reduced and the flame temperature increased resulting in increased engine efficiency. Reddy et al [55] established in their experiment to improve the performance of a two-stroke spark ignition engine, coated the combustion chamber by partially stabilised zirconia, improves the brake thermal efficiency and reduces HC and CO emissions. Wear would be reduced giving longer times between routine services and a considerably extended engine life. There are also components in the engine which are limited by wear, particularly in the valve train, such as cams, cam followers, tappets, and exhaust valves (Fig 2.8). All these components have been fabricated using zirconia and are under test [56]. A rotary engine has been constructed using a silicon nitride casing and a zirconia rotor. If testing results proved to be positive, zirconia could be used extensively in automotive parts.

(a) Piston crown (b) Piston liner (c) cams (d) Tappets (e) Exhaust gas valves

Figure 2.8 Different engines parts coated with zirconia.

Zirconia-bearing ceramics have other applications that include:

- Refractory components and bricks for high temperature furnaces for metallurgical processing
- Refractory fibers that provide thermal insulation to separators in aerospace batteries, hot gas filters, and electrolysis diaphragms
- Thermal barrier coatings for equiaxed, directionally solidified, and single-crystal superalloy turbine blades [33,57,58,59]
- Furnace heating elements
- Oxygen sensors, fuel cells and catalytic membrane [24,60]

2.6 Materials processing and properties

2.6.1 Compaction

Compaction is one of the most important stages in sinter-forming route. It gives the powder an initial shape and provides necessary strength for handling of further processes. It depends on an external source of pressure for deforming the powders into a relatively high density mass, also providing shape and dimensional control to the powder. The pressure determines the densities of the components. With sufficiently high green density, it is possible to produce high density with small grain size at relatively low sintering temperature. Chen et al [61] pressed 3Y-TZ powder to a relative green density of 58%, afterwards sintered, and achieved 99.9% theoretical density with a grain size of 85 nm.

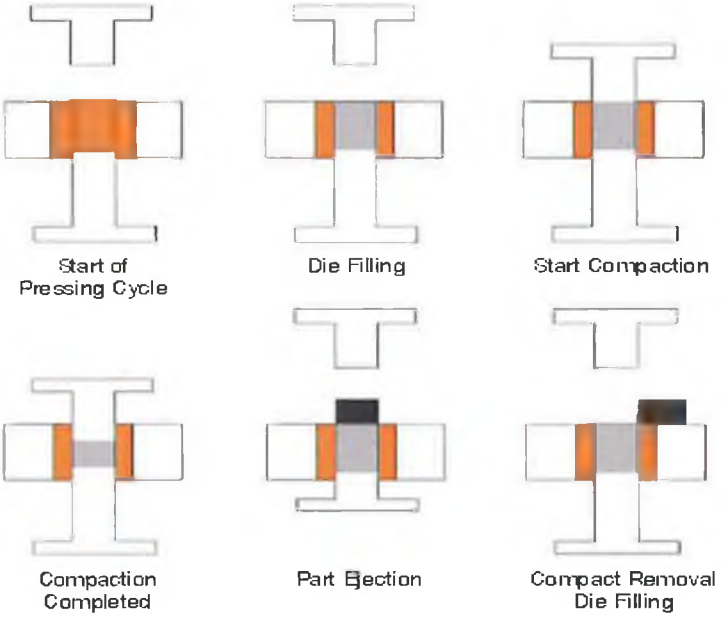

Figure 2.9 Typical compaction cycle [59].

Cutler et al [28] used TZ-3Y Daiichi powder and formed uniaxially at 35 MPa and subsequently isostatically pressed at 200 MPa. Kim [21] used Tosoh 3Y-TZP powder and using same uniaxial pressure but followed by140 MPa isostatic pressure.

Esquivias et al [3] used 5 mol% yttria doped zirconia powder which is cold uniaxially pressed at 75 MPa leads the green compacts ~39% of theoretical density. Vleugels et al [12,15,16] always shaped as-synthesized TZP powders by cold isostatic pressing (CIP) at 300 MPa. Most of cases cold isostatic pressing (CIP) ranged from 150-300 MPa was used for Y-TZP ceramic powders [11,29,42]. Rafferty et al [63] used manual 150 KN hydraulic press (Specac Ltd. Kent, UK) and a 7 mm evacuable pellet die. They developed and optimise the pressing procedure for multilayer pellets comprising ferrite, multilayer and varistor where first powder is added to the die and pressed for 20 s under 10 MPa pressure to form a pellet. Then the second powder is added to the die and pressed against the previously formed pellet for 20 s, leading to a co-pressed bi-layer sample. Finally the third powder is added to the die and pressed with the previously co-pressed sample for 60 s, resulting in a triple layered device. Esquivias et al [3] stated, in relation to characterize the green bodies of 5 mol% yttria dopes zirconia powder, the compaction process of powders is controlled by a crushing phenomenon of their agglomerate and do not stand after applying uniaxial pressure of 75 MPa. Laberty-Robert et al [24] studied green microstructure and sintering behaviour of 8 mol% Y_2O_3-ZrO_2 powders which were uniaxially cold pressed up to 160 KN. They found out that the density increases from 35 to 50% of theoretical densities with increasing the compaction force from 20 to 110 KN. The green density remains same up to 140 KN and beyond that start decreasing. They also investigated the influence of pressure time for compaction pressure and no influence observed.

2.6.2 Sintering

2.6.2.1 Sintering phenomenon

Sintering means the bonding together of particles when heated to high temperatures. This bonding occurs as cohesive necks (weld bonds) grow at the points of contact between particles when seen on a microstructural scale. Figure 2.10 shows scanning electron micrograph of neck formation between sintering particles. Such neck growth causes all of the property changes associated with sintering. Several laws guide the application of sintering fundamentals to practical situations [64,65].

Figure 2.10 Scanning electron micrograph of neck formation between spherical particles induced by sintering [66].

Atomic motions sinter the particles and these motions eliminate the high surface energy associated with an unsintered powder. The surface energy per unit volume is inversely proportional to the particle diameter. Therefore, smaller particles have more energy and sinter more rapidly than larger particles. However, all of the surface energy is not essentially available as a driving force for sintering. In case of a crystalline solid, nearly every particle contact will evolve a grain boundary with associated grain boundary energy. These grain boundaries are important to atomic motion because the boundaries are defective regions with high atomic mobility.

Neck growth by the movement of mass to the neck is desirable during sintering since it reduces the surface energy by decreasing the total surface area. The structural changes related with neck growth depend on a number of possible transport mechanisms. The majority of these mechanisms are diffusion processes. Diffusion is thermally activated. It means there is minimum energy necessary for atomic or ionic movement and available sites are essential. This motion depends on the atoms or ions getting energy equal to or above the activation energy necessary to break free from their present sites and moving into other available sites. The Arrhenius temperature relation shows that both the population of available sites and the number of atoms with sufficient energy to move into these sites vary,

$$N/N_o = \exp(-E/kT) \qquad (2.1)$$

where N/N_o is the ratio of available sites or activated atoms to total atoms, E is the appropriate activation energy, k is the Boltzmann constant, and T is the absolute

temperature. Therefore, sintering is faster at higher temperatures due to the increased number of active atoms and available sites.

Since the elimination of surface energy is the main objective of sintering, one obvious way in achieving this goal is the surface area. The surface area declines rapidly from an initial value and provides a gauge of the degree of sintering. The surface area could be measured using microscopic analysis, gas adsorption, or gas permeability techniques [65].

Relative neck size ratio is another measure of sintering. Mathematically, it is X/D, where X is defined as the neck diameter divided by the particle diameter, D. Besides undergoing neck growth, a sintered compact generally shrinks, densifies, and increases in strength. The shrinkage, $\Delta L/Lo$, is the change in compact length from the initial dimension, ΔL, divided by the initial dimension, Lo. Due to shrinkage, the compact densifies from the fractional green density f_g to the fractional sintered density f_s according to the relation

$$f_s = f_g (1 - \Delta L/Lo)^{-3} \qquad (2.2)$$

The densification, ψ, is the change in density due to sintering divided by the change needed to attain a pore-free solid:

$$\psi = (f_s - f_g) / (1 - f_g) \qquad (2.3)$$

Densification, final density, neck size, surface area, and shrinkage are related measures of the pore elimination process during sintering. At high temperatures, sintering is more rapid, consequently shorter times are needed to attain an equivalent degree of sintering.

2.6.2.2 Stages of sintering

The entire process of sintering can be categorized into three stages:

- Stage 1: The particle contacts are transformed to sintered contacts or necks. Powder particles remain detached. At the plane of contact grain boundaries can be created between two contiguous particles.

- Stage 2: It's the intermediate stage where single particles resume loosing their identity when the x: a ratio goes over a certain value after strong neck growth. Pores form a consistent network and grain growth occurs, that result in the formation of a new microstructure. This stage witnesses the most of the shrinkages.
- Stage 3: At the point when the apparent density becomes 90 to 95% of the theoretical density, the relative proportion of the closed pore spaces increase very rapidly and the isolated pores turn into spheroidised. If cannot diffused, gas stay enclosed in the porosity and further densification becomes impossible as the gas pressure reaches equilibrium with the pressure due to surface tension [67]. For fine grained microstructures, some additional slow densification can occur when gases trapped is easy to diffuse in the solid matrix or pores are empty.

2.6.2.3 Effects of sintering on pore structure

The sintering rate is governed by the geometry of the grain boundary and the pore during intermediate stage. At the onset of the intermediate stage, the pore geometry is extremely convoluted and the pores are situated at grain boundary intersections. As sintering continues, the pore geometry comes close to a cylindrical shape in which densification happens by decreasing of the pore radius [68]. For the period of sintering, the interaction between pores and grain boundaries can have three forms as follows:

- Pores can slow down grain growth
- Pores can be dragged by the moving grain boundaries at the time of any grain growth
- Grain boundaries can disintegrate from the pores, leaving pores isolated in the grain interior

Most materials show moderate to high grain growth rates at the temperatures typical of sintering; any differences in initial grain sizes produce forces on the grain boundaries that cause grain growth. When the temperature is increased, the rate of grain boundary motion also increases. The reason of Breaking away of the boundaries from the pores occurs is that the pores are slower moving than the grain boundaries [69]. When tension is created by a moving grain boundary, pores can move by volume or surface diffusion or even by evaporation-condensation across the pore. However, this requires close control of the heating rate, using a process termed rate-controlled sintering [70].

2.6.2.4 Densification

During densification process, the lower mobility of the pores coupled to the diminishing pinning force allows breakaway. Separation of the pores from the boundaries confines the potential final density. Therefore, it is important to minimize breakaway by careful processing control. A combination of large pore size and grain size spearheads towards breakaway during grain growth. In the ideal case, the large pores are immobile in the early stages of sintering and are pinned against, the grain boundaries to maintain a small grain size. During the later stages of sintering, the pores become fewer in number and diminish in size due to shrinkage. Even though the grains are relatively large, the pores are sufficiently mobile to migrate with the boundaries. Densification depends on the rate of pore shrinkage while this situation persists and high grain boundary diffusivity is helpful. During the process, as the pore size decreases, there is less inhibition to grain growth and pore mobility is a greater concern. For the pores to remain on the moving grain boundaries, it is essential to increase their mobility, for instance, by increasing surface diffusivity. Rapid grain growth should be avoided as invariably the densification rate is low [71].

Ceramic materials that show a high sensitivity to residual porosity could be improved in properties by the understanding of the mechanisms by which the breakaway event can be avoided. The dominant factor in the rate of densification is the effect of temperature among other factors including grain size, density, and time. In case bulk diffusion is inactive at the end of the initial stage of sintering, there will be no densification. However, pore growth and possibly grain growth might be active. Pore rounding takes place simultaneously with densification.

When the pores spheroidise into a closed structure, approximately 8% porosity, the final stage of sintering occurs. Most materials are sintered to densities over 92% of theoretical and send into the final stage. During intermediate stage sintering, Surface transport is active. It helps to smooth the pore structure and allow pore migration with grain boundaries during grain growth. However, surface transport does not contribute to densification or shrinkage. The specific sintering events depend on the microstructure (grain size, pore size, and pore spacing). Besides, since the microstructure is continually changing, the influence of temperature can be quite prominent. A high diffusivity and a small grain size [72] enhance the densification rate. Grain growth is slowed down by pores, dispersoids, and second phase inclusions. So these can be used to improve densification.

Final stage sintering is a process where spherical pores shrink by a diffusion mechanism and thus it's a slow one. Should the pores have a trapped gas, then solubility of the gas in the matrix will influence the rate of pore elimination. Because of this, it is preferable to sinter in vacuum or to use an atmosphere that is soluble in the sintering material. When a gas is sealed in the pores, internal gas pressure controls the densification rate. If the closed pores are mobile enough to stay coupled to the grain structure, then shrinkage will go on further to the final stage. A homogeneous grain size and sintering in a vacuum helps densification in the final stage

In the final stage in most materials, the distributions in particle size and packing create a pore size distribution. The longer the sintering times the lesser is the number of pores. Besides, pore size coarsens in that case while the total porosity may even increase. Differences in pore curvature will result in the growth of the larger pores at the expense of the smaller, less stable pores. This process is well-known as Ostwald ripening. To attain 100% density by sintering, it requires precise manipulation of the initial powder microstructure and heating cycle, because several factors can inhibit final pore elimination.

2.6.2.5 Factors affecting sintering profile

The main objective for sintering is to improve such compact properties as hardness, strength, transparency, toughness, electrical conductivity, thermal expansion, magnetic saturation, and corrosion resistance. Generally each of these properties improves with the degree of densification. Thus it is always desired for high strength materials because of stronger dependency of strength data upon porosity and grain size. The advantages and disadvantages of some of the adjustable processing variables in sintering are depicted in Table 3.

Particle size:

With regard to a sintering perspective, a decrease in particle size is favourable, because smaller particles exhibit faster neck growth and need less sintering time or a lower sintering temperature to achieve an equivalent degree of sintering. Generally, large particles leads to a slower sinter and require higher sintering temperature or longer sintering times to attain an equivalent degree of densification. Smaller particle size plays a major key role to achieve improved sinter densification [73]

Grain Size:

With higher density, grain size increases. This situation should be taken into account when a sintering cycle needs to be optimized to provide high density and small grain size. It is possible to sinter the commercial powders to full density at temperatures below 1400°C to give a fine grained tetragonal ceramic. There is usually a small percentage of the cubic phase present, readily identifiable as larger grains, typically 4 to 8 μm compared to the tetragonal phase grains which are usually less than 1.0 μm. A critical grain size was reported which spontaneous transformation occurred resulting in lower strength (Fig 2.11). The effect of composition and sintering temperature on the mechanical properties of commercially available material is now well established [74].

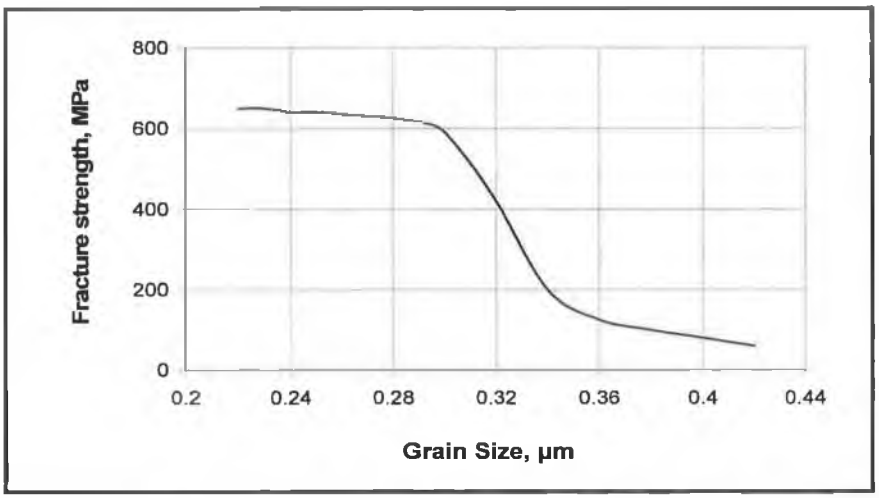

Figure 2.11 Influence of grain size on fracture strength [32].

It has been found that a critical grain size exist, which is dependent on the yttria concentration and the degree of mechanical constraint. Such factors are inter-dependent, as illustrated by the relationship of the critical grain size with stabiliser content on tetragonal zirconia in Fig 2.12. Above the critical grain size spontaneous t-m transformation of grains take place, whereas this transformation would be inhibited in a too fine grained structure [75]. Theunissen et al also stated [76] the critical grain size for retainment of the tetragonal phase at room temperature is larger in the Y, Ce-TZP systems compared to the Y-TZP and Ce-TZP systems. The chemical stability increased by doping Y-TZP with cerium or titanium.

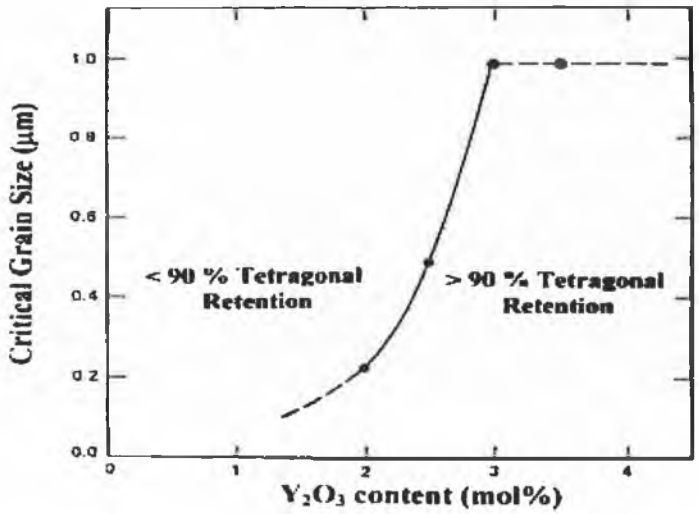

Figure 2.12 Dependence of the critical grain size on the yttria content in tetragonal zirconia [1].

Sintering Temperature:

Among all sintering variables, the sintering temperature is one of the most influential ones. Higher sintering temperatures entail more rapid sintering. However, it is to be considered carefully as it is not always favourable, due to the greater expense in furnace design, the higher energy costs and the possible grain boundary separation from the pores. Compositional changes can also improve sintered properties. It is possible to considerably strengthen the material by adjusting the composition. This adjustment also assists sintering densification. Therefore, another goal of sintering could be stated as to attain desirable diffusional homogenization responses during the high-temperature portion of the sintering cycle. Sagel-Ransijn et al [77] studied the function of temperature effect on grain growth in dense ultrafine-grained (120-600 nm) tetragonal ZrO_2-Y_2O_3 ceramics. He concluded the temperature effect in three segments. At temperature equal or below 1150°C grain growth is not significantly impeded by (solid solution) segregation or by phase partitioning. Above 1150°C grain growth is inhibited by both strain energy which arise from phase partitioning and solid solution segregation depending on exerted condition. When phase partitioning is completed, grain growth can only be restricted by drag caused by solid solution segregation. Cubic grain growth can restrict by segregation as well as by the presence of smaller tetragonal grains. Esquivias et al [3] reported, in their characterize of 5 mol% yttria dopes zirconia powder, that increase of sintering temperature from 1400 to 1600°C causes the average grain increase from 350nm to 950nm and the grain size distribution broaden from 0.16 to 3.3 μm. From XRD analysis it was revealed that the larger grains have the cubic structure, whereas the smaller grains are tetragonal.

Sintering time:

A long sintering time normally improve the degree of sintering. But it is not always favourable as it will invariably incur more expense in processing. Xu et al [16] studied the effect of sintering time for Nd_2O_3/Y_2O_3 coated zirconia ceramics. They sintered samples at 1450°C as a function of sintering time (1-5 hrs) and found out that for the (1.5 Nd_2O_3, 1.5 Y_2O)-ZrO_2 grade ceramic, fully dense materials can be obtained when sintered for 2-4 hours and for (2.0 Nd_2O_3, 1.5 Y_2O)-ZrO_2, full density

could be obtained when sintering for 2-3 hours. At longer sintering time, the density of the samples decrease. XRD analysis revealed that the decrease in density is due to the formation and increase of m- ZrO_2 which has lower density (5.68 g/cm^3) compared with t- ZrO_2 (6.05 g/cm^3). They noticed that one hour of sintering is not enough to reach fully dense samples because of the remaining closed porosity. Hardness slightly increased with time and maximum when sintering 2-3 hours. The fracture toughness strongly related to sintering time, and increases with increasing sintering time up to a maximum of 11.0-11.5 MPa $m^{1/2}$ after 2-3hours and then sharply decreased with increasing sintering time. They also concluded that the grain size of maximum toughness reaches the critical grain size as the retention of t- ZrO_2 phase after sintering is possible if the grain size of the dense crystalline materials is smaller than a critical size.

Sintering Atmosphere:

For sintering operation, a protective atmosphere/shield is required since the involvement of the large surface areas, and at temperatures between 60 and 90% of the melting-point of the particular metal or alloys [78]. But Bartolome et al and Deville et al [11] studied the aging behaviour of 3Y-TZP ceramics sintered in air and in reduced condition (90% Ar / 10% H_2) and reported that aging rate increased of about 50% in samples sintered in reducing condition compare to samples with similar density and average grain size but obtained by sintering in air.

Table 2.3 Results of modification in processing designed to aid the sintering process

	Processing change					
Result of processing change	Decrease in particle size	Increase in time	Increase in temperature	Increase in packing density	Increase in alloying level	Use of sintering aids
Thermal decomposition	...	...	X	...	...	...
Slower debinding	...	...	...	X	...	...
Reduced productivity	...	X	...	...	...	...
Pore coarsening	...	...	X	...	...	...
More rapid densification	...	...	...	...	...	X
Lower toughness	...	...	...	...	...	X
Lower sintering temperature	...	...	...	...	...	X
Less shrinkage	...	...	...	X	...	...
Less binder	...	...	...	X	...	...
Increased health hazards	X	...	...	...	...	...
Homogeneity concerns	...	...	...	...	X	...
Higher strength	...	...	...	...	X	...
Higher impurity level	X	...	...	...	...	...
Higher final density	...	...	...	...	...	X
Higher density	...	...	X	...	...	...
Greater expense	X	X	X	...	...	...
Grain growth	...	X	X	...	...	X
Furnace limitations	...	...	X	...	...	...
Faster sintering	X	...	X	...	...	...
Distortion	...	...	...	...	...	X
Degrade creep strength	...	...	...	...	...	X

2.7 Y-TZP sintering profile

In the research of some authors, it was reported that fully dense sintered ceramics appeared, after hot pressing for 1 hr at 1450°C [18,28]. Esquivias et al [3] reported, in their characterize of 5 mol% yttria dopes zirconia powder, that the sintering schedule that gave the smallest grain size (average grain size < 300 nm) was heating at 5°C/min up to 1100°C and then 1°C/min up to 1400°C holding this temperature for 2 hours. Duran et al [79] proposed sintering schedule, where Y-TZP (3 mol% Y_2O_3) was prepares by a chemically coprecipitation method having crystalline size of 6 nm, allowed to achieve fully dense bodies with 80 nm grain size by pressureless sintering at a temperature as low as 1000°C for 2 hours. Ran et al [52] used both 0.8 mol%-CuO doped 3Y-TZP and undoped 3Y-TZP, and study their sintering behaviour in air and in oxygen where they heated the sample at a rate of 2°C/m, hold for 2 hours at 1400°C and finally cooled by 4°C/min. They found out the grain size of Y-TZP phase was less than 1 μm which indicated the grain growth of Y-TZP was not significantly large during sintering and is about the same for pure 3Y-TZP system. Sagel-Ransijn et al [77] investigated the grain growth properties of nanosized ZrO_2-Y_2O_3 ceramics where they pressed the powder isostatically at 400 MPa and sintered at temperature ranging from 1070° to 1375°C using heating rate 2°C/m and cooling rate 4°C/m. Barrera-Solano et al [3] in their study with 5 mol% yttria doped zirconia powders from gel, optimised sintering schedule that gave the smallest grain size (average grain size < 300nm) was heating at 5°C/min up to 1100°C and then at 1°C/min up to 1400°C and holding for 2 hours in that peak temperature. Some authors used same sintering schedule of heating rate at 10°C/m to the desired peak temperature (1450° to 1700°C), holding for 0.5 to 10 hours at the peak temperature, followed by cooling to room temperature at a rate of 10°C/m [11,23,24,80].

Nevertheless, other authors have investigated the possibility of using two-step sintering to achieve high densities and fine grain sizes. In two steps sintering the sample is first heated at a higher temperature to achieve an intermediate density, then cooled and held at a lower temperature until it is fully dense without further grain growth [20]. Lee [23] used rate-controlled; two step sintering to sinter 3mol% Y_2O_3 stabilised zirconia. Bending strengths of two-step sintered samples were four times

greater than those of samples sintered using conventional sintering. Lee ascribed this to denser microstructures and finer grain size. Laberty-Robert et al [24] synthesized nanocrystalline YSZ powders using a modified Pechini process. They found that a high density (>98% D_{th}) and fine average grain size (5μm) could be achieved by using two-step sintering. Chen et al [81] proposed a two-step sintering method for Y_2O_3, where they initially heated to 1310°C and then cooling down to 1150°C for 20 hours, can successfully retain the grain size of 60 nm which is about 4-6 times the starting powder size. They explained the reason behind to minimize the grain growth in way of exploiting the kinetic window that separates grain-boundary diffusion from grain growth. Whereas wang et al [82] studied two-step sintering in Y_2O_3 and found out a coarsening ratio of 2 using 200 nm powders and 6 for 10 nm, from powder particle size to dense ceramic grain size which is much lower than conventional sintering. Zhou-Berbon et al [83] used double sintering method (presenting and sintering) where they presintered the samples with a heating rate of 2 °C/m up to temperature of 1008°C based on dilatometric measurement and sintered again to two different temperature (1650°C for 2 h and 1550°C for 1 h). They found high density (>99% D_{th}) with average grain size 1.5 μm for 1650°C for 2 h and fully dense with average grain size ≈ 0.67 μm 1for 1550°C for 1 h.

CHAPTER THREE
EXPERIMENTAL TECHNIQUES

CHAPTER THREE
EXPERIMENTAL TECHNIQUES

3.1 Materials

Two grades of commercially available nano-sized, 3 mol% yttria-stabilised zirconia (3Y-TZP) powders were procured. The powders were binder-added and non-binder added Tosoh E-grade (Tosoh Ltd., Japan) and Technox 2000 grade (Dynamic-Ceramic Ltd., UK). Pure, un-stabilised zirconia powder (American Premalox Ceramics Ltd.) was also investigated in this work for characterisation and comparison purposes.

3.2. Particle size analysis

Particle size analysis of the starting material was carried out using a Malvern Mastersizer S (Malvern Ltd., UK). See Fig. 3.1 Powder was dispersed in water mixed with dispersants and agitated in an ultrasonic bath for five minutes. Dispersants used included calgon and Daxad 11 [GEO Speciality Chemicals Ltd. USA].

Figure 3.1 Mastersizer S particle size analyzer.

3.2.1 Attrition milling

Powders were milled using a Netzsch attrition mill (Netzsch Ltd. Germany) as shown in Fig 3.2, fitted with an alumina grinding tank. 120 g of powder was dispersed in 180 ml of propan-2-ol and added to this was 360 g of 0.5 mm MgO-stabilised ZrO_2 media. Milling speed was 2300 rpm for 1 hr. Following attrition milling the samples were dried in a drying oven for 30 minutes at 120°C.

Figure.3.2 Netzsch attrition milling.

3.2.2 Surface area analysis

BET surface area analysis (Micromeritics Ltd., USA) was carried out. Powders were outgassed under helium at 200°C for 2 hours prior to analysis. See Fig. 3.3

Figure 3.3 Gemini III 2375 surface area analyzer.

3.2.3 Transmission Electron Microscopy (TEM)

High resolution transmission electron microscopy (JEOL 100 CX Transmission electron microscope, JEOL UK Ltd.) was also used to measure the particle size and shape of the powders under investigation [Fig. 3.4].

Figure 3.4 High resolution transmission electron microscope.

3.3 Powder density measurement

A small volume helium pycnometer (Accupyc 1330, Micromeritics Ltd., UK) was used to measure the density of as-received powder. Mean values and standard deviations were determined from five successive measurements.

Figure 3.5 Micromeritics Accupyc 1330 helium pycnometer.

3.4 Thermal analysis

Differential Thermal Analysis/Thermo Gravimetric Analysis (DTA/TGA) (Stanton Redcroft, UK) was carried out under nitrogen and air atmospheres at a heating rate of 10°C/min to 1450°C, using alumina powder as a reference material, see Fig. 3.6.

Figure 3.6 Stanton Redcroft TGA/DTA analyzer.

3.5 Powder compaction

3.5.1 Powder compaction apparatus

Two steel die set were used to form discs. The dies used for sintering and measuring Young's Modulus were 26 mm and 55 mm diameter respectively. The punch tips and the die were made of steel material. See Fig. 3.7. To aid compaction, graphite powder was used to lubricate the die. Approximately 3 g of powder was added to a 26 mm diameter steel die to make individual discs.

Figure 3.7 Pellet die.

3.5.2 Powder pressing

A uniaxial press (Moore & Son, Birmingham, UK) with a maximum load of 50 tonnes was used to press discs, see Fig. 3.8. A pressure of 20 kg/cm^2 was applied for 20 s.

Figure 3.8 Uniaxial press (Moore & Son, Birmingham, UK).

3.6 Sintering furnace

Discs were sintered in a horizontal tube furnace (Carbolite Ltd., Sheffield, UK), in air using a ramp rate of 2°C/min and holding for 2 hours at 1350°C, 1400°C, 1450°C, and 1500°C. Cooling rate was 3°C/min to room temperature. For two-step sintering, discs were heated up to 1000°C at 30°C/min and then to 1500°C at 20°C/min. The samples were then cooled down to 1380°C using a cooling rate of 40°C/min. Discs were held for 4-16 hours and then cooled to room temperature with a cooling rate of 3°C/min.

Figure 3.9 Horizontal tube furnace (Carbolite, Sheffield, UK).

3.7 Density measurement

Densities of sintered discs were calculated by simple geometric method. Thickness (t) and diameter was measured using a vernier callipers to an accuracy of 0.01 mm. Mass was measured using a precision balance to an accuracy of 0.0001 g. The sample density, i.e. the mass/volume, was then determined where the disc volume was calculated from the formula $\pi r^2.t$. Average values of two diameter measurements and four thickness measurements were used to account for variations caused by uneven pressing or warping during sintering.

Densities of the sintered discs were also measured, according to the Archimedes method (Sartorius AG, Weighing Technology Ltd.) using a water medium. Mean values were determined from three successive measurements.

3.8 Dilatometry analysis

Bar shaped samples were made by uniaxially pressing powder in a custom made steel die under a load of 20 kg/cm^2 for 20 s. Sample dimensions were 5 x 5 x 2 mm. Dilatometry (Model 402 E, Netzsch Ltd., Germany) measurements were carried out in air from room temperature to 1540°C, using heating and cooling rates of 10°C/min. See Fig. 3.10.

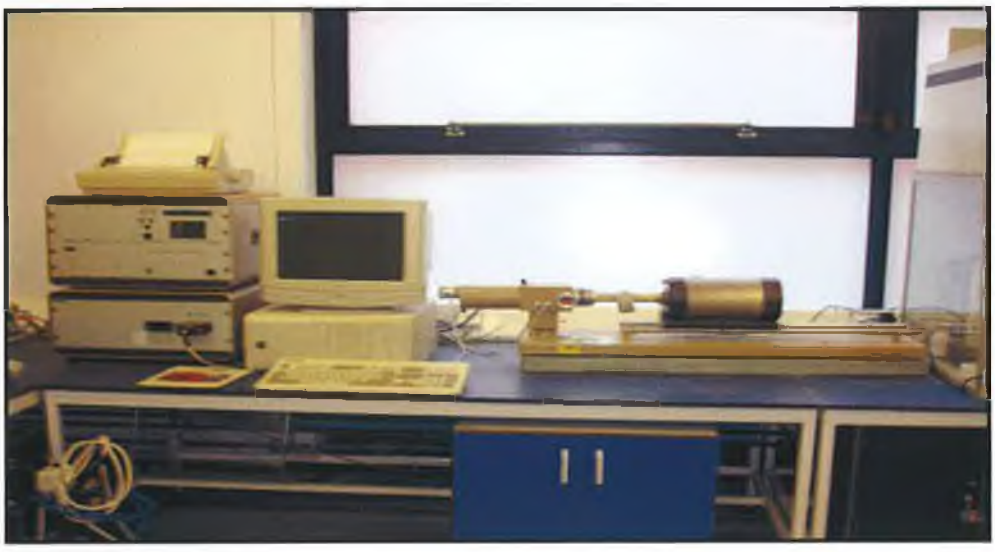

Figure 3.10 Netzsch Model 402 E Dilatometer.

3.9 Young's Modulus testing

Disc shaped samples were uniaxially pressed and sintered. Sintered discs of diameter 41.1 mm and thickness 3.1 mm were set on narrow strips of plastic foam; completely isolated from solid contact. The strips were used to support the discs in the four nodal lines of the torsional vibration as shown in Fig. 3.11.

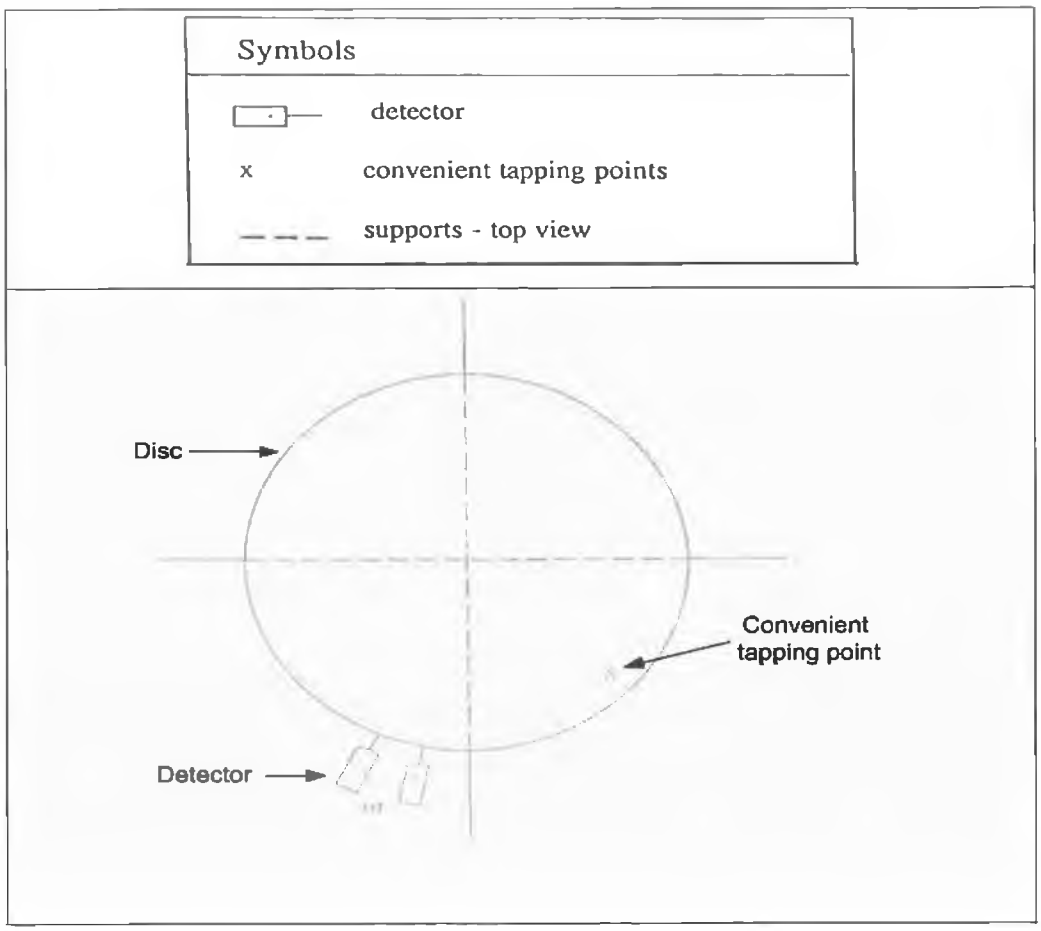

Figure 3.11 Nodal zones of the torsional vibration measurement.

The impulse excitation technique is described in detail in ASTM standard C1259 [84]. Basically, a small hammer or impulse tool strikes a solid and creates a standing wave. An impulse-excited body can vibrate in several different modes, such as flexural or transverse (bending), torsional (twisting), and longitudinal, and each mode has a fundamental resonant frequency and higher frequency overtones associated with it. The sample is struck at one of the antinodes, and the frequency of vibration is then measured at another antinode using a microphone and frequency analyzer or frequency counter. Tapping on the surface of the disc, near the rim,

causes a point of maximum vibration in that area. The resultant standing wave creates another maximum (same amplitude, same phase) at the point at 180 degrees. Two other maxima (same amplitude, opposite phase) are created at 90 degrees and 270 degrees. Two perpendicular nodal diameters are created at 45 degrees relative to the point of impact and discs are supported in four points situated on these nodal lines. The point of impact is selected in the middle, some smaller or larger angle, but not in the nodal points. The impacting pulse creates an antinode in the centre of the discs and the whole periphery acts as another antinode. A nodal circle, as shown in Fig 3.12, are selected and the discs are supported any points of this circle. The detector is held anywhere on the periphery.

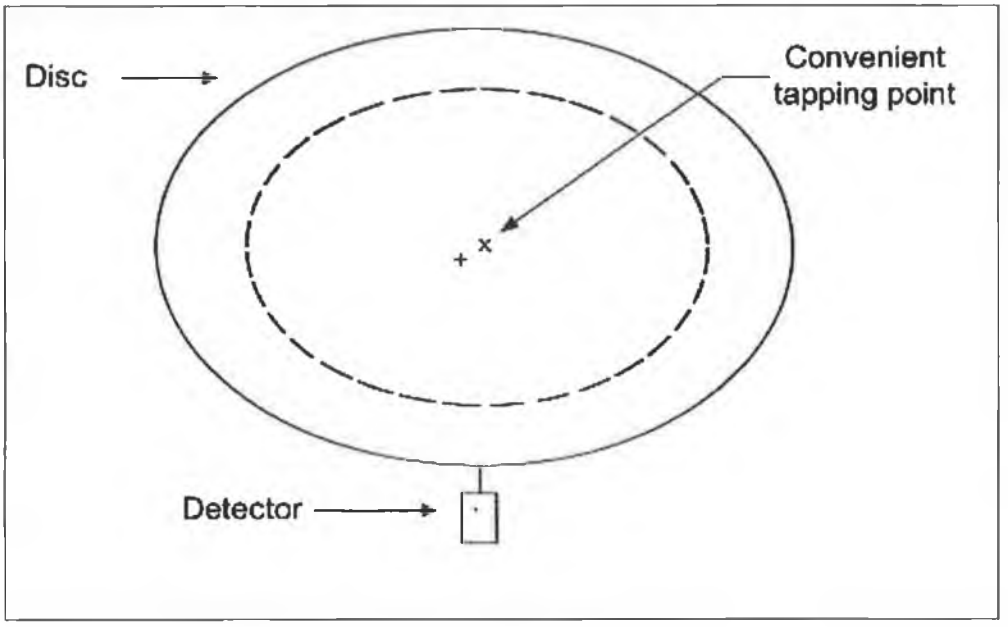

Figure 3.12 Flexural vibration measurement set-up.

An impulse excitation frequency tester (Lemmens Electronika Grindosonic) was used to measure the resonant frequency. This frequency, along with the diameter, thickness, and density of the material were used to calculate Young's modulus. The formulas used are described details in two references [85 and 86]. The fundamental equation defining the relationship between the natural resonant frequency, the material properties, and the specimen dimensions is given in [85] as:

$$f_1 = \frac{k_1}{2\pi r^2}\sqrt{\frac{A}{\rho t}} \qquad (3.1)$$

where f_1 is the resonant frequency, k_1 is the geometric factor for that resonant frequency, r is the radius of the disc, A is the plate constant ($A= Et^3/[12(1-\mu^2)]$), t is the disc thickness, μ is the Poisson's ratio for the disc material, E is Young's modulus, and ρ is the density of the disc. For the Young's modulus of a disc, two calculations of E (E_1 and E_2) are made independently from the two resonant frequency measurements, and a final value E is determined by averaging the two calculated vales E_1 and E_2. Mean values were determined from three successive measurements.

$$E_1 = [37.6991 f_1^2 D^2 m(1-\mu^2)]/(K_1^2 t^3)$$
$$E_2 = [37.6991 f_2^2 D^2 m(1-\mu^2)]/(K_2^2 t^3) \quad (3.2)$$
$$E = (E_1 + E_2)/2$$

where:

E = Young's Modulus (Pa)
E_1 = Torsional nature calculation of Young's Modulus
E_2 = Flexural nature calculation of Young's Modulus
f_1 = Torsional nature resonant frequency (Hz) of the disc
f_2 = Flexural nature resonant frequency (Hz) of the disc
D = Diameter (mm) of the disc
m = Mass (g) of the disc
μ = Poisson's ratio for the disc
K_1 = Torsional nature of geometric factor
K_2 = Flexural nature of geometric factor
t = Thickness (mm) of the disc
r = Radius (mm) of the disc

3.10 Hardness measurement

Vickers hardness was measured on a Zwick hardness tester (Type 5030 SKV, Indentec Ltd., UK) with a standard diamond indenter. Ten measurements were taken to obtain an average value under a load of 20 kg for 10 s. The two diagonals, d_1 and d_2 of the indentation left in the surface of the material after the removal of the load were measured by adjusting two lines controlled by large diameter thumb wheels. The lines enable the corners of the diamond shaped indentation to be precisely

located on a CCTV screen. The diagonal measurements and the hardness reading were displayed on a digital display. Mean values were determined from ten successive measurements. The formula (3.3) used to calculate Vickers hardness is:

$$Hv = \frac{2F \sin \frac{136^{0}}{2}}{d^{2}} \approx 1.854 \frac{F}{d^{2}} \qquad (3.3)$$

Where:

H_V: Vickers hardness in ($kgf.mm^{-2}$)

F: Load in kg-force

d: Arithmetic mean of two diagonals, d_1 and d_2 (mm)

Figure 3.13 Zwick hardness and toughness tester.

3.11 Fracture toughness

Fracture toughness was measured on the same Zwick hardness tester (Type 5030 SKV, Indentec Ltd., UK). The values were calculated by measuring the lengths of the radial cracks emanating from the indentations formed during hardness testing. Two different methods were employed to calculate fracture toughness. The first was

the indentation method of Lawn and Wilshaw [87]. Ten measurements of the radial crack lengths were taken to obtain an average value. Equation (3.4)

$$K_{c,idt} = \psi_b \left(\frac{P}{C_0^{\frac{3}{2}}} \right) \qquad (3.4)$$

Where:

$K_{C,idt}$: is the fracture toughness (GPa)

ψ_b : is the half angle of Vickers indenter (68°)

P: is the indentation load (MN)

C_O: is the radial crack length (m)

The second method used was that of Anstis et al [88], using the formula (3.5)

$$K_{c,idt} = 0.016 \left(\frac{E}{H} \right)^{\frac{1}{2}} \frac{P}{c_0^{\frac{3}{2}}} \qquad \mathbf{(3.5)}$$

Where:

E: Young's modulus (GPa)

H: Hardness (GPa)

3.12 Grinding and polishing

Samples were mounted in bakelite, using a hot-compression mounting process. The Buehler Simplimet 2000 Mounting Press (shown in Fig. 3.14 (a) was set to the operating parameters shown in Table 3.1

Table 3.1 The operating parameters involved in the mounting process

Equipment	Buehler Simplimet 2000 Mounting Press
Resin	High quality brown bakelite thermosetting resin
Temperature	Hot 150°C and cold 15°C
Time	8 minutes hot followed by 4 minutes cold
Pressure	2 MPa

Grinding and polishing were performed using a Buehler Motopol 2000 Semi-Automatic Specimen Preparation unit. See Fig. 3.14 (b). They were ground with silicon carbide paper of 120 grit (20 min), 240 grit (20 min), 600 grit (10 min) and 1200 grit (5 min). Samples were polished using napless paper (DP-Cloth, Struers Ltd., Denmark) with water-based diamond suspensions of 3 μm and 1 μm (See Table 3.2). A wheel speed of 200 rpm and platen pressure of 20 N was used for each step.

Table 3.2 Grinding and polishing step parameters

Stage	Paper/Suspension	Abrasive Size	Time (minute)	Speed (rpm)
1	Silicon Carbide	P120	20	200
2	Silicon Carbide	P 240	10	200
3	Silicon Carbide	P 600	5	200
4	Silicon Carbide	P 800	5	200
5	Silicon Carbide	P 1200	5	200
6	Diamond	3.00 μm	5	200
7	Diamond	1.00 μm	5	200

(a) (b)

Figure 3.14 (a) The Buehler Simplimet 2000 Mounting Press and (b) The Buehler Motopol 2000 Semi-Automatic Specimen Preparation unit.

3.13 Scanning Electronic Microscopy (SEM)

Polished samples were preliminarily thermally etched [2,11,12,15,16,18,23] in air at 1400 °C for 30 minutes but this proved ineffective. Chemical etching [89,90] was carried out on polished discs by etching with phosphoric acid (85%) for 2 minutes at 250°C [91]. Scanning electronic microscope (Model: 95-C1805-400,

JEOL Ltd., Japan) was used to investigate the microstructure of the sintered discs. A Back-scattering detector was employed for observation of grain boundaries on unetched samples.

Figure 3.15 JEOL Scanning Electronic Microscope.

3.14 Optical microscopy

An (MeF2 Universal Camera Optical Microscope) optical microscope was used for bright field examination of polished metallographic sintered discs. See Fig. 3.16. Buehler Omnimet image analysis software was used to determine the grain size of sintered discs. The analysis involves setting the grey-level on the microscope picture to a separate colour, to distinguish various features (such as void/pores) from the rest of the microstructure (rest of the picture set to its original colour). The area of one

feature can be numerically related to the total area of the picture, as the program counts the number of one colour type pixels and sets that as a ratio of the total number of pixels in the picture (total area).

Figure 3.16 Reichert MeF2 Universal Camera Optical Microscope.

3.15 X-Ray Diffraction analysis (XRD)

X-Ray diffraction (Bruker AXS D8 Advance, USA) analysis with Cu-Kα radiation was carried out to determine the phase structure of powders and sintered disc samples. See Fig. 3.17.

Figure 3.17 Bruker AXS D8 Advance XRD analyzer

CHAPTER FOUR

RESULTS AND DISCUSSION

CHAPTER FOUR
RESULTS AND DISCUSSION

4.1 Powders characterisation

4.1.1 Particle size analysis

4.1.1.1 Laser-diffraction based particle size analysis

As-received nano-powders were dispersed in water and agitated in an ultrasonic bath. Particle size analysis values of D [4, 3] were 1.29 μm (Tosoh) and 1.78 μm (Technox). The particle size distribution is shown in Fig. 4.1.

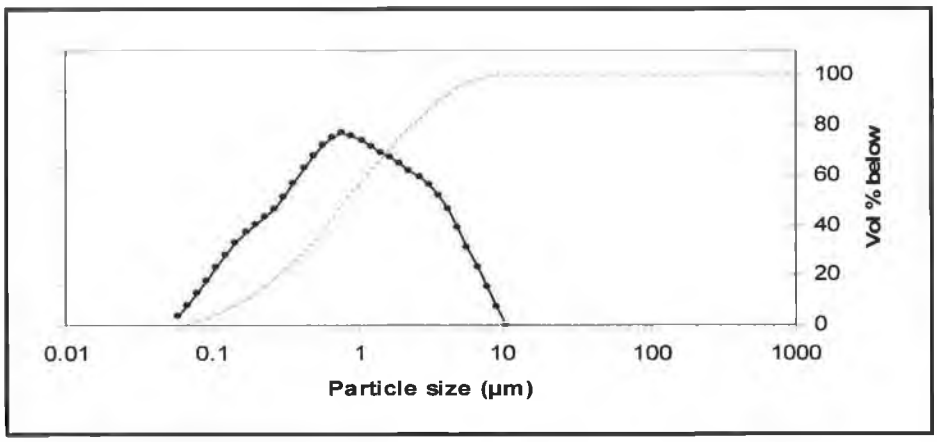

(a)

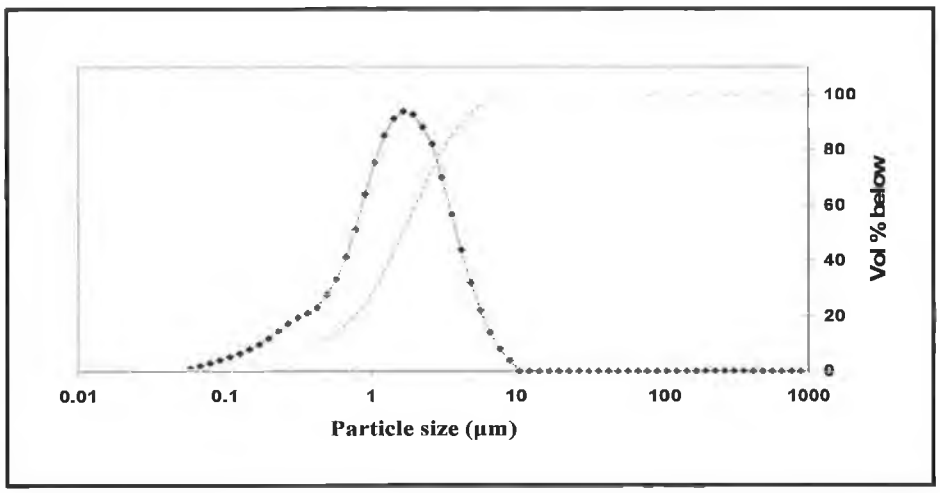

(b)

Figure 4.1 Particle size distribution pattern for (a) Tosoh powder (b) Technox powder.

From Fig. 4.1 it can be seen that only 13% of Tosoh powder and 4% of Technox powder has particle size <200 nm. It was therefore assumed that water caused this powder to agglomerate. Attrition milling of the powder failed to produce a measured reduction in particle size. It was appeared that the nano-powder was heavily prone to agglomeration. Another possibility was that the powder particle size was close to the lower limit of the instruments specified size range measurement capability of 0.05 – 880 μm. An alternative particle size analyser (Malvern, HPP5001 HPPS (high performance particle sizer) with a measurement range of 0.6 nm – 6000 nm was also employed. Powder (Tosoh) dispersed in de-ionised water again yielded particle sizes in the μm regime. A sample of powder was then filtered through a 0.45μm filter (Acrodisc, Sigma Aldrich), resulting in the result shown in Fig. 4.2 and an average particle size of 147 nm.

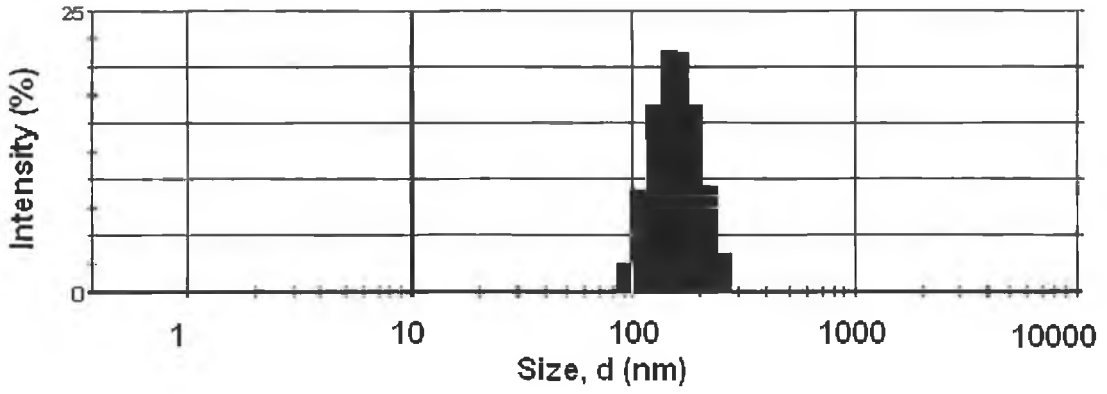

Figure 4.2 Particle size distribution pattern for TZ-3Y-E powder filtered through 0.45 μm.

Repeated analyses consistently yielded 147 nm, which showed that this powder was finely dispersed and not agglomerating over time. However, without filtering this result could not be achieved. It was unclear then if the value 147 nm simply represented the quantity of powder <200 nm observed in Fig. 4.2. Daxad 11 was used to avoid agglomeration but same result was obtained. Unfortunately, a definite conclusion about particle size of the non-filtered sample could not be reached as the possibility of water–induced agglomeration was a real problem.

Attrition milling was attempted with the Tosoh powders in order to reduce particle size and break up agglomerates. Yuan et al [92] in their study of micron-sized, yttria-stabilised zirconia and aluminium described attrition milling as an

effective way to reduce particle size, to change the particle size distribution, to change particle shape and to disperse agglomerates [93]. However, for the nano-sized powder studied here, no real decrease was realised through attrition milling. As can be seen in Fig. 4.3 the main particle size distribution peak shifted slightly to lower particle size. However, a new secondary peak also formed between 10 and 100 μm, which was not present for the un-milled powder. It is possible that the attrition milling process is de-agglomerating some particles, but deleteriously causing others to agglomerate further. However, in light of the fact that these powders are believed to be prone to water–induced agglomeration, it is difficult to make any definite conclusions about the usefulness of attrition milling to de-agglomerate these powders, from wet-based particle size analysis.

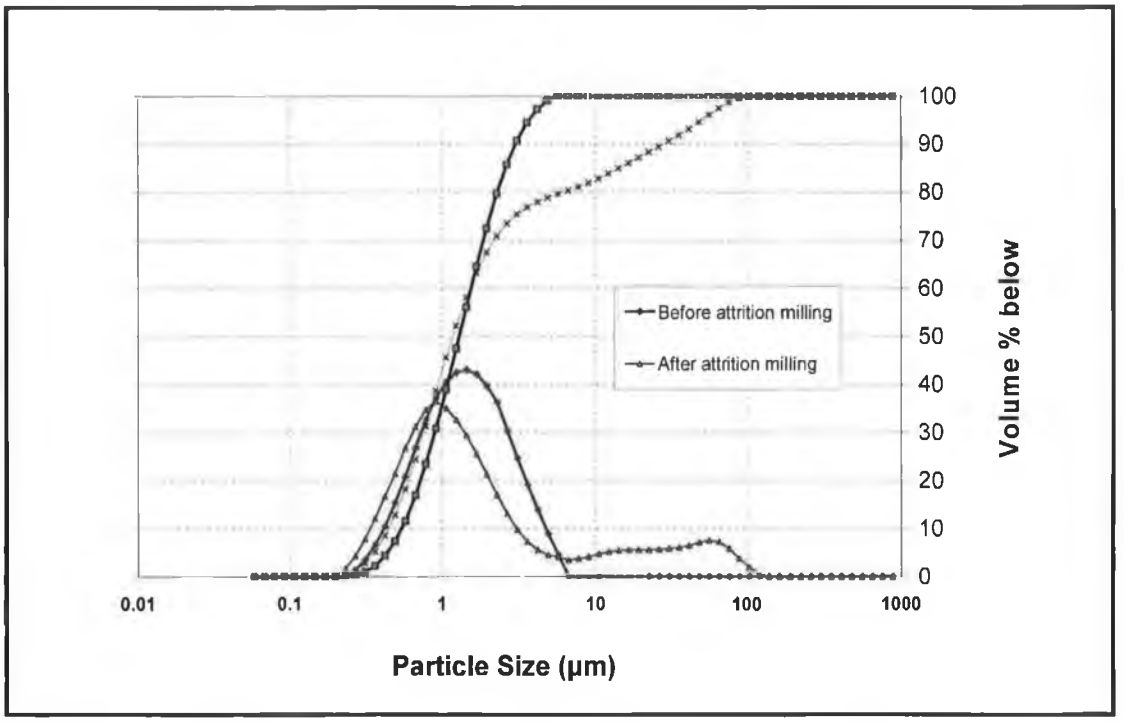

Figure 4.3 Attrition milled and non-attrition milled TZ-3Y-E grade powder.

Many authors [3,79,94,95] use a dry spherical equivalent diameter approach to avoid the problem of agglomeration when analysing nano-powders. Seidensticker et al [94] used this approach for 3Y-TZP (Tosoh) powder and calculated a BET equivalent diameter of 61.2 nm, based on a BET surface area of 16.1 m^2/g and a powder density of 6.08 g/cm^3. Seidensticker et al [94] used sedimentation size analysis to measure a mean particle diameter of 170 nm for this powder. However,

there are conflicting reports when wet methods are used. Liu et al used Tosoh TZ-3Y-E powder for hollow fiber membrane applications but only refer to the powder as having sub-μm particle diameters. Kunes et al [96] investigated the same powder for slip-casting applications. They used the alkali-free polyelectrolyte Dolapix CE64 as a deflocculant and measured a mean X_{50} particle size of 280 nm by low-angle laser light scattering (LALLS). Tuan et al, [4] carried out particle size analysis on this powder and arrived at a particle size of 230 nm.

4.1.1.2 Particle size from equivalent spherical diameter theory

In order to measure primary particle size, the specific surface area of the powders was measured. This yielded a value of 14.52 m^2/g for Tosoh and 6.42 m^2/g for Technox 2000. The equivalent spherical diameter (ESD_{BET}) was calculated from the following equation: [95]

$$ESD = \frac{6}{\rho_{part} SSA} \tag{4.1}$$

Where ρ_{part} is the density of the powder particle and SSA is the specific surface area of the powder. The density of the powder was 5.98 g/cm^3 for Tosoh and 6.03 g/cm^3 for Technox as determined from pycnometry analysis. This translated to particle sizes of 69 nm and 155 nm respectively using equation (4.1). However, from ESD theory, these results are in good agreement with the suppliers specifications. Considering the results obtained from laser diffraction based particle size analysis, it would appear that these powders are heavily prone to agglomeration in water, and are not suited to wet-based analysis.

4.1.1.3 Transmission Electron Microscopy

Fig. 4.4 shows transmission electron micrographs of both Tosoh and Technox powder with and without binder. Tosoh powder particles are spherical with uniform size distribution of around 40-70 nm. This result is in good agreement with particle size obtained using equivalent spherical diameter (ESD_{BET}). Technox powder particles are also spherical and uniformly distributed. TEM observation in Fig. 4.4 (d), shows a weakly agglomerated powder in which some agglomerate like chains consisting of primary crystallites with binder are present. The average particle size for Technox powder seems to be <100 nm which is less than results obtained using equivalent spherical diameter (ESD_{BET}). The TEM micrographs revealed agglomeration of the nanopowders.

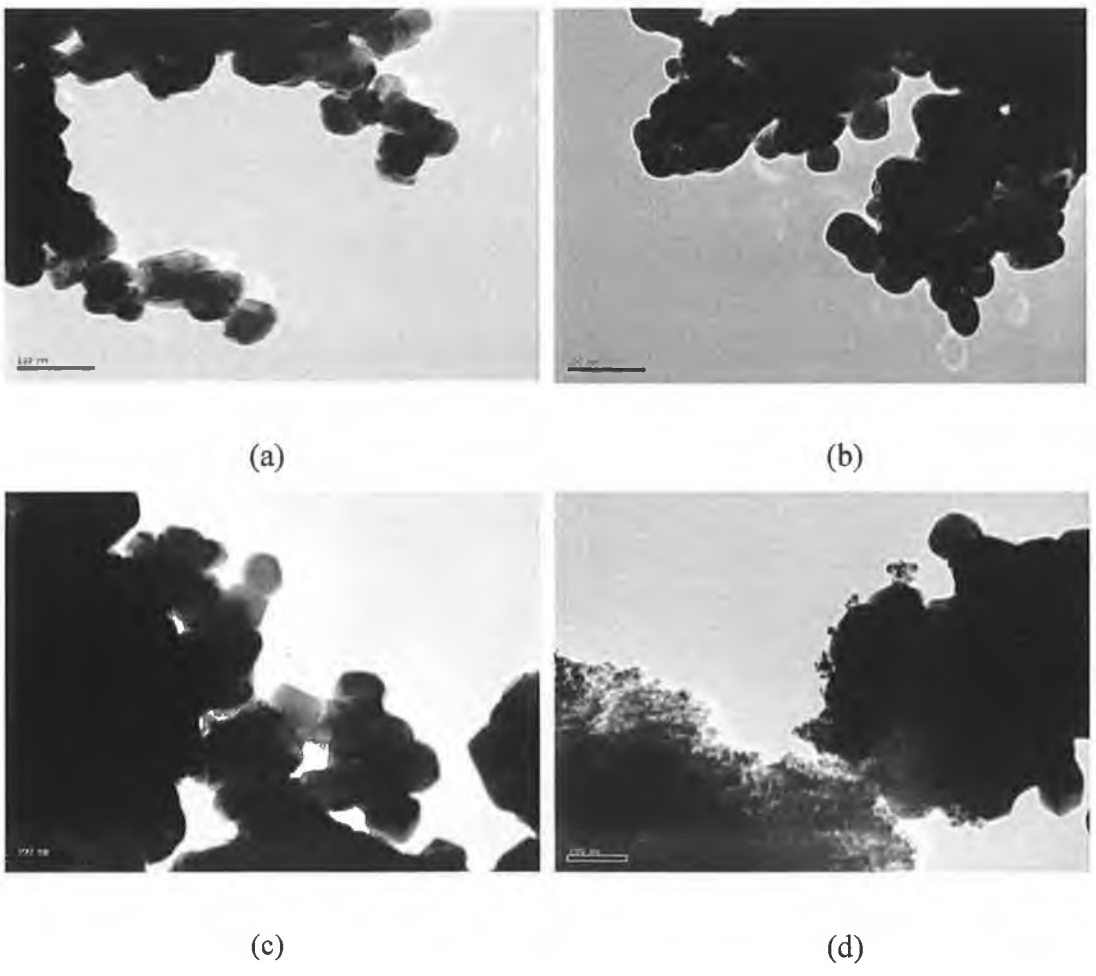

Figure 4.4 High-resolution transmission electron microscopy of (a) Tosoh powder without binder (TZ-3Y-E), (b) Tosoh powder with binder (TZ-3Y-BE), (c) Technox powder without binder and (d) Technox powder with binder.

4.1.2 Powder density measurement

Care had to be taken when carrying out pycnometry of the powder samples. Anomalous density readings were observed for small quantities of powder. Tamari [97] highlights the importance of sample chamber filling. According to Tamari, the authors Consolmango and Britt [98], observed that the volume of small meteorites could not be determined accurately and that the relative uncertainty in the measurement of sample volume decreases when the meteorite size and thus the filling factor, increases. Stabilisation of density results occurred only for quantities >8 g for Tosoh powder and between 6 to 7 g for Technox. Interestingly, 12 g of Tosoh powder (the maximum amount which could fit in the sample chamber) only corresponded to 16.6% sample chamber volume filled illustrating the difficulty in achieving high packing of this powder. The final three readings taken for 8 g, 10 g and 12 g were 5.99 g/cm^3, 5.98 g/cm^3 and 5.97 g/cm^3 respectively. From these values, an average was taken yielding a density value of 5.98 g/cm^3 for the as-received, nano-zirconia powder. The reason for the difficulty in achieving a stable result for the zirconia powder could be due to the relatively low volume of chamber filling. This is due to the high density of the zirconia powder. Lower density powders would allow greater volumes to be packed into the sample chamber, thus improving the chamber volume filled, and improving the accuracy of the result. The fact that it is nano powders which are under investigation could potentially mean that some powder is being displaced during the gas fill step by the high gas pressure. The importance of powder quantity becomes apparent. Tamari [97] recommends submitting the powder to an initial low gas pressure, a result that was employed in this study. Also, samples were weighed before and after analysis on a precision balance (accuracy 0.0001 g) and no loss of weight was recorded.

4.1.3 Thermal Analysis

Thermal analysis was carried out on the as-received, binder containing Tosoh powder. See Fig. 4.5 (a). For the sample run under nitrogen, binder burnout commenced at approximately 150°C and was completed by 475°C, corresponding to

about 3 % weight loss. A broad exothermic peak began at around 300°C and ended at around 440°C, corresponding to binder burn out. No other peaks were observed above 450°C. Similarly, on cooling, no peaks were observed. The sample run under "static air" behaved differently. See Fig. 4.5 (a). A small exothermic peak was observed at ~175°C and a large sharp exothermic peak at ~375°C. The peak at ~175°C is believed due to combustion of organics, a reaction which is prevented under nitrogen. The position of the second peak occurs at a lower temperature in air than in nitrogen. This suggests that the binder burn-off is aided by the air and is occurring at lower temperatures as a result. A percentage weight loss of ~3.6% was recorded in air compared with ~3.1% in nitrogen, indicating that residual unreacted carbon remains when a nitrogen atmosphere is used. The fact that the second peak is exothermic under air and under nitrogen suggests that decomposition and not combustion of the binder is occurring in this temperature range.

The Technox powder sample run under air behaved almost the same as Tosoh powder [Fig. 4.5 (b)]. Binder began to burn out with a sharp gradient near 200°C and ended up at around 440°C. The weight loss is about 5.05% which revealed that the Technox powder contained almost twice as much binder compared with Tosoh powder. DTA pattern showed two peaks, one small exothermic peak at about 240°C which correspond to combustion of organics. The second one is exothermic at about 342°C and related to combustion of binder [Fig. 4.5 (b)].

Duran et al [79], carried out DTA/TG analysis in air with as dried co-precipitated nanosized Y-TZP powders, observed three peaks for DTA analysis where first endothermic peak at about 120°C which corresponded to the loss of organic solvent. The second one is exothermic at about 280°C correspond to the combustion of alcoholic groups, and the third peak at 445°C , also exothermic, related to the crystallization temperature of the amorphous powder to tetragonal zirconia. They also described the main weight loss (about 10 %), which took place from 150°C to 400°C, probably due to burning of isopropyl groups.

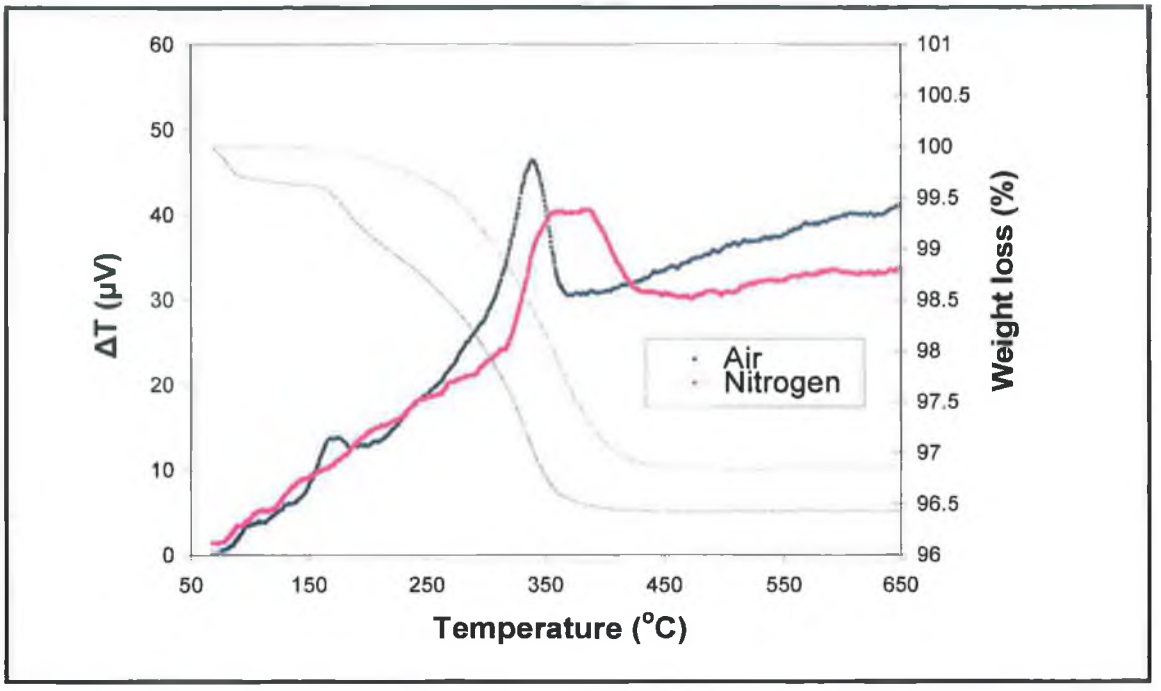

(a)

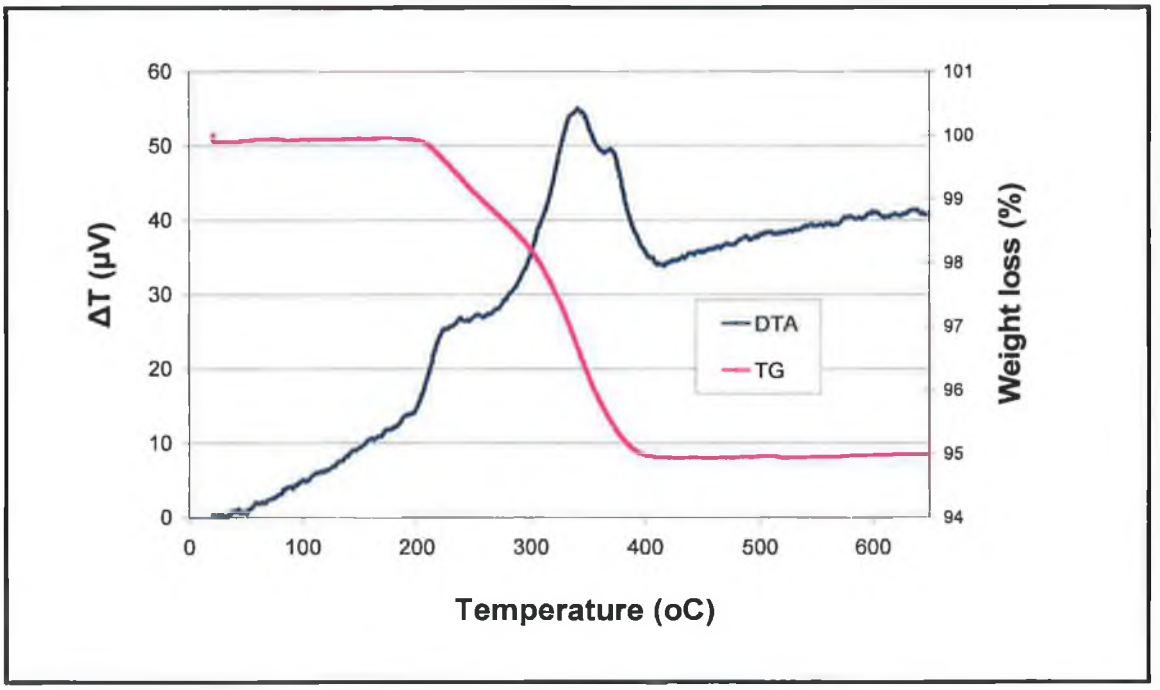

(b)

Figure 4.5 DTA/TGA curves for (a) Tosoh grade powder under static air and flowing nitrogen atmospheres and (b) Technox 2000 grade powder under air.

Of interest in this work was the retention of the tetragonal phase after sintering. For this reason, thermal analysis was carried out on Tosoh powder and also on un-stabilised monoclinic zirconia powder for comparison purposes. These powders didn't contain any binder. Fig. 4.6 shows DTA data for these powders cooled from 1450°C. For the monoclinic powder, a shift in the curve was observed during cooling at about 910°C (shown by the arrow in Fig. 4.6), believed due to tetragonal to monoclinic phase transformation. According to Piconi [1], for pure zirconia during cooling, a T-M transformation takes place in the temperature range of about 100°C below 1070°C; this transformation is associated with a volume expansion of approximately 3-4%. Tosoh recommend a cooling rate of 200°C/hr after sintering. Slow cooling rates reduce the risk of spontaneous transformation from tetragonal to monoclinic which could lead to deleterious cracking of the sintered part. From Fig. 4.6 there is no evidence of a T → M transformation for the Tosoh sample.

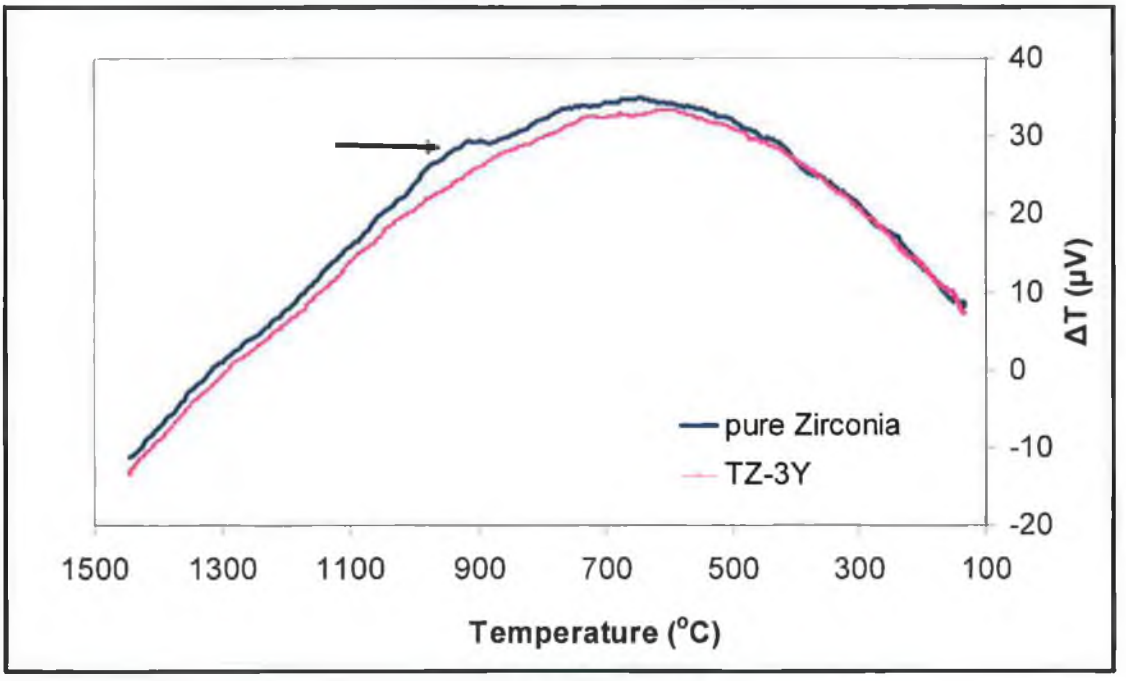

Figure 4.6 DTA curves for TZ-3Y (Tosoh) and monoclinic powder cooled from 1450°C at a rate of 10°C/min to room temperature under flowing nitrogen.

4.1.4 Dilatometry data

Dilatometry was also employed to detect the T → M transition for the monoclinic powder and both Tosoh and Technox powders. Fig. 4.7 plots the shrinkage/expansion on cooling from 1400°C.

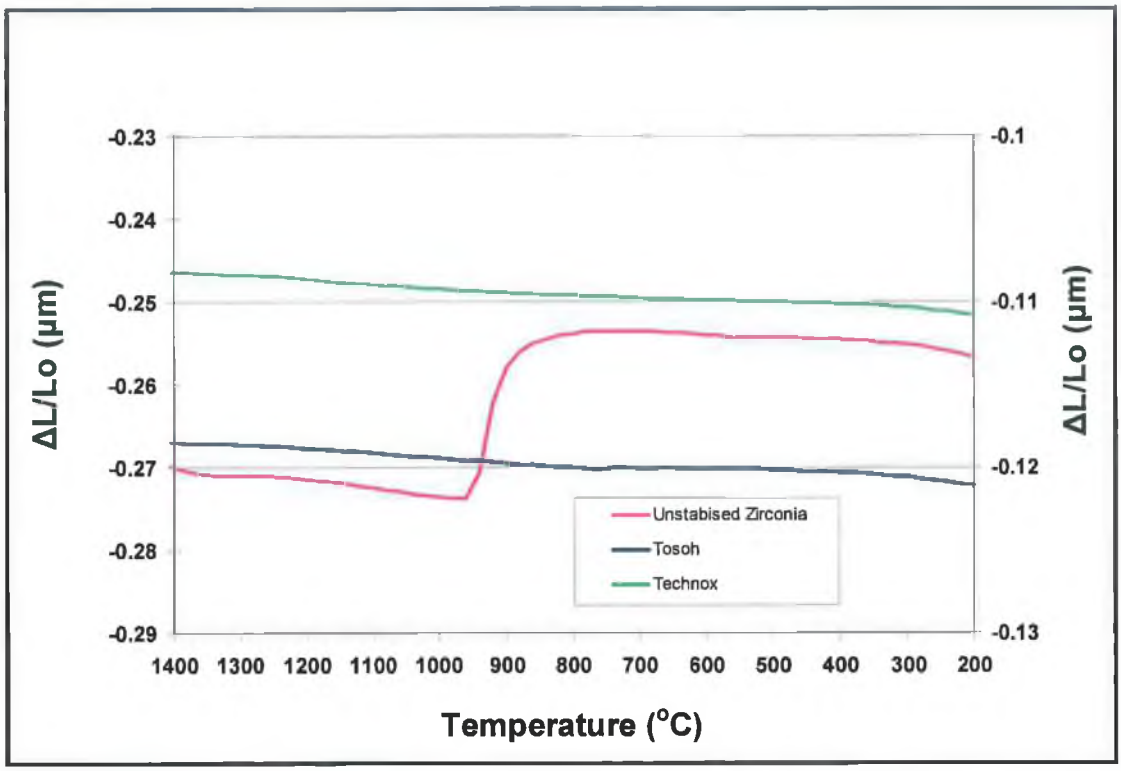

Figure 4.7 Dilatometric analysis of unstabilised zirconia, Tosoh and Technox samples cooled from 1400°C.

A sharp expansion was observed for the monoclinic sample in the region 880-960°C, as compared with the Tosoh and Technox samples, which both shrunk slightly over the cooling range. The temperature where expansion was observed for the monoclinic sample was in good agreement with the shift in the DTA curve observed in Fig. 4.6.

While the presence of tetragonal and/or monoclinic phase after sintering is important, equally important is the final density of the ceramic. Dilatometry was also used here to investigate the densification behaviour of both powders during sintering. In Fig. 4.8, shrinkage and densification rate are plotted against temperature.

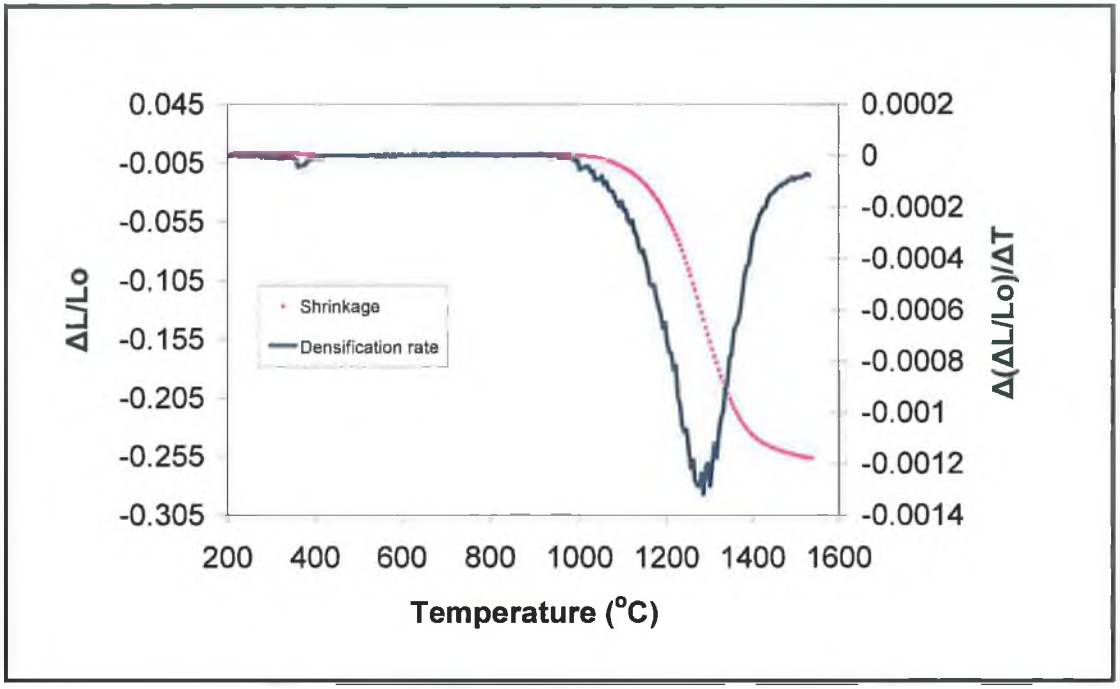

(a)

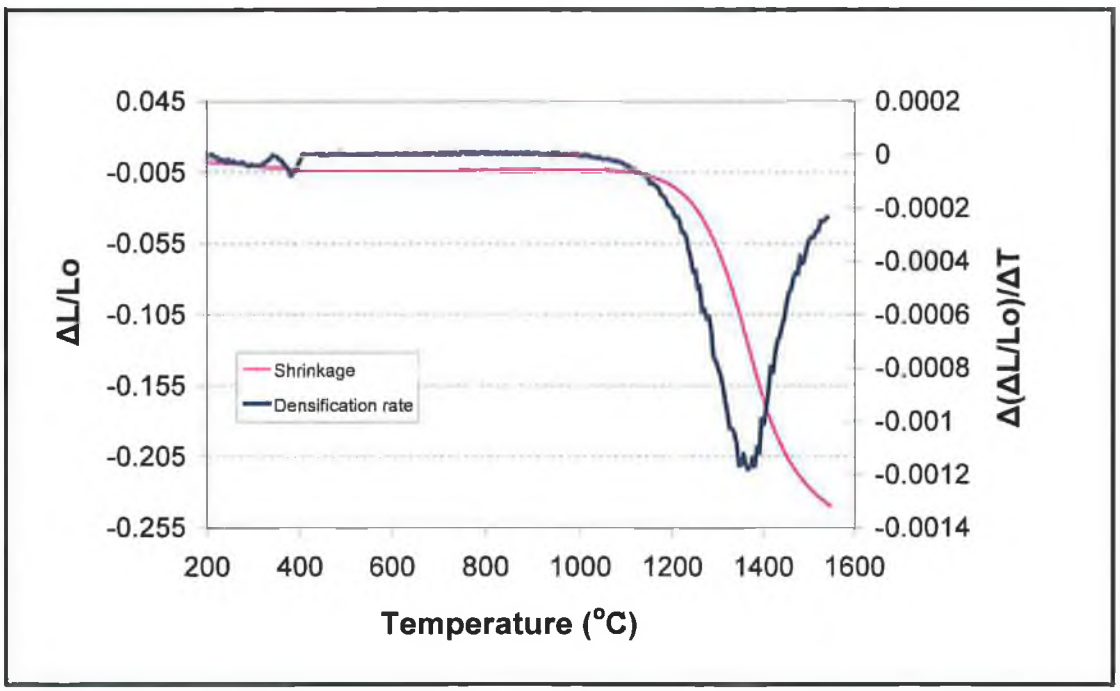

(b)

Figure 4.8 Shrinkage (pink line) and densification rate (blue line) of 3Y-TZP (a) Tosoh (b) Technox bar, as measured using dilatometry in static air with an isothermal heating rate of 10°C/min.

For the Tosoh sample (Fig. 4.8 a), a small peak at ~350°C corresponded to the elimination of binder. Shrinkage initiated at about 990°C. The shrinkage gradient was sharp with a final linear shrinkage of approximately 25.6%. The densification

rate reached a maximum at 1284°C. Shrinkage reached completion by about 1530°C. The Technox sample behaved somewhat differently (Fig. 4.8 b). Shrinkage initiated at about 1060°C. Densification does not seem to have reached completion by 1540°C, as the shrinkage has not levelled out, as compared with the Tosoh sample. The maximum densification rate is occurring at 1370°C, approximately 100°C higher than for the Tosoh sample. This is in good agreement with literature survey where it stated smaller particles exhibit faster neck growth and need less sintering time or a lower sintering temperature to achieve an equivalent degree of sintering. Generally, large particles lead to a slower sinter and require higher sintering temperature or longer sintering time to attain an equivalent degree of densification [73]. Duran et al [79], in their study of nanosized (7 nm) Y-TZP (Tosoh), observed a major densification rate peak at about 1200°C. Above 1200°C, densification increased up to about 96% D_{th} at 1300°C, and density achieved at the end which corresponded to a maximum in densification of about 99.6% $D_{th.}$ Duran et al [99] also studied densification behaviour of high-purity barium titanate. They observed a major densification rate peak at 1250°C which corresponded to a maximum in densification of about 99.3% D_{th}. Above 1250°C a small de-densification occurred and densification decreased up to about 97% D_{th} at 1300°C, which they attributed to gas release from the decomposition of barium carbonate in the barium titanate environment and the high mobility of the grain boundaries. Shi et al [100] studied the sintering behaviour of fully agglomerated 7 mol % yttria stabilised zirconia and correlated pore behaviour with densification. According to their study, the volume of the primary pores reduces to only 10 % of that sintered at 1000°C and almost completely eliminated when heated at 1400°C, showing full densification but the removal of the secondary pores become significant only at temperatures above 1400°C.

4.2 Compaction and sintering

4.2.1 Compaction

Disc samples were prepared by pressing and sintering. From Table 4.1 and Table 4.2, it can be seen that green density of compact was around ~40 % D_{th} achieved by applying a load of 20kg/cm^2 for 20 s. Duran at el [79] described compaction

behaviour of isopropanol-washed calcined Y-TZP powder. The powder was isostatically pressed in the range of 20 to 350 MPa and found out the relative density increased with increasing applied pressure and finally reached 43 % of D_{th}. They found that a clear transition in the consolidation behaviour occurs at a compaction pressure of about 32 MPa which is lower than the result reported for the Tosoh powder ($\geq$ 40 MPa) [79,101].

4.2.2 Sintering

Almost full density is being achieved by using isothermal ramping and single dwell time sintering. However, it is likely that such an approach is not optimum in terms of grain size, a parameter which is critical for zirconia ceramics. Two-step sintering as discovered by Chen & Wang is fast gaining in popularity particularly for nano-powders [81]. Many authors advocate two-step sintering in order to achieve full densification, while maintaining fine grain sizes. Barba et al [102] claimed that when relative density reaches critical values (~90%), temperature should be decreased and dwell time increased, to maximise the potential for complete densification. In the case of the Technox powder studied here it appeared that 1380°C as a dwell temperature might be suitable if employed in a two step sintering strategy as it coincides with the onset of maximum densification rate.

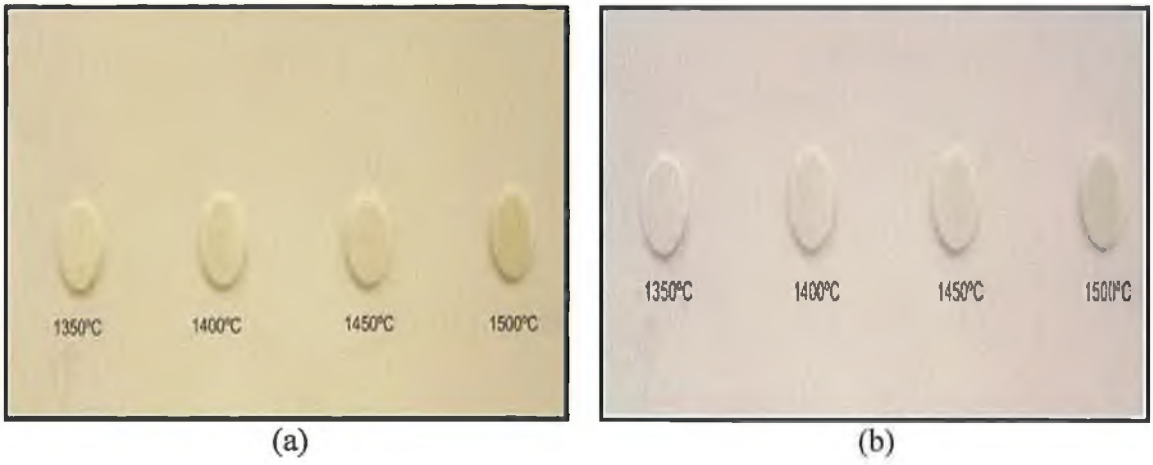

(a) (b)

Figure 4.9 Images of sintered discs (a) Tosoh and (b) Technox.

4.2.2.1 Densities of sintered discs

In order to further investigate the densification of these powders, discs were sintered in the temperature range 1350-1500°C. Two different methods were used to measure the density. The results are summarized in Table 4.1 and Table 4.2

Table 4.1 Green density and sintered density of Tosoh discs

Sintering Temperature (°C)	Green Density % D_{th}	Sintered Density (Callipers) % D_{th}	Sintered Density (Archimedes) % D_{th}
1350	40.11	97.46	97.40
1400	41.38	99.47	98.95
1450	40.94	99.64	99.44
1500	40.96	99.72	99.31

The % D_{th} value was calculated based on taking a density value of 6.08 g/cm^3 for Tosoh. This value was chosen based on work carried out by Basu et al [18]. Basu et al reported a density of 6.08 for TZ-3Y (Tosoh) which was hot-pressed at 1450°C for 1 h in a vacuum. This is the highest value reported for this material in the literature and it is reasonable to assume that it represents an almost if not fully dense part. The manufacturer quotes a value of 6.05 g/cm^3 for sintered part. Normally, the percentage theoretical density of sintered parts would be calculated based on the density of starting powder. However, in this work a value of 5.98 g/cm^3 was recorded using pycnometry and it was therefore felt that the powder was not 100% tetragonal. This was later confirmed by XRD analysis (Fig. 4.20). During sintering, any monoclinic phase would transform to tetragonal, thus leading to a density increase. After sintering, the value of 5.98 g/cm^3 would then no longer be valid as a reference density.

Table 4.2 Green density and sintered density of Technox discs

Sintering Temperature (°C)	Green Density % D_{th}	Sintered Density (Callipers) % D_{th}	Sintered Density (Archimedes) % D_{th}
1350	40.75	91.64	94.67
1400	41.98	93.53	96.89
1450	40.99	94.41	97.57
1500	40.88	96.49	98.05
1550	40.68	97.61	99.11

From Table 4.1 it is clear that the Tosoh powder sintered very readily and reached a maximum density of 99.31 % D_{th} under conventional one-step sintering conditions. Technox powder needs higher temperatures to yield % D_{th} more than 99 % as shown in Table 4.2. The dilatometry analysis data (Fig. 4.8) did show that the maximum densification rate of Technox powder occurred at higher temperature than for Tosoh powder. To achieve higher density using Technox powder, discs were sintered at 1500°C with different holding time as shown in Fig. 4.10. It suggests that the % D_{th} increases sharply with time and then falls with further increasing time. % D_{th} increases with temperature regardless of the powders. Laberty-Robert et al [24] studied green microstructure and sintering behaviour of 8 mol% Y_2O_3-ZrO_2 powders and observed the relative densities as a function of sintering temperature. They reported that the densification increased with the sintering temperature.

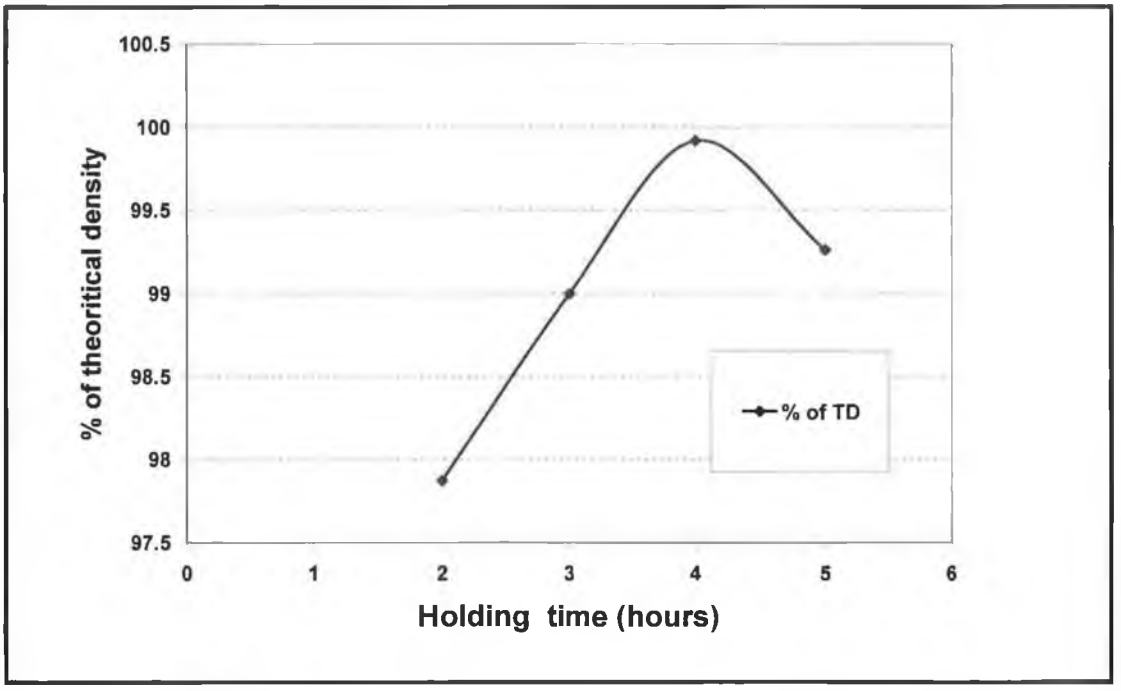

Figure 4.10 Technox sample sintered at 1500°C with different holding time.

Two-step sintering was employed for the Technox powder based on the dilatometry data from Fig. 4.8 (b). As can be seen from Table 4.3, density increased with increasing hold time at 1380°C and finally reached 98.58 % D_{th} applying holding time of 16 h. Polotai et al [20] produced a fine grained barium titanate ceramic with a %D_{th} of 99.7% using two-step sintering combined with rate

controlled sintering. The first sintering step produced and froze in place a uniform pore microstructure while minimising grain growth. The diffusion distance was thus minimised during constant grain-size sintering which maximised densification kinetics leading to an almost fully dense ceramic.

Table 4.3 Sintered density of Technox samples for two-step sintering

Sintering Temperature (°C)	Holding time	Sintered Density (Callipers) % D_{th}	Sintered Density (Archimedes) % D_{th}
1380	4	96.46	96.05
1380	8	96.87	97.40
1380	12	97.94	98.47
1380	16	98.12	98.58

4.3 Mechanical properties determination

4.3.1. Vickers hardness

Mechanical properties of sintered samples are given in Table 4.4, Table 4.5 and Table 4.6. The hardness measurement was carried out using a load of 20 kg. The indentation load was critical in the measurement of hardness and fracture toughness using the indentation method. The amount of load could affect the indentation size and crack length. Many ceramic shows a decrease of hardness with the load increase. This problem can be solved by carrying out the Vickers hardness measurement in raised loads, above 50 N, where the influence of the hardness decreases and so the standard hardness can be obtained [103, 104]. An important observation was the development of transformation-induced uplift around the indents evident from the optical microscopy (Fig. 4.11). Well-defined cracks grew from the indent diagonals for both Tosoh (Fig. 4.11 a) and Technox (Fig. 4.11 b) samples. The tortuosity of the cracks does not change in spite of variation of powders and sintering route.

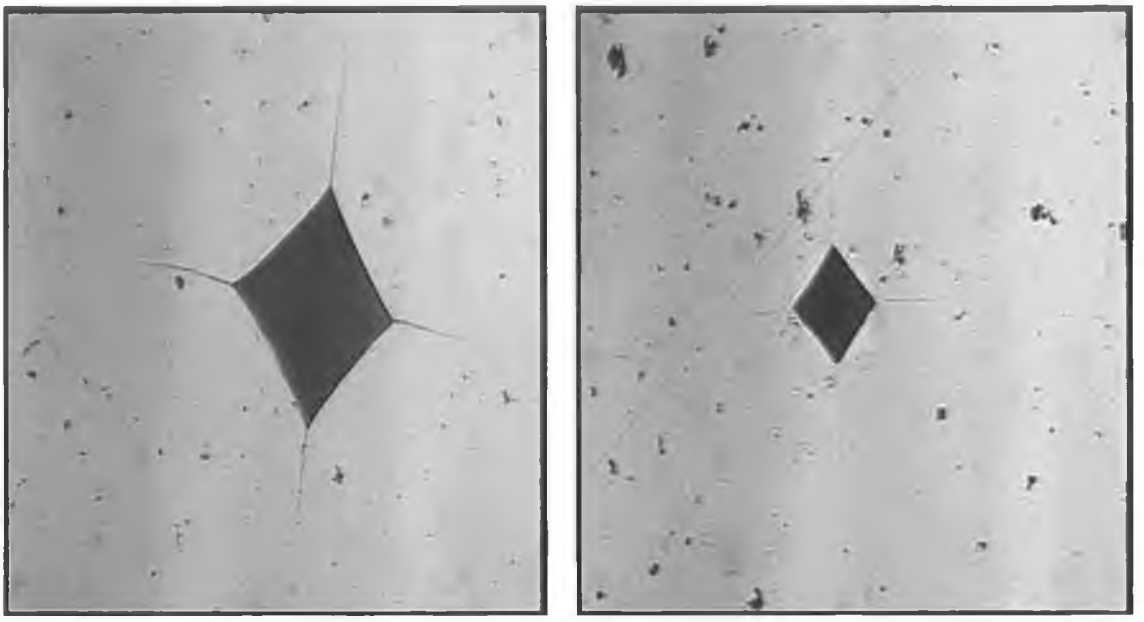

(a) Tosoh (b) Technox

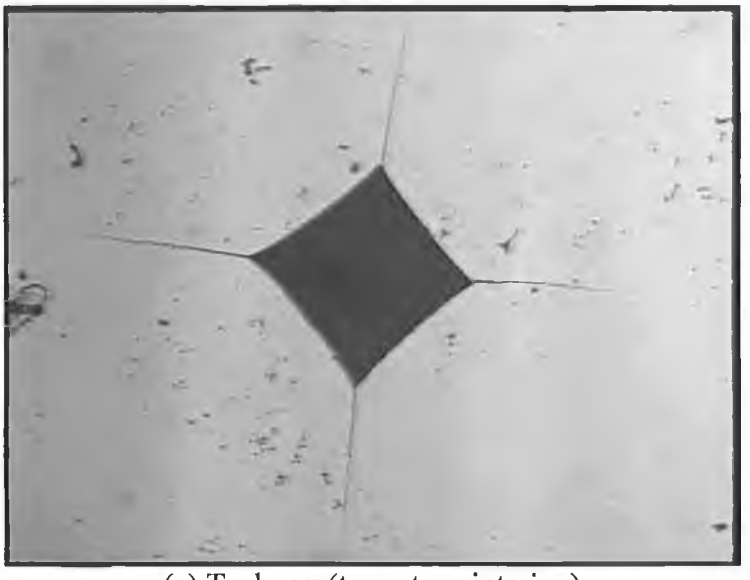

(c) Technox (two-step sintering)

Figure 4.11 Vickers indentation for 3Y-TZP ceramics with a load of 20 kg: (a) Tosoh sample, (b) Technox sample and (c) Technox sample using two-step sintering.

The dependence of Vickers hardness on the sintering temperature and time is shown in Fig. 4.12 and Fig. 4.13, respectively. Although the hardness of Tosoh sample was higher than that of Technox sample both had same trend of increasing with temperature and reached a maximum. Above the maximum, the hardness decreased with increasing sintering temperature, which could be attributed to grain growth. Tosoh samples reached maximum hardness at lower temperature compared with Technox samples which is in good agreement with the dilatometry analysis data

(Fig. 4.8 where it showed that maximum densification rate of Technox powder occurred at higher temperature than for Tosoh powder. Vickers hardness increased with sintering time and reached a maximum value of 12.87 ± 0.29 GPa when sintering for 16 h at lower temperature in two-step sintering. Above the maximum, the hardness levelled off.

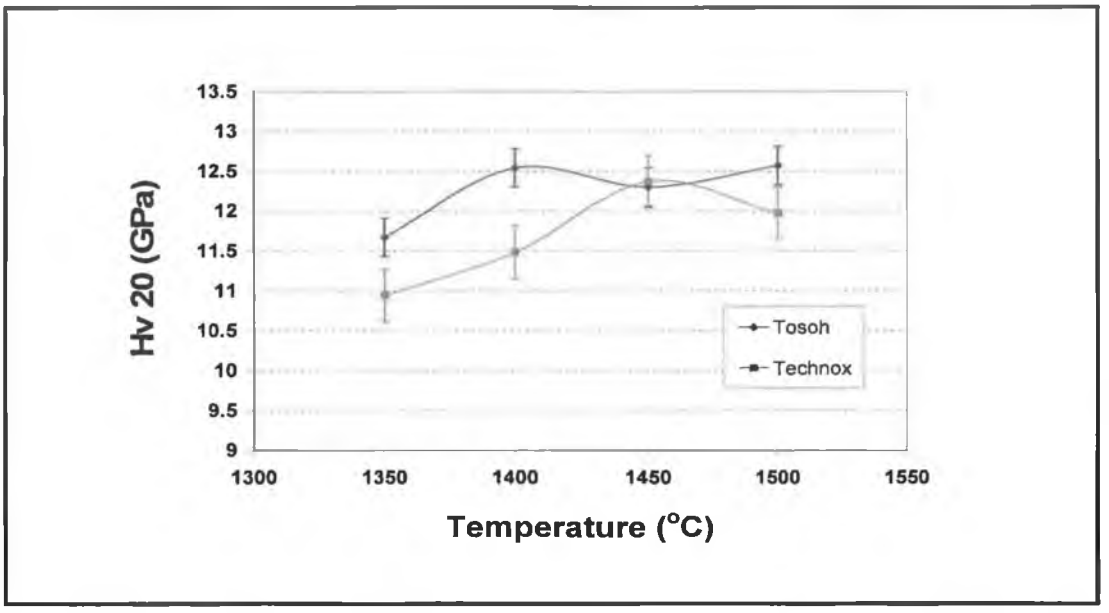

Figure 4.12 Vickers hardness of the sintered samples as a function of sintering temperature.

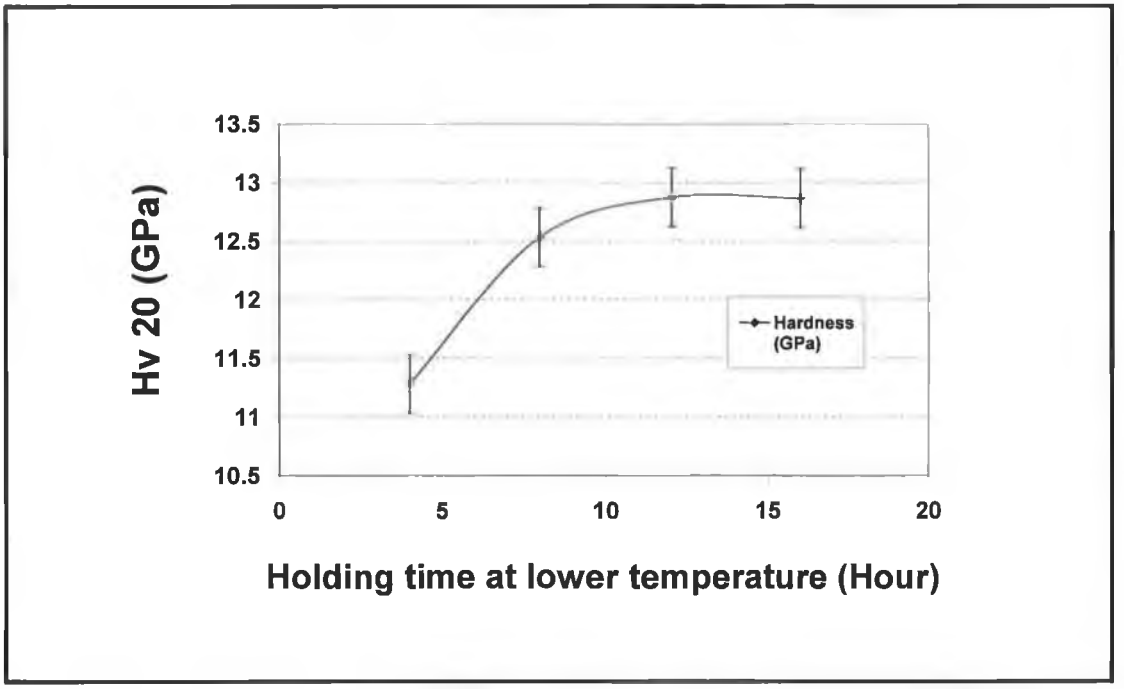

Figure 4.13 Vickers hardness of 2-step sintered Technox sample as a function of sintering time.

Table 4.4 Mechanical properties of Tosoh samples

Sintering Temperature (°C)	Vickers Hardness Hv (GPa)	Fracture toughness K_{IC} (MPa.m$^{1/2}$)
1350	11.67 ± 0.30	5.49 ± 0.34
1400	12.54 ± 0.23	4.88 ± 0.28
1450	12.30 ± 0.24	4.97 ± 0.25
1500	12.57 ± 0.17	4.20 ± 0.38

Table 4.5 Mechanical properties of Technox samples

Sintering Temperature (°C)	Vickers Hardness Hv (GPa)	Fracture toughness K_{IC} (MPa.m$^{1/2}$)
1350	10.94 ± 0.34	5.14 ± 0.25
1400	11.48 ± 0.21	5.08 ± 0.23
1450	12.37 ± 0.37	4.82 ± 0.26
1500	11.97 ± 0.39	5.47 ± 0.34
1550	12.19 ± 0.31	5.20 ± 0.26

Table 4.6 Mechanical properties of Technox samples using two-step sintering

Sintering Temperature (°C)	Holding time	Vickers Hardness Hv (GPa)	Fracture toughness K_{IC} (MPa.m$^{1/2}$)
1380	4	11.28 ± 0.20	5.48 ± 0.36
1380	8	12.53 ± 0.33	4.84 ± 0.37
1380	12	12.87 ± 0.19	4.96 ± 0.25
1380	16	12.87 ± 0.29	6.12 ± 0.46

4.3.2 Fracture toughness

The dependence of fracture toughness on sintering temperature was not very pronounced as can be seen from Fig. 4.14. For Tosoh samples, it was higher (5.49 ± 0.34 MPa.m$^{1/2}$) at lower temperature and gradually decreased with temperature. For Technox sample it is almost constant with temperature. Fracture toughness varied with sintering time (Fig. 4.15). As the dwell time increases, for Technox sample at lower temperature (2-step sintering), fracture toughness also increases and finally

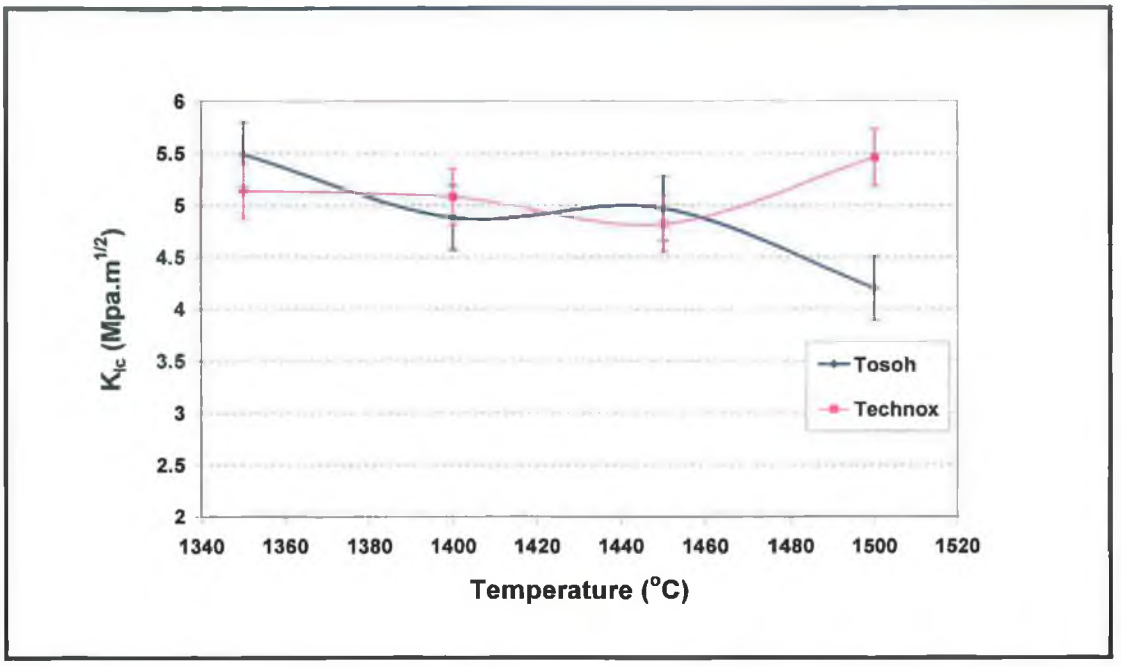

Figure 4.14 Fracture toughness of the sintered samples as a function of sintering temperature.

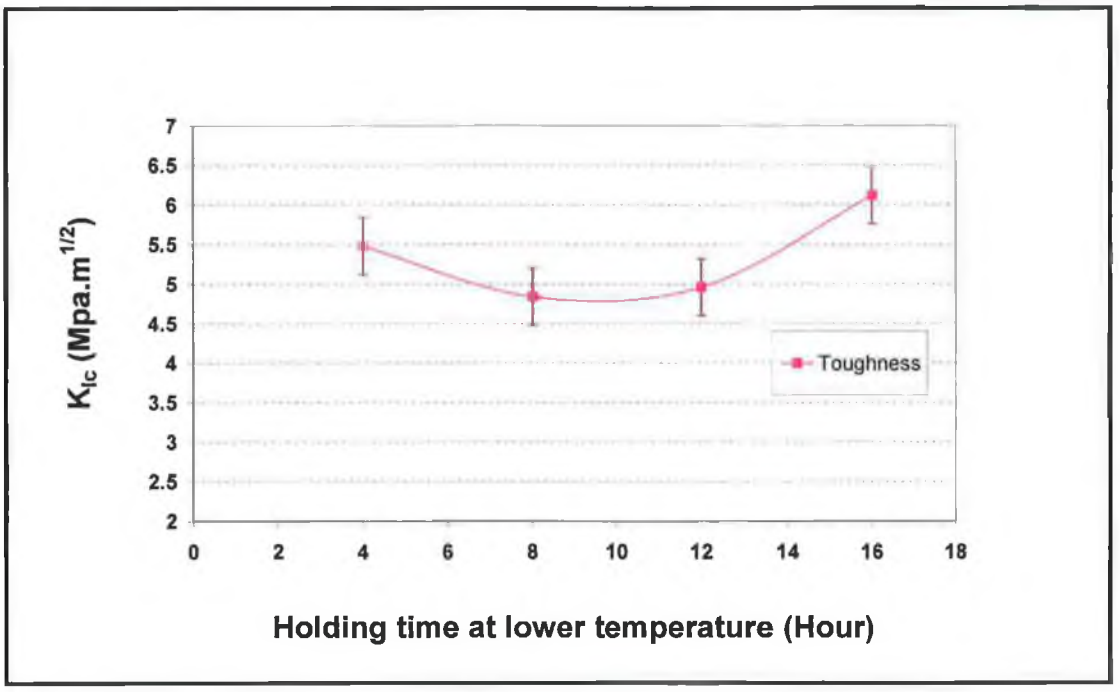

Figure 4.15 Fracture toughness of 2-step sintered Technox sample as a function of sintering time.

reached maximum value of 6.12 ± 0.46 MPa.m$^{1/2}$ applying holding time of 16 h. Pedzick et al [30] investigated slow crack propagation using commercially available 3Y-TZP powder (Tosoh). They reported the fracture toughness value of 5.0±05

$MPa.m^{1/2}$ by Vickers indentation. Chung et al [29] reported a fracture toughness value of 4.8±02 $MPa.m^{1/2}$, using commercially available 3Y-TZP powder (Tosoh), for samples sintered at 1600°C for 3 h in air. Basu et al [18] investigated a simple but innovative route based on the mixing and hot pressing (under identical conditions) of TZ-3Y (Tosoh) zirconia powders. The experimental results yielded a fracture toughness of 3.3±0.3 $MPa.m^{1/2}$ using 30 kg indentation load. Cutler et al [28] also hot pressed TZ-3Y (Tosoh) zirconia powder and measured fracture toughness of 3.54±0.12 $MPa.m^{1/2}$.

4.3.3 Young's Modulus

Measurements of E from the resonant frequency gave values which are within 140-194 GPa for three zirconia samples. Most of the authors reported the values of E for 3Y-TZP in the range of 194-210 GPa [18, 103, 104]. The employment of various techniques to measure fracture toughness would yield different results possibly due to difference of crack mechanisms induced, although, arguments may be just due to different toughness equation used (Table 4.7). Moraes et al [103] used three different equations for calculating indentation fracture toughness and found out a difference of 50 % for K_{IC} values for the same composition.

Table 4.7 Mechanical properties and comparison between Lawn & Wilishaw and Anstis method

Material	Sintering Temperature (°C)	Holding time	Young's modulus E (GPa)	Fracture toughness Lawn & Wilshaw K_{IC} ($MPa.m^{1/2}$)	Fracture toughness Anthis K_{IC} ($MPa.m^{1/2}$)
Tosoh	1450	2	194	4.97	4.32
Technox	1500	2	153	5.47	4.29
2-step sintered	1380	16	140	6.12	4.43

4.4 Microstructure analysis

SEM was attempted to study the microstructure but no clear image was observed using standard polishing route followed by chemical etching as thermal etching did not work out efficiently. From the optical micrograph (Fig. 4.19), the grain size was measured by using linear intercept method [105]. The average grain size for Tosoh

sintered samples increased up to 13 μm and for Technox, it was 15 μm. The grain size was also measured using Buehler Omnimet image analysis software as shown in Fig. 4.16 to Fig. 4. 18.

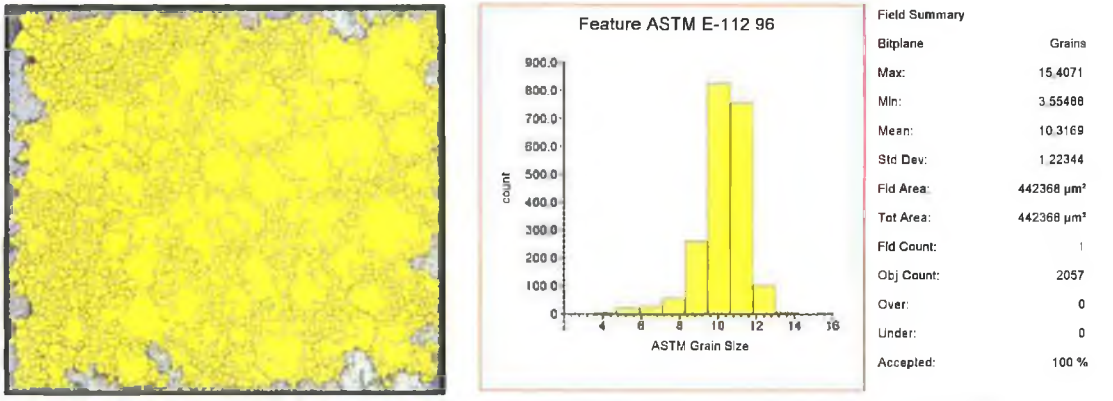

Figure 4.16 Grain size analysis of Tosoh sintered at 1350°C by using Buehler Omnimet image analysis software.

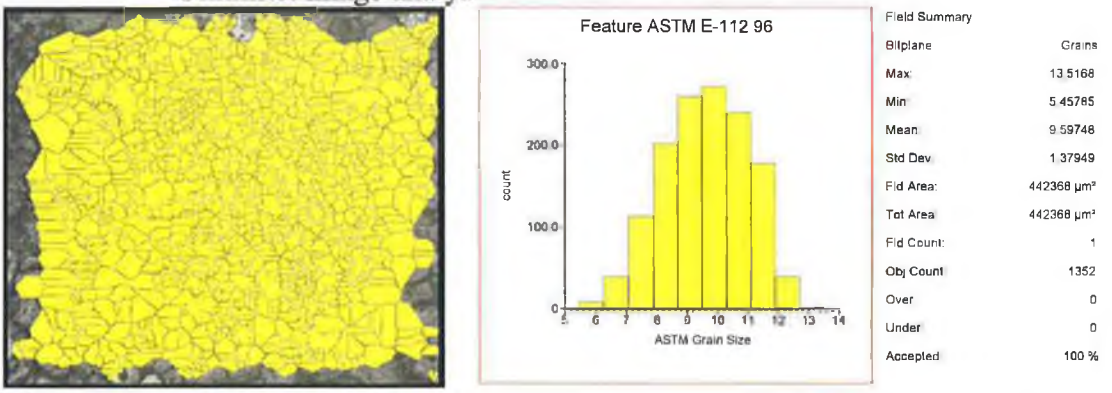

Figure 4.17 Grain size analysis of Technox sintered at 1400°C by using Buehler Omnimet image analysis software.

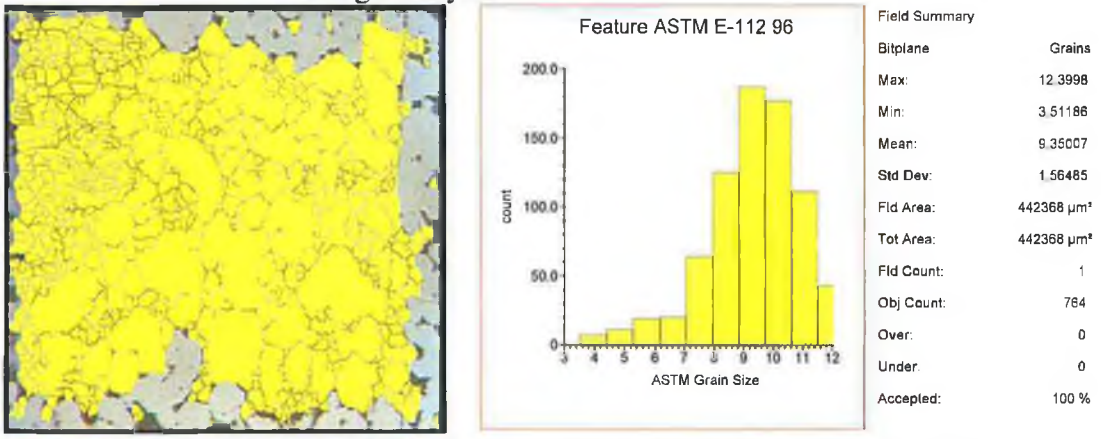

Figure 4.18 Grain size analysis of Technox two-step sintered (8 hrs) sample by using Buehler Omnimet image analysis software.

The grain size increased with increasing sintering temperature and maximum was reported 10.55 μm for Tosoh sample sintered at 1500°C. Applying two-step sintering, appeared to be an effective method for restraining grain growth. Polotai et al [20] reported a grain growth factor of 12 for fine grained barium titanate ceramic

using two-step sintering which is 5 times smaller than that observed for conventional sintering. Wang et al [82] applied two-step sintering to 200 nm Y_2O_3 powder and reported a coarsening ratio of 2, from powder particle size to dense ceramic grain size. The ratio was 6 for 10 nm powders, which is much lower than for conventional sintering. Laberty-Robert et al [24] in their study of green microstructure and sintering behaviour of 8 mol% Y_2O_3-ZrO_2, investigated the effect of dwelling time at 1450°C in order to control grain size. They observed that for a short dwelling time of 4h, the grain size of fully dense ceramics was around 5 μm, about 10 times more than the starting powder size.

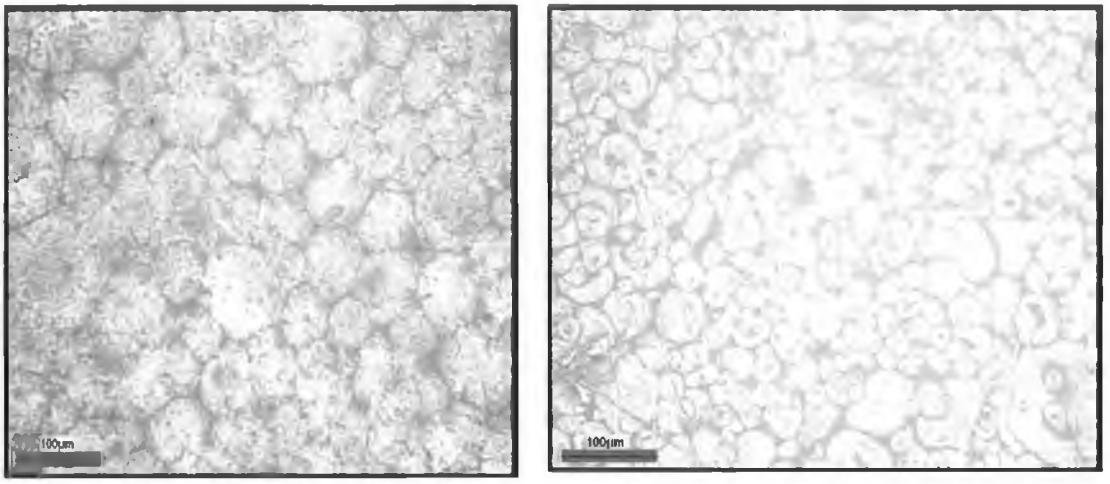

(a) (b)

Figure 4.19 Optical micrograph of polished (a) Tosoh and (b) Technox samples at 1500°C.

4.5 Phase study

X-ray diffraction analysis was conducted, the patterns of which are shown in Fig. 4.20. The un-stabilised powder showed a classic monoclinic pattern (Fig. 4.20 a). The Tosoh disc after sintering (Fig. 4.20 b) was found to be wholly tetragonal. The splitting of the (110) and (002) peak at 2Θ (~35°) was a clear indication of the presence of tetragonal phase [106]. The Technox powder was very similar and also found to be tetragonal after sintering (Fig 4.20 d). The powder sample of Tosoh (Fig. 4.20 c) revealed the presence of some monoclinic phase in this material, i.e. secondary peaks are observed at ~28° and ~31.5°. The presence of this monoclinic phase explains the value of 5.98 g/cm^3 obtained by pycnometry for this powder. This phase was then being transformed to tetragonal during sintering.

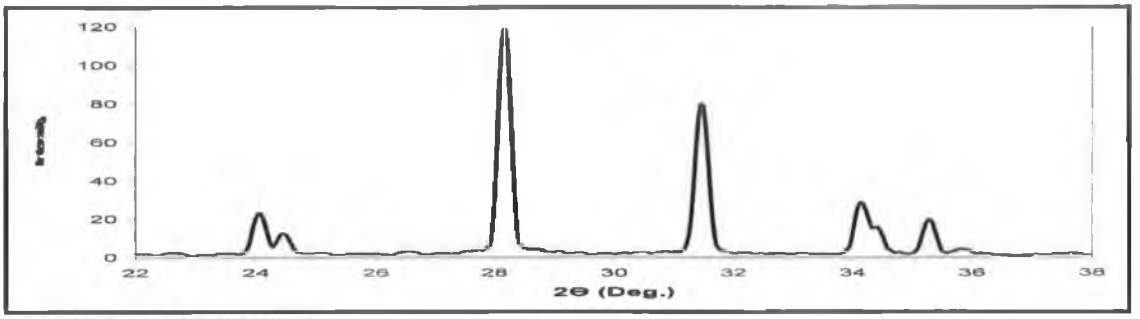

(a) Monoclinic powder

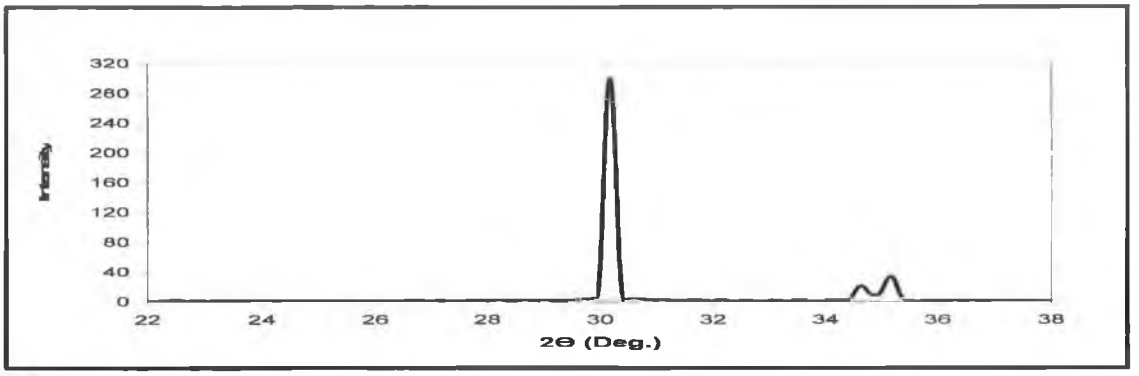

(b) Sintered Tosoh disc

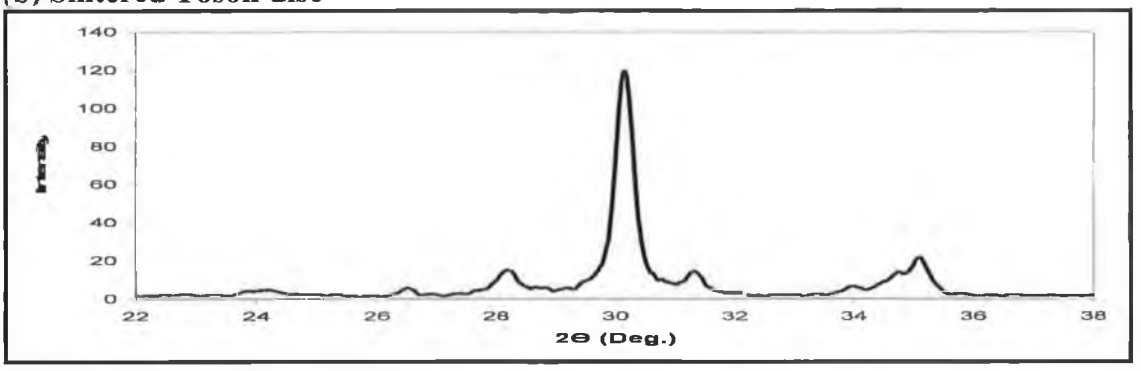

(c) Tosoh powder

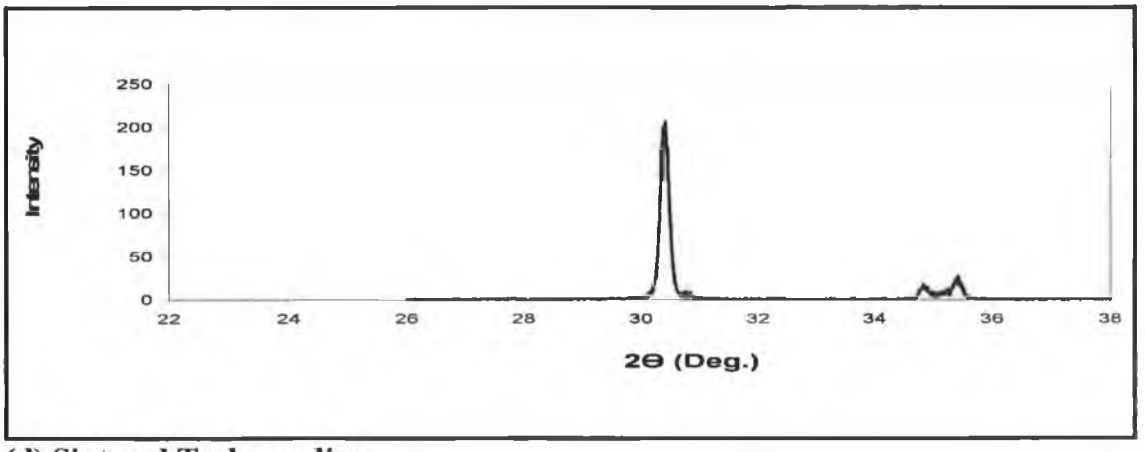

(d) Sintered Technox disc

Figure 4.20 XRD pattern of (a) Monoclinic zirconia powder (b) Sintered Tosoh disc (c) Tosoh powder (d) Sintered Technox disc.

CHAPTER FIVE
CONCLUSIONS AND FUTURE WORK

CHAPTER FIVE
CONCLUSIONS AND FUTURE WORK

5.1 Conclusions

The following conclusions have been drawn from this work:

1. Two different 3Y-TZP nano powders were investigated and wet laser diffraction based particle size analysis indicated the powders appeared to be heavily prone to agglomeration in water.

2. Attrition milling was found to be a technique for reducing the particle size.

3. Equivalent spherical diameter calculation (ESD_{BET}) resulted in a particle sizes of 69 nm and 155 nm. This result also is in good agreement with TEM micrograph and suppliers specifications.

4. The density of the powders (5.98 g/cm^3 and 6.03 g/cm^3) measured by pycnometry was lower than expected due to the presence of a small amount of monoclinic phase (verified by XRD analysis of the powder, see Fig. 4.20).

5. Thermal analysis revealed that one of the powders contained almost twice as much binder as the other and weight loss during heating was about 3-5 % due to binder burn out.

6. Binder burn-off was aided by air and occurred at lower temperatures compared with under nitrogen.

7. Bars made from both of the 3Y-TZP powders showed similar final shrinkages, of approximately 25%, but the point of maximum densification rate occurred at a much higher temperature for the powder of greater particle size.

8. Sintered discs exhibited densities > 99 % theoretical, and no evidence of a t→m transformation was detected.

9. Hardness increased with temperature irrespective of powders and sintering method. A maximum was recorded for samples sintered for 16 hours at lower temperature using two-step sintering.

10. Fracture toughness decreased with increasing temperature due to considerable grain growth in conventional sintering but fracture toughness strongly related to sintering time in case of two-step sintering, and increased with increasing sintering time up to a maximum of 6.12 MPa $m^{1/2}$ after 16 hours at lower temperature.

11. Acquiring high quality powders and effective sintering led to highly dense (>99%) sintered discs with desired hardness and toughness that retained tetragonal phase at room temperature.

5.2 Future work

1. Work more on conventional and two-step sintering schedule to minimise the grain size.

2. Study the degradation properties of 3 mol% yttria stabilised zirconia through experimental work.

3. Study the effect of sintering on pore structure.

REFERENCES

REFERENCES

[1] C. Piconi and G. Macauro, Zirconia as a ceramic biomaterial, Biomaterials, 20 (1991) pp 1-25.

[2] B. Basu, J. Vleugels, and O. V. D. Biest, Transformation behaviour of tetragonal zirconia: role of dopant content and distribution, Materials Science and Engineering, A366 (2004) pp 338-347.

[3] L. Esquivias, C. B. Solano, and M. Piñero, 5YSZ powder from gels: densification and microstructure characterization, Journal of European Ceramic Society, 18 (1998) pp 1429-1438.

[4] H. Lu and S. Chen., Low-temperature aging of t-ZrO_2 polycrystals with 3 mol% Y_2O_3, J. Am.Ceram. Soc., 70, 8, (1987) pp 537-41.

[5] R. H. J. Hannink, P. M. Kelly, and B. C. Muddle, Transformation toughening in zirconia-containing ceramics, J. Am.Ceram. Soc., 83, 3, (2000) pp 461-87.

[6] R. A. Kimel and J. H. Adair, Aqueous degradation and chemical passivation of yttria-tetragonally-stabilized zirconia at 25°C, J. Am.Ceram. Soc., 85, 6, (2002) pp 403-408.

[7] H. Lu and S. Chen , Low-temperature aging of t-ZrO_2 polycrystals with 3 mol% Y_2O_3, J. Am.Ceram. Soc., 70, 8, (1987) pp 537-41.

[8] A. Hirvonen, R. Nowak, Y. Yamamoto, T. Sekino, K. Niihara., Fabrication, structure, mechanical and thermal properties of zirconia-based new ceramic nanocomposites, Journal of European Ceramic Society, 26 (2006) pp 1497-1505.

[9] H. Tsubakino and N. Matsuura, Relationship between transformation temperature and time-temperature-transformation curve of tetragonal-to-monoclinic martensitic transformation in zirconia-yttria system, J. Am.Ceram. Soc., 85, 8, (2002) pp 2102-106.

[10] F. F. Lange, Transformation-toughened ZrO_2: correlation between grain size control and composition in the system ZrO_2-Y_2O_3, J. Am.Ceram. Soc., 69, 3, (1986) pp 240-42.

[11] J. F. Bartolomé, I. Montero, M. Diaz, S. Lopez-Esteban, and J. S. Moya, accelerated aging in 3-mol%-yttria-stabilized tetragonal zirconia ceramics sintered in reduced condition, J. Am.Ceram. Soc., 87, 12, (2004) pp 2282-2285.

[12] T. Xu, J. Vleugels, O. V . Biest, and P. Wang. Phase stability and mechanical properties of TZP with low mixed Nd_2O_3/Y_2O_3, Material Science and Engineering, A374 (2004) pp 239-243.

[13] C. Zhao, J. Vleugels, L. Vandeperre, B. Basu, O. V. Biest, Y-TZP/Ce-TZP functionally graded composite, Journal of Materials Science letters, 17 (1998) pp 1453-1455.

[14] M. W. Barsoum, Fundamentals of ceramics, Institute of Physics Publishing, Bristol and Philadelphia, (2003) pp 382-385.

[15] T. Xu, J. Vleugels, O. V. D. Biest, and P. Wang, Fabrication and characterization of (Nd,Y)-TZP ceramics from stabilizer-coated nanopowder, Materials Letter, 58 (2004) pp 3353-3357.

[16] T. Xu, J. Vleugels, O. V. D. Biest, and P. Wang, Mechanical properties of Nd_2O_3/Y_2O_3-coated zirconia ceramics, Material Science and Engineering, A374 (2004) pp 239-243.

[17] S. G. Huang, J. Vleugels, L. Li, O. V. D. Biest, and P. L. Wang, Composition design and mechanical properties of mixed (Ce,Y)-TZP ceramics obtained from coated starting powders, Journal of European Ceramic Society, 25 (2005) pp 3109-3115.

[18] B. Basu, J. Vleugels, and O. V. D. Biest, Toughness tailoring of yttria-doped zirconia ceramics, Materials Science and Engineering, A380 (2004) pp 215-221.

[19] S. Lawson, Environmental degradation of zirconia ceramics, Journal of European Ceramic Society, 15 (1995) pp 485-502.

[20] A. Polotai, K. Breece, E. Dickey, and C. Randall, A novel approach to sintering nanocrystalline barium titanate ceramics, J. Am.Ceram. Soc., 88, 11, (2005) pp 3008-3012.

[21] D. Kim, Effect of heating rate on pore shrinkage in yttria-doped zirconia, Am.Ceram. Soc., 76, 7, (1993) pp 1877-1878.

[22] X. H. Wang, X. Y. Deng, H. Bai, H. Zhou, W. Qu, and L. T. Li, Two-step sintering of ceramics with constant grain-size, II: $BaTiO_3$ and Ni-Cu-Zn ferrite, Am.Ceram. Soc., 89, 2, (2006) pp 438-443.

[23] A. Lee, Sintering behaviour and mechanical properties of injection-molded zirconia powder, Ceramics International, 30 (2004) pp 579-584.

[24] C. Robert, F. Ansart, C. Deloget, M. Gaudon, and A. Rousset, Dense yttria stabolized zirconia: sintering and microstructure, Ceramics International, 29 (2003) pp 151-158.

[25] Encyclopedia of Materials Science and Engineering, The MIT Press, 7 (1986) pp 5130.

[26] P. H. Rieth, J. S. Reed, A. W. Naumann, Fabrication and flexural strength of ultra-fine grained yttria-stabilised zirconia, Am Ceram Soc, 55 (1976) pp 717.

[27] T. K. Gupta, J. H. Bechtold, R. C. Kuznickie, L. H. Cadoff, B. R. Rossing, Stabilization of tetragonal phase in polycrystalline zirconia, J Mater Sci., 13 (1978) pp 1464.

[28] R. A. Cutler, J. R. Reynolds, and A. Jones, Sintering and characterization of polycrystalline monoclinic, tetragonal, and cubic zirconia, J. Am. Ceram. Soc., 75, 8, (1992) pp 2173-2183.

[29] T-J. Chung, H. Song, G-H. Kim, and D-Y. Kim, Microstructure and phase stability of yttria-doped tetragonal zirconia polycrystals heat treated in nitrogen atmosphere, J. Am. Ceram. Soc., 80, 10, (1997) pp 2607-2612.

[30] Z. Pedzich, and C. Wajler, Slow crack propagation in Y-TZP/metal composites, Journal of European Ceramic Society, 26 (2006) pp 679-682.

[31] R. C. Garvie, R. H. Hannick, R. T. Pascoe, Ceramic steel?, Nature, 258 (1975) pp 703-704.

[32] Ceramics and glasses, Engineering materials handbook, ASM international, 4 (1991) pp 775-786

[33] P. Boch, P. Fauchais, B. Lombard, B. Rogeaux, and M. Vardelle, plasma sprayed zirconia coatings, Science and Technology of Zirconia-II, Advances in Ceramics, N. Claussen, M. RUhle, and A.H. Heuer, Ed., American Ceramic Society, 12 (1983) pp 488-502.

[34] T. Sato and M. Shimada, Transformation of Yttria doped tetragonal zirconia polycrystals by annealing in water, J. Am. Ceram. Soc., 68 (1985) pp 356.

[35] T. Masaki, Mechanical properties of Y-PSZ after ageing at low temperatures, Int. J. High Tech. Ceram., (1986), pp 85-98.

[36] F.F. Lange, G.L. Dunlop, and B.I. Davis, Degradation during ageing of transformation toughened ZrO_2- Y_2O_3 materials at 250°C , J. Am. Ceram. Soc., 69, 3, (1986) pp 237-240.

[37] S. Schmauder and H. Schubert, Significance of internal stresses for themartensitic transformation in yttria-stabilized tetragonal-zirconia polycrystals during degradation, J. Am. Ceram. Soc., 69, 7, (1986) pp 534–40.

[38] R. H. J. Hannink and M. V. Swain, Progress in transformation toughening of ceramics, Ann. Rev. Mater. Sci., 24 (1994) pp 359–408.

[39] T. Sato, A. Ohtaki, T. Endo, and M. Shimada, Transformation of yttria-doped tetragonal-ZrO2 polycrystals by annealing under controlled humidity conditions, J. Am. Ceram. Soc., 68, 12, (1985) pp 320–322.

[40] k. Tsuma, Y. Kubota, and T. Tsukidate, thermal and mechanical properties of Y_2O_3-stabilized tetragonal zirconia polycrystals; science and technology of zirconia II, Advances in Ceramics, Edited by N. Claussen, M. Ruhle, and A. H. Heuer, American Ceramic Society, Columbus, OH, 12 (1984).pp 382-90.

[41] B. Basu, J. Vleugels, and V. D. Biest, Transformation behaviour of yttria stabilized tetragonal zirconia polycrystal-TiB_2 composites, J. Materials research, 16, 7, (2001) pp 2158-2169.

[42] P. J. Whalen, F. Reidinger, and R. F. Antrim, Prevention of low-temperature surface transformation by surface recrystallization in yttria-doped tetragonal zirconia, J. Am. Ceram. Soc., 72, 2, (1989) pp 319-321.

[43] A.A. Griffith, The phenomena of rupture and flow in solids, Philos. Trans. R. Soc. London, A221 (1920) pp 163.

[44] E. Orowan, Fracture and strength of solids, Rep. Prog. Phys., 12 (1949) pp 185.

[45] Engineered Material Handbook, ASM International, 4 (1991) pp 782.

[46] T. E. Fischer, M. P. Anderson, and S. Jahanmir, Influence of fracture toughness on the wear resistance of yttria-doped zirconiaum oxide, J. Am. Ceram. Soc., 72, 2, 1989 pp 252-257.

[47] C. Piconi, W. Burger, H.G. Richter, A. Cittadini, G. Maccauro, V. Covacci, N. Bruzzese and G.A. Ricci, E. Marmo, Y-TZP ceramics for artificial joint replacements, Biomaterials, 19 (1998) pp 1489-1494.

[48] R. C. Garvie, C. Urbani, D. R. Kennedy, and J. C. McNeuer, Biocompatibility of magnesia partially stabilised zirconia (Mg-PSZ) ceramics, J. Mater. Sci., 19 (1984) pp 3224-3228.

[49] B. Cales, High reliable zirconia ceramics for orthopedics, In Trans 5th World Biomaterials Congress, June (1996), Toronto, Canada.

[50] http://hcd2.bupa.co.uk/images/factsheets/hip_replacement.gif

[51] http://www.llnl.gov/etr/pdfs/10_94.2.pdf. 16.08.2006

[52] S. Ran, L. Winnubst, W. Wiratha, and D. H. A. Blank, Sintering behaviour of 0.8 mol%-CuO-doped 3Y-TZP ceramics, J. Am.Ceram. Soc., 89, 1, (2006) pp 151-155.

[53] R. C. Garvie, Structural application of ZrO_2-bearing materials, Am. Ceram. Soc., 12 (1984) pp 465-79.

[54] S. T. Gulati, J. D. Helfinstine, and A. D. Davis, Determination of some useful properties of partially stabilized zirconia and the application to extrusion dies, J. Am. Ceram. Soc., 69, 2, (1980) pp 211-219.

[55] K. A. Reddy and A.Ramesh, Modifications on a small two wheeler two stroke si engine for reducing fuel consumption and exhaust emissions, RIO 5 - World Climate & Energy Event, 15-17 February (2005), Rio de Janeiro, Brazil.

[56] M. Marmach, D. Servent, R.H.J. Hannink, M.J. Murray, and M.V. Swain, Toughened PSZ ceramics-their role as advanced engine components, MPR, Jan (1984) pp 7-12.

[57] R.J. Bratton and S.K. Lau, Zirconia thermal barrier coatings, Science and technology of zirconia , Advances in Ceramics, A.H. Heuer and L.W. Hobbs, Ed., American Ceramic Society, 3 (1981) pp 226.

[58] D.S. Suhr, T.E. Mitchell, and R.J. Keller, Microstructure and durability of zirconia thermal barrier coatings, Science and Technology of Zirconia-II, Advances in Ceramics, N. Claussen, M. Riihle, and A.H. Heuer, Ed., American Ceramic Society, 12 (1983) pp 503-517.

[59] A.S. Grot and J.K. Martyn, Behaviour of plasma sprayed ceramic thermal barrier coatings for gas turbine applications, Am. Ceram. Soc., 60, 8, (1981) pp 807.

[60] B. C. H. Steele and T. Takahashi, High conductivity solid ionic conductors, recent trends and applications, World Scientific, Singapore, (1998) pp. 402.

[61] D. L. Chen and M. J Mayo, Densification and grain growth of ultrafine 3 mol% Y2O3-ZrO2 ceramics, Nanosructred Materials, 2 (1993) pp 469-478.

[62] http://www.azom.com/details.asp?ArticleID=155, 01.08.2006.

[63] A. Rafferty, Y. Gun'ko, and R. Raghavendra, An investigation of co-fired varistor-ferrite materials, Journal of the European Ceramic Society, 24 (2004) pp 2005–2013.

[64] F. V. Lenel, Powder metallurgy principles and applications, Metal powder Industries Fedaration, (1980) pp 211-267.

[65] R. M. German, Powder metallurgy science, Metal Powder Industries Fedaration, (1984) pp 145-200.

[66] http://www.turkcadcam.net/rapor/otoinsa/images/sintering-neck-formation.jpg. 16.08.2006

[67] J. P. Smith and G. L. Messing, Sintering of biomodally distributed alumina powders, J. Am. Ceram. Soc., 67 (1984) pp 238-242.

[68] R. L Coble, Sintering Crystalline Solids. I Intermediate and final state diffusion models, J. Appl. Phys., 32 (1961) pp 787-792.

[69] R. J Brook, Pore-grain boundary interactions and grain growth, J. Am. Ceram. Soc., 52 (1969) pp 339-340.

[70] H. palmour and T. M. Hare, Rate controlled sintering revisited, sintering '85, G. C. Kucczynski, D. P. Uskokovic, H. Palmour, and M. M. Ristic, Ed., Plenum Press, (1987) pp 17-34.

[71] M. F Yan, Sintering of ceramics and metals. Advance in powder technology, G. Y. Chin, Ed., American Society for Metals, (1982) pp 99-133.

[72] M. F. Yan, R. M. Cannon, and K. H. Bowen, Grain boundary migration in ceramics, Ceramic microstructure '76, R. M. Fulrath and J. A. Pask, Ed., west-view press, (1977) pp 276-307.

[73] B. R. Patterson and J. A. Griffin, Effect of particle size distribution on sintering of tungsten, modern development in powder metallurgy, Metal Powder Industries Federation, 15 (1985) pp 279-288.

[74] Y. L Krasulin, V. N. Timofeev, S. M. Barinov, and A. B. Ivanov, Strength and fracture of porous ceramic sintered from spherical particles, J. Matar. Sci., 15 (1980) pp 1402-1406.

[75] G. S. A. M. Theunissen, A. J. A. Winnubst, and A. J. Burggraaf, Mechanical properties of ultra-fine grained zirconia ceramics, J Mater Sci., 27 (1992) pp 4429-38.

[76] G. S. A. M. Theunissen, A. J. A Winnubst., and. A. J. Burggraaf, Effect of dopants on the sintering behaviour and stability of tetragonal zirconia ceramics, Journal of the European Ceramic Society, 9 (1992) pp 251-263.

[77] C. D. Sagel-Ransijn, A. J. A. Winnubst, A. J. Burggraaf, and H. Verweij, Grain growth in ultrafine-grained Y-TZP, Journal of European Ceramic Society, 17 (1997), pp 1133-1141.

[78] R. Haynes, The Mechanical behaviour of sintered metals, Reviews on the deformation behaviour of materials, 3 (1981) pp 1-101.

[79] P. Duran, M. Villegas, J. F. Fernandez, F. Capel, and C. Moure, Theoretically dense and nanostructured ceramics by pressureless sintering of nanosized Y-TZP powders, Materials Science and Engineering, A232 (1997) pp 168-176.

[80] P. F. Becher, and M. V. Swain, Grain-size-dependent transformation behaviour in polycrystalline tetragonal zirconia, J. Am. Ceram. Soc., 75, 3, (1992) pp 493-502.

[81] I. Chen and X.-H Wang, Sintering dense nanocrystalline ceramics without final-stage grain growth, Nature, 404 (2000) pp 168-171.

[82] X. H. Wang, P. L. Chen, and I. W. Chen, Two-step sintering of ceramics with constant grain-size, I: Y_2O_3, Am.Ceram. Soc., 89, 2, (2006) pp 431-437.

[83] M. Zhou-Berbon, O. T. Sorensen, and T. G. Langdon, A simple technique for the preparation of tensile specimens of yttria-stabilized zirconia, Materials Letters, 27 (1996) pp 211-214.

[84] Standard test method for dynamic Young's Modulus, Shear Modulus, and Poisson's ratio for advanced ceramics by impulse excitation of vibration, ASTM, C 1259-1298 (2001) pp 1-18.

[85] G. Martincek, The determination of Poisson's ratio and the dynamic Modulus of Elasticity from the frequency of natural vibration in thick circular plates, Journal of Sound Vibration, 2, 2, (1965) pp 116-127.

[86] J. C. Glandus, Rupture fragile et résistance aux choes thermiques de céramiques a usages mechaniques, Thesis, University of Limoges, France, (1981).

[87] B. Lawn, Fracture of brittle solids, Cambridge University press, (2^{nd} Ed.) (1993) pp 3-7.

[88] G. R. Anstis., P. Chantikul, B. R. Lawn, and D. B. Marshall, Critical evaluation of indentation techniques for measuring fracture toughness: I direct crack measurements, J. Am.Ceram. Soc., 64 (1981) pp 533-538.

[89] M. S. Kaliszewski, G. Behrens, A. H. Heuer, M. C. Shaw, D. B. Marshall, G. W. Dransmann, R. W. Steinbrech, A. Pajares, F. Guiberteau, F. L. Cumbrera, and A. Dominguez-Rodriguez, Indentation studies on Y_2O_3-stabilized ZrO_2: I,

development of indentation-induced cracks, J. Am. Ceram. Soc., 77, 5, (1994) pp 1185-1193.

[90] P. S. Anderson, X. Wang, and P. Xiao, Effect of isothermal heat treatment on plasma-sprayed yttria-stabilized zirconia studied by impedance spectroscopy, J. Am. Ceram. Soc., 88, 2, (2005) pp 324-330.

[91] P. G. etzow, Metallographic etching, ASM International, (2nd Edition) (1999) pp 167.

[92] Y. Yuan, X. Wang and P. Xiao, Attrition milling of metallic-ceramic particles in acetyl-acetone, Journal of European Ceramic Society, 24 (2004) pp 2233-2240.

[93] W. Summers, Broad scope particle size reduction by means of vibratory grinding, J. Am. Ceram. Soc., 62, 2, (1983) pp 212-215.

[94] J. R. Seidensticker, M. J. Mayo, and K. O. Asare, Adsorption as a method of doping 3-mol%-yttria-stabilized zirconia powder with copper oxide, J. Am.Ceram. Soc., 76, 7, (1993) pp 1844-1848.

[95] R.A. Kimel and J. H. Adair, Aqueous synthesis at 200 °c of sub-10 nanometeryttria tetragonally stabilized zirconia using a metal-ligand approach, J. Am.Ceram. Soc., 88, 5, (2005) pp 1133-1138.

[96] K Kunes, J. Havrda, K. Hronikova, E. Gregorova, W. Pabst, Stabilization of bioceramic suspensions prepared from alumina-containing zirconia powders, Ceramics-Silikáty, 44, 1, (2000) pp 1-8.

[97] S. Tamari, Optimum design of the constant-volume gas pycnometer for determining the volume of solid particles, Meas. Sci. Technol, 15 (2004) pp 549-558.

[98] G. J. Consolmagno and D. T. Britt, The density and porosity of meteorites from vatican collection, Meteorit. Planet. Sci., 33 (1998) pp 1231-1241.

[99] P. Duran, J. Tartaj and C. Moure, Sintering behaviour and microstructural evolution of agglomerated spherical particles of high-purity barium titanate, Ceramic International, 29 (2003) pp 419-425.

[100] J.-L. Shi, J.-H Gao, Z-X. Lin, and T-S. Yen, Sintering behavior of fully agglomerated zirconia compacts, J. Am. Ceram. Soc., 74[5] (1991) pp 994-997.

[101] W. F. M. Groot Zevert, A. J. A. Winnubst, G. S. A. M. Theunissen and A. J. Burggraaf, Powder preparation and compaction behaviour of fine-grained Y-TZP, J. Mater. Sci, 25 (1990), pp. 3449.

[102] A Barba, C. Clausell, C. Feliu, and M. Monzo, Sintering of ($Cu_{0.25}Ni_{0.25}Zn_{0.50}$) Fe_2O_4 ferrite, J. Am.Ceram. Soc., 87, 4, (2004) pp 571-77.

[103] M. C. B. Moraes, C. N. Elias, J. D. Filho, and L. G. Oliveira, Mechanical properties of alumina-zirconia composites for ceramic abutments, Materials Research, 7, 2, (2004) pp 643-649

[104] A. Celli, A. Tucci, L. Esposito, and C. Palmonari, Fractal análysis of cracks in alumina-zirconia composites, Journal of European Ceramic Society, 23 (2003) pp 469-479.

[105] Standard test methods for determining average grain size, ASTM, E 112-96, (1996) pp 227-249.

[106] A. Ghosh, A. K. Suri, M. Pandey, S. Thomas, T.R. Rama Mohan, B.T. Rao. Nanocrystalline zirconia-yttria system-a Raman study, Materials Letters, 60 (2006) pp 1170-1173.

APPENDIX A

Temperature equivalence of the horizontal furnace

Furnace Temp (Heating cycle) (°C)	*,**Thermocouple (Heating cycle) (°C)	Furnace Temp (Cooling cycle) (°C)	*,**Thermocouple (Cooling cycle) (°C)
50	31	1500	1473
100	53	1450	1427
150	105	1400	1385
200	147	1350	1344
250	200	1300	1304
300	258	1250	1256
350	316	1200	1210
400	372	1150	1165
450	428	1100	1119
500	481	1050	1075
550	534	1000	1030
600	586	950	984
650	635	900	938
700	688	850	891
750	735	800	844
800	786	750	794
850	834	700	745
900	880	650	696
950	927	600	648
1000	989	550	598
1050	1024	500	544
1100	1075	450	491
1150	1125	400	445
1200	1174	350	398
1250	1222	300	348
1300	1274	250	291
1350	1320	200	245
1400	1369	150	145
1450	1419	100	138
1500	1469	50	96

* = R type (Platinum-13 % Rhodium vs Platinum) thermocouple was used (TC Ltd., UK).
** = TC-08 thermocouple data logger with picolog data acquisition software was used (Pico Technology Ltd., UK).

APPENDIX B

Table of Vickers hardness data

1. Hardness test data sheet for Tosoh (TZ-3Y-BE grade) powder

Single-step		20 kg				
	Tosoh			Hardness		
No.	Sample	d1 (mm)	d2 (mm)	Hv 20	Hv 20 (GPa)	STDEV
1	Tosoh 1350	176.4	174.8	1202.7	11.7948789	
2	Tosoh 1350	175.1	177.8	1190.5	11.6752335	
3	Tosoh 1350	174	173.8	1226.3	12.0263241	
4	Tosoh 1350	174.2	178.9	1189.1	11.6615037	
5	Tosoh 1350	178.7	181.3	1144.6	11.2250922	
6	Tosoh 1350	174.4	173.1	1227.7	12.0400539	
7	Tosoh 1350	172.4	175.5	1224.9	12.0125943	
8	Tosoh 1350	178.3	179.1	1161.3	11.3888691	
9	Tosoh 1350	177	177.7	1178.4	11.5565688	
10	Tosoh 1350	177.8	180.3	1156.2	11.3388534	
			Avg=	1190.17	11.67199719	0.297477222
No.	Sample	d1 (mm)	d2 (mm)	Hv 20	Hv 20 (GPa)	STDEV
1	Tosoh 1400	170.9	173.7	1249.2	12.2509044	
2	Tosoh 1400	169.9	170.7	1278.7	12.5402109	
3	Tosoh 1400	168.9	172	1275.7	12.5107899	
4	Tosoh 1400	167	169.4	1310.9	12.8559963	
5	Tosoh 1400	169.2	173.1	1265.3	12.4087971	
6	Tosoh 1400	168.3	171.3	1286.3	12.6147441	
7	Tosoh 1400	171.8	174.8	1234.8	12.1096836	
8	Tosoh 1400	168.4	171.4	1284.8	12.6000336	
9	Tosoh 1400	168.1	169.9	1298.5	12.7343895	
10	Tosoh 1400	168.7	169.2	1298.5	12.7343895	
			Avg=	1278.27	12.53599389	0.228831414
No.	Sample	d1 (mm)	d2 (mm)	Hv 20	Hv 20 (GPa)	STDEV
1	Tosoh 1450	170.8	170.7	1271.3	12.4676391	
2	Tosoh 1450	172.3	172.3	1249.2	12.2509044	
3	Tosoh 1450	168.4	170.1	1293.9	12.6892773	
4	Tosoh 1450	173.1	173.1	1237.7	12.1381239	
5	Tosoh 1450	172.3	167.2	1286.3	12.6147441	
6	Tosoh 1450	173.9	171.7	1240	12.16068	
7	Tosoh 1450	173.6	174.5	1223.5	11.9988645	
8	Tosoh 1450	171.5	168.5	1283.2	12.5843424	
9	Tosoh 1450	172.4	174.2	1234.8	12.1096836	
10	Tosoh 1450	171	171.5	1263.8	12.3940866	
			Avg=	1258.37	12.34083459	0.241904255

No.	Sample	d1 (mm)	d2 (mm)	Hv 20	Hv 20 (GPa)	STDEV
1	Tosoh 1500	177.2	170.2	1229.2	12.0547644	
2	Tosoh 1500	170	171.8	1269.8	12.4529286	
3	Tosoh 1500	170.5	171.7	1266.8	12.4235076	
4	Tosoh 1500	170.2	170.3	1278.7	12.5402109	
5	Tosoh 1500	172.4	170.9	1258	12.337206	
6	Tosoh 1500	171.4	168.9	1280.2	12.5549214	
7	Tosoh 1500	171.9	168.8	1277.2	12.5255004	
8	Tosoh 1500	172.5	167.4	1283.2	12.5843424	
9	Tosoh 1500	169	169.8	1292.4	12.6745668	
10	Tosoh 1500	170.5	169.7	1281.7	12.5696319	
			Avg=	1271.72	12.47175804	0.174020019

2. Hardness test data sheet for Technox 2000 grade (with binder) powder

Single-step		20 kg				
	Technox			Hardness		
No.	Sample	d1 (mm)	d2 (mm)	Hv 20	Hv 20 (GPa)	STDEV
1	Tecnx1350	177.8	178.3	1169.2	11.4663444	
2	Tecnx1350	176.6	180.7	1161.3	11.3888691	
3	Tecnx1350	184	185.1	1088.3	10.6729581	
4	Tecnx1350	181.1	180.7	1133.3	11.1142731	
5	Tecnx1350	181.6	187.2	1090.6	10.6955142	
6	Tecnx1350	184.1	182.6	1102.6	10.8131982	
7	Tecnx1350	181.9	186.2	1094.2	10.7308194	
8	Tecnx1350	181.6	183.7	1111	10.895577	
9	Tecnx1350	187.3	186.7	1060.5	10.4003235	
10	Tecnx1350	179.5	180.6	1143.4	11.2133238	
			Avg=	1115.44	10.93912008	0.344437577
No.	Sample	d1 (mm)	d2 (mm)	Hv 20	Hv 20 (GPa)	STDEV
1	Tecnx1400	178.1	177.6	1171.8	11.4918426	
2	Tecnx1400	176.5	177.9	1181.1	11.5830477	
3	Tecnx1400	176.9	175.8	1191.8	11.6879826	
4	Tecnx1400	181.4	177.1	1155.6	11.3329692	
5	Tecnx1400	177.9	175	1190.5	11.6752335	
6	Tecnx1400	177.4	176.6	1183.8	11.6095266	
7	Tecnx1400	179.1	178.2	1161.3	11.3888691	
8	Tecnx1400	181.5	182.4	1119.6	10.9799172	
9	Tecnx1400	178.1	178.9	1163.9	11.4143673	
10	Tecnx1400	176.4	177.8	1182.4	11.5957968	
			Avg=	1170.18	11.47595526	0.212516078

No.	Sample	d1 (mm)	d2 (mm)	Hv 20	Hv 20 (GPa)	STDEV
1	Tecnx1450	171.3	172.4	1255	12.307785	
2	Tecnx1450	170.1	170.1	1281.7	12.5696319	
3	Tecnx1450	172.2	171.7	1253.6	12.4087971	
4	Tecnx1450	171.1	171.3	1265.3	12.3803568	
5	Tecnx1450	170	172.7	1262.4	12.7186983	
6	Tecnx1450	170	168.2	1296.9	12.9324909	
7	Tecnx1450	166.7	168.7	1318.7	11.7546702	
8	Tecnx1450	174.5	177.3	1198.6	11.7684	
9	Tecnx1450	174.4	177.1	1200	12.4676391	
10	Tecnx1450	171.7	169.9	1271.3	12.36025245	
			Avg=	1260.35	12.36025245	0.370196119

No.	Sample	d1 (mm)	d2 (mm)	Hv 20	Hv 20 (GPa)	STDEV
1	Tecnx1500	173.3	171.6	1246.3	12.2224641	
2	Tecnx1500	174.4	177.8	1195.9	11.7281913	
3	Tecnx1500	175.1	178.9	1183.8	11.6095266	
4	Tecnx1500	170.4	169.2	1286.5	12.6167055	
5	Tecnx1500	168.8	170.2	1290.8	12.6588756	
6	Tecnx1500	176.3	175.3	1200	11.7684	
7	Tecnx1500	175.3	178.7	1183.8	11.6095266	
8	Tecnx1500	176	175.9	1197.2	11.7409404	
9	Tecnx1500	178.2	172.9	1202.7	11.7948789	
10	Tecnx1500	173.5	175.1	1220.7	11.9714049	
			Avg=	1220.77	11.97209139	0.394208885

No.	Sample	d1 (mm)	d2 (mm)	Hv 20	Hv 20 (GPa)	STDEV
1	Tecnx1550	175.5	178.9	1181.1	11.5830477	
2	Tecnx1550	174.2	175	1216.5	11.9302155	
3	Tecnx1550	173.1	177	1209.6	11.8625472	
4	Tecnx1550	171.2	173.2	1250.7	12.2656149	
5	Tecnx1550	170.4	175.2	1242	12.180294	
6	Tecnx1550	167.8	172	1284.8	12.6000336	
7	Tecnx1550	171.1	172.2	1258	12.337206	
8	Tecnx1550	171.4	172.3	1255	12.307785	
9	Tecnx1550	172.8	171.9	1247.8	12.2371746	
10	Tecnx1550	171.7	168.7	1280.2	12.5549214	
			Avg=	1242.57	12.18588399	0.314078964

3. Two-step sintering hardness test data sheet for Technox 2000 grade powder

2-step Sintering	20 kg			Hardness		
No.	Sample	d1 (mm)	d2 (mm)	Hv 20	Hv 20 (GPa)	STDEV
1	Tecnox 4 hrs	180.8	184.1	1113.5	10.9200945	
2	Tecnox 4 hrs	177.3	183.9	1137	11.150559	
3	Tecnox 4 hrs	179.4	181.6	1138.3	11.1633081	
4	Tecnox 4 hrs	180.4	178.8	1149.7	11.2751079	

5	Tecnox 4 hrs	176	179	1177.1	11.5438197	
6	Tecnox 4 hrs	177.4	179.2	1166.6	11.4408462	
7	Tecnox 4 hrs	180.1	180.3	1142.1	11.2005747	
8	Tecnox 4 hrs	180.2	180.5	1139.6	11.1760572	
9	Tecnox 4 hrs	180.2	175.9	1169.2	11.4663444	
10	Tecnox 4 hrs	176.5	179.5	1170.5	11.4790935	
			Avg=	1150.36	11.28158052	0.196313289

No.	Sample	d1 (mm)	d2 (mm)	Hv 20	Hv 20 (GPa)	STDEV
1	Tecnox 8 hrs	169.7	170.5	1281.8	12.5706126	
2	Tecnox 8 hrs	168.4	167.8	1312.4	12.8707068	
3	Tecnox 8 hrs	168.9	168.1	1304.7	12.7951929	
4	Tecnox 8 hrs	169.4	167.7	1275.7	12.5107899	
5	Tecnox 8 hrs	169.6	171.3	1277.2	12.5255004	
6	Tecnox 8 hrs	173.5	167.3	1206.9	11.8360683	
7	Tecnox 8 hrs	168.9	169.3	1312.4	12.8707068	
8	Tecnox 8 hrs	169	167.2	1296.9	12.7186983	
9	Tecnox 8 hrs	167.1	171.1	1268.3	12.4382181	
10	Tecnox 8 hrs	171.6	170.3	1242	12.180294	
			Avg=	1277.83	12.53167881	0.325297548

No.	Sample	d1 (mm)	d2 (mm)	Hv 20	Hv 20 (GPa)	STDEV
1	Tecnox 12 hrs	167.4	168.5	1314	12.886398	
2	Tecnox 12 hrs	168.2	168.8	1306.2	12.8099034	
3	Tecnox 12 hrs	168.4	166.8	1320.3	12.9481821	
4	Tecnox 12 hrs	170	170	1283.2	12.5843424	
5	Tecnox 12 hrs	166.7	166.7	1326.6	13.0099662	
6	Tecnox 12 hrs	169.3	169.3	1307.8	12.8255946	
7	Tecnox 12 hrs	166.7	166.7	1337.8	13.1198046	
8	Tecnox 12 hrs	167.6	167.6	1318.7	12.9324909	
9	Tecnox 12 hrs	166.3	166.3	1333	13.072731	
10	Tecnox 12 hrs	171.1	171.1	1278.7	12.5402109	
			Avg=	1312.63	12.87296241	0.191263628

No.	Sample	d1 (mm)	d2 (mm)	Hv 20	Hv 20 (GPa)	STDEV
1	Tecnox 16 hrs	167.3	166	1334.6	13.0884222	
2	Tecnox 16 hrs	168.7	171.2	1283.2	12.5843424	
3	Tecnox 16 hrs	169.7	168.3	1298.5	12.7343895	
4	Tecnox 16 hrs	168.3	168.3	1309.3	12.8403051	
5	Tecnox 16 hrs	168.1	165.9	1329.8	13.0413486	
6	Tecnox 16 hrs	167.6	167.4	1321.8	12.9628926	
7	Tecnox 16 hrs	170.3	169	1287.8	12.6294546	
8	Tecnox 16 hrs	169.3	167.4	1367.8	13.4140146	
9	Tecnox 16 hrs	169.8	172.6	1265.3	12.4087971	
10	Tecnox 16 hrs	168.1	167.1	1320.3	12.9481821	
			Avg=	1311.84	12.86521488	0.290397324

APPENDIX C

Table of fracture toughness data

1. Lawn and Wilshaw method for Tosoh (TZ-3Y-BE grade) powder

				Lawn & Wilshaw 1975			
Single-step	Tosoh	20 kg				Toughness	
No.	Sample	Crack 1	Crack 2	Avg in µm	Avg in meter	Kc, MPa.m$^{1/2}$	STDEV
1	Tosoh 1350	354.9	419.2	387.05	0.00038705	5.290054442	
2	Tosoh 1350	356.1	434.2	395.15	0.00039515	5.128233246	
3	Tosoh 1350	406.7	404.1	405.4	0.0004054	4.934976997	
4	Tosoh 1350	368.3	401.3	384.8	0.0003848	5.336520157	
5	Tosoh 1350	372.2	373.4	372.8	0.0003728	5.596247247	
6	Tosoh 1350	373.5	387.2	380.35	0.00038035	5.430447487	
7	Tosoh 1350	381.5	339.3	360.4	0.0003604	5.887536001	
8	Tosoh 1350	368.6	365.8	367.2	0.0003672	5.72475283	
9	Tosoh 1350	368.3	376.4	372.35	0.00037235	5.606395247	
10	Tosoh 1350	368.1	343	355.55	0.00035555	6.008412276	
					Avg=	5.494357593	0.335418
No.	Sample	Crack 1	Crack 2	Avg in µm	Avg in meter	Kc, MPa.m$^{1/2}$	STDEV
1	Tosoh 1400	410.9	428.3	419.6	0.0004196	4.686596134	
2	Tosoh 1400	416.5	446.6	431.55	0.00043155	4.493286055	
3	Tosoh 1400	396.1	444.2	420.15	0.00042015	4.677396619	
4	Tosoh 1400	414.3	418.8	416.55	0.00041655	4.73816348	
5	Tosoh 1400	401.4	441.7	421.55	0.00042155	4.654114985	
6	Tosoh 1400	384	407.9	395.95	0.00039595	5.112699036	
7	Tosoh 1400	396.7	417.2	406.95	0.00040695	4.90680919	
8	Tosoh 1400	382.8	418.6	400.7	0.0004007	5.022058133	
9	Tosoh 1400	329.2	439.1	384.15	0.00038415	5.350070352	
10	Tosoh 1400	411	372.2	391.6	0.0003916	5.198125068	
					Avg=	4.883931905	
							0.27813
No.	Sample	Crack 1	Crack 2	Avg in µm	Avg in meter	Kc, MPa.m$^{1/2}$	STDEV
1	Tosoh 1450	368.9	448.6	408.75	0.00040875	4.874432949	
2	Tosoh 1450	413.1	371.2	392.15	0.00039215	5.187193157	
3	Tosoh 1450	375	450.5	412.75	0.00041275	4.803747001	
4	Tosoh 1450	367.4	399	383.2	0.0003832	5.369977903	
5	Tosoh 1450	320.1	474.7	397.4	0.0003974	5.084742391	
6	Tosoh 1450	406.8	363.2	385	0.000385	5.33236237	
7	Tosoh 1450	388.4	449.5	418.95	0.00041895	4.697507229	
8	Tosoh 1450	434.5	386.1	410.3	0.0004103	4.846837661	
9	Tosoh 1450	401.9	427.9	414.9	0.0004149	4.766456095	
10	Tosoh 1450	433.7	400.8	417.25	0.00041725	4.726245003	
					Avg=	4.968950176	0.253565

No.	Sample	Crack 1	Crack 2	Avg in µm	Avg in meter	Kc, MPa.m$^{1/2}$	STDEV
1	Tosoh 1500	457.1	447	452.05	0.00045205	4.191129102	
2	Tosoh 1500	554.7	474.7	514.7	0.0005147	3.449685449	
3	Tosoh 1500	423.2	382.9	403.05	0.00040305	4.978200235	
4	Tosoh 1500	459.5	433	446.25	0.00044625	4.273103436	
5	Tosoh 1500	363.8	524.3	444.05	0.00044405	4.304898712	
6	Tosoh 1500	574.4	361.6	468	0.000468	3.978707106	
7	Tosoh 1500	464	418.6	441.3	0.0004413	4.345200872	
8	Tosoh 1500	417.3	470.4	443.85	0.00044385	4.307808739	
9	Tosoh 1500	391.9	523.7	457.8	0.0004578	4.112416251	
10	Tosoh 1500	498.6	431.8	465.2	0.0004652	4.014682363	
					Avg=	4.195583227	0.381297

2. Lawn and Wilshaw method for Technox 2000 grade powder

				Lawn & Wilshaw 1975			
Single-step No.	Technox Sample	20 kg Crack 1	Crack 2	Avg in µm	Avg in meter	Toughness Kc, MPa.m$^{1/2}$	STDEV
1	Tecnx1350	397.8	399	398.4	0.0003984	5.065610048	
2	Tecnx1350	409.8	392.8	401.3	0.0004013	5.010799318	
3	Tecnx1350	409.8	391.1	400.45	0.00040045	5.026761756	
4	Tecnx1350	393.3	431.9	412.6	0.0004126	4.80636683	
5	Tecnx1350	407	378.6	392.8	0.0003928	5.174322942	
6	Tecnx1350	396	358.7	377.35	0.00037735	5.495335572	
7	Tecnx1350	412.5	400	406.25	0.00040625	4.919496866	
8	Tecnx1350	393.2	350	371.6	0.0003716	5.623376883	
9	Tecnx1350	395.8	386.4	391.1	0.0003911	5.208096532	
10	Tecnx1350	402.8	398.3	400.55	0.00040055	5.024879426	
					Avg=	5.135504617	0.2524909
No.	Sample	Crack 1	Crack 2	Avg in µm	Avg in meter	Kc, MPa.m$^{1/2}$	STDEV
1	Tecnx1400	401.4	396.8	399.1	0.0003991	5.052288681	
2	Tecnx1400	333.7	472.3	403	0.000403	4.979126728	
3	Tecnx1400	400.7	378.8	389.75	0.00038975	5.235179336	
4	Tecnx1400	364.6	430.9	397.75	0.00039775	5.078032391	
5	Tecnx1400	406.9	392.8	399.85	0.00039985	5.038080456	
6	Tecnx1400	401.1	419.7	410.4	0.0004104	4.845066264	
7	Tecnx1400	371.9	394	382.95	0.00038295	5.375237259	
8	Tecnx1400	415.6	427.6	421.6	0.0004216	4.653287071	
9	Tecnx1400	419.7	369.9	394.8	0.0003948	5.135054216	
10	Tecnx1400	338	424.4	381.2	0.0003812	5.412294393	
					Avg=	5.080364679	0.229656
No.	Sample	Crack 1	Crack 2	Avg in µm	Avg in meter	Kc, MPa.m$^{1/2}$	STDEV
1	Tecnx1450	420.1	381.5	400.8	0.0004008	5.020178737	
2	Tecnx1450	432.3	425.1	428.7	0.0004287	4.538167528	
3	Tecnx1450	446.6	411.4	429	0.000429	4.533408045	
4	Tecnx1450	432.9	406.2	419.55	0.00041955	4.687433949	

5	Tecnx1450	378.1	418.1	398.1	0.0003981	5.071337136	
6	Tecnx1450	420	424.4	422.2	0.0004222	4.643371226	
7	Tecnx1450	453	370.3	411.65	0.00041165	4.823014522	
8	Tecnx1450	432.9	415	423.95	0.00042395	4.614650239	
9	Tecnx1450	417.6	355.1	386.35	0.00038635	5.30443796	
10	Tecnx1450	395.1	410.5	402.8	0.0004028	4.982835575	
					Avg=	4.821883492	0.2618132

No.	Sample	Crack 1	Crack 2	Avg in µm	Avg in meter	Kc, MPa.m$^{1/2}$	STDEV
1	Tecnx1500	324.7	395.7	360.2	0.0003602	5.892440238	
2	Tecnx1500	412.8	342.8	377.8	0.0003778	5.485520203	
3	Tecnx1500	318.8	394.1	356.45	0.00035645	5.985670701	
4	Tecnx1500	352.9	383.5	368.2	0.0003682	5.701446757	
5	Tecnx1500	405.6	342.4	374	0.000374	5.569335053	
6	Tecnx1500	385.4	370	377.7	0.0003777	5.48769887	
7	Tecnx1500	375.6	422.2	398.9	0.0003989	5.056088822	
8	Tecnx1500	400.7	381.2	390.95	0.00039095	5.21109419	
9	Tecnx1500	367.2	405	386.1	0.0003861	5.309590735	
10	Tecnx1500	408.5	398.7	403.6	0.0004036	4.968027748	
					Avg=	5.466691332	0.3373613

No.	Sample	Crack 1	Crack 2	Avg in µm	Avg in meter	Kc, MPa.m$^{1/2}$	STDEV
1	Tecnx1550	414	378.8	396.4	0.0003964	5.103995473	
2	Tecnx1550	436.5	355.7	396.1	0.0003961	5.109795101	
3	Tecnx1550	419.5	367.3	393.4	0.0003934	5.16248991	
4	Tecnx1550	418.7	361	389.85	0.00038985	5.23316516	
5	Tecnx1550	395.5	350.5	373	0.000373	5.591746847	
6	Tecnx1550	415.7	384.7	400.2	0.0004002	5.031472725	
7	Tecnx1550	426.5	364.9	395.7	0.0003957	5.117545043	
8	Tecnx1550	442.9	384.5	413.7	0.0004137	4.787209877	
9	Tecnx1550	397.2	342.9	370.05	0.00037005	5.658745165	
10	Tecnx1550	357.4	420.3	388.85	0.00038885	5.253365218	
					Avg=	5.204953052	0.2564657

3. Lawn and Wilshaw method for two-step sintering (Technox 2000 grade powder)

				Lawn & Wilshaw 1975			
No.	2-step Sintering Sample	20 kg Crack 1	Crack 2	Avg in µm	Avg in meter	Toughness Kc, MPa.m$^{1/2}$	STDEV
1	Tecnox 4 hrs	404	378.1	391.05	0.00039105	5.209095432	
2	Tecnox 4 hrs	383.5	395.5	389.5	0.0003895	5.240220433	
3	Tecnox 4 hrs	361	432.2	396.6	0.0003966	5.100135146	
4	Tecnox 4 hrs	402.2	375.4	388.8	0.0003888	5.254378631	
5	Tecnox 4 hrs	337.1	399.5	368.3	0.0003683	5.699124848	
6	Tecnox 4 hrs	365.5	331.7	348.6	0.0003486	6.188988491	
7	Tecnox 4 hrs	417.2	349.1	383.15	0.00038315	5.371029088	
8	Tecnox 4 hrs	382.1	404.4	393.25	0.00039325	5.165443937	
9	Tecnox 4 hrs	361.8	366.5	364.15	0.00036415	5.796826176	
10	Tecnox 4 hrs	378.6	355.3	366.95	0.00036695	5.730604166	
					Avg=	5.475584635	0.357549175

No.	Sample	Crack 1	Crack 2	Avg in μm	Avg in meter	Kc, MPa.m$^{1/2}$	STDEV
1	Tecnox 8 hrs	408.1	429.3	418.7	0.0004187	4.701715082	
2	Tecnox 8 hrs	380.1	447.6	413.85	0.00041385	4.784607425	
3	Tecnox 8 hrs	414.7	453.1	433.9	0.0004339	4.456832106	
4	Tecnox 8 hrs	368.7	411.9	390.3	0.0003903	5.22411733	
5	Tecnox 8 hrs	422.2	440.4	431.3	0.0004313	4.497193373	
6	Tecnox 8 hrs	408	397.2	402.6	0.0004026	4.986549028	
7	Tecnox 8 hrs	446.1	421.9	434	0.000434	4.455291815	
8	Tecnox 8 hrs	336	452.3	394.15	0.00039415	5.14776192	
9	Tecnox 8 hrs	438.6	420.3	429.45	0.00042945	4.526284401	
10	Tecnox 8 hrs	367.8	379.4	373.6	0.0003736	5.578281774	
					Avg=	4.835863426	0.386087489

No.	Sample	Crack 1	Crack 2	Avg in μm	Avg in meter	Kc, MPa.m$^{1/2}$	STDEV
1	Tecnox 12 hrs	409.4	431.3	420.35	0.00042035	4.674058801	
2	Tecnox 12 hrs	409.2	428.8	419	0.000419	4.696666411	
3	Tecnox 12 hrs	426.5	430.6	428.55	0.00042855	4.540550394	
4	Tecnox 12 hrs	367.8	407.2	387.5	0.0003875	5.280842184	
5	Tecnox 12 hrs	399.2	410.9	405.05	0.00040505	4.941374782	
6	Tecnox 12 hrs	350.3	497.7	424	0.000424	4.613833992	
7	Tecnox 12 hrs	436.8	406.1	421.45	0.00042145	4.655771548	
8	Tecnox 12 hrs	402.1	429	415.55	0.00041555	4.755276991	
9	Tecnox 12 hrs	402	465.5	433.75	0.00043375	4.459144207	
10	Tecnox 12 hrs	410.5	407.2	408.85	0.00040885	6.962970611	
					Avg=	4.958048992	0.245202315

No.	Sample	Crack 1	Crack 2	Avg in μm	Avg in meter	Kc, MPa.m$^{1/2}$	STDEV
1	Tecnox 16 hrs	398	336.3	367.15	0.00036715	5.7259223	
2	Tecnox 16 hrs	337.3	300.8	319.05	0.00031905	7.068424537	
3	Tecnox 16 hrs	379.8	349.3	364.55	0.00036455	5.787288002	
4	Tecnox 16 hrs	313.7	391.5	352.6	0.0003526	6.08397313	
5	Tecnox 16 hrs	364.6	364.6	364.6	0.0003646	5.786097569	
6	Tecnox 16 hrs	330.7	394.7	362.7	0.0003627	5.831622674	
7	Tecnox 16 hrs	376.4	350.5	363.45	0.00036345	5.813581156	
8	Tecnox 16 hrs	314.7	340.6	327.65	0.00032765	6.791965806	
9	Tecnox 16 hrs	350.4	351.8	351.1	0.0003511	6.123003463	
10	Tecnox 16 hrs	345	354.7	349.85	0.00034985	6.155848626	
					Avg=	6.116772726	0.460443555

APPENDIX D

Table of densities measured by Archimedes method

1. Density test data sheet for Tosoh (TZ-3Y-BE grade) discs.

Density measurement by using Density Measuring Kit

Single step

Density of water at 20°C ρ (fl) = 0.99823

Temperature 1500°C

	Density(g/cc)	Average	STDEV	W (a)	G	% of TD
Sample A	6.04168545			2.89198	0.478	
Sample B	6.033891262	6.037788	0.005511	2.9384	0.4863	99.47577
Sample C	6.068804009			2.8764	0.4733	

Temperature 1450°C

	Density	Average	STDEV	W (a)	G	% of TD
Sample A	6.05731636			2.8291	0.4664	
Sample B	6.067506267	6.046006	0.028868	2.877	0.4735	99.44089
sample C	6.013195395			2.9229	0.4854	

Temperature 1400°C

	Density	Average	STDEV	W (a)	G	% of TD
Sample A	6.023283863			2.9459	0.4884	
Sample B	6.007924401	6.016618	0.007878	2.8698	0.477	98.95753
sample C	6.018644475			2.8701	0.4762	

Temperature 1350°C

	Density	Average	STDEV	W (a)	G	% of TD
Sample A	5.956254976			2.9149	0.4887	
Sample B	5.919974895	5.922233	0.032951	3.008	0.5074	97.40515
sample C	5.890469097			2.9234	0.4956	

2. Density test data sheet for Technox 2000 grade (with binder) discs.

Density measurement by using Density Measuring Kit

Single step

Density of water at 20°C ρ (fl) = 0.99833

Temperature 1500°C

	Density(g/cc)	Average	STDEV	W (a)	G	% of TD
Sample A	5.944291176			2.87185	0.4825	
Sample B	5.953920936	5.96118	0.02146	2.90035	0.4865	98.04573
sample C	5.985329028			2.83115	0.4724	

Temperature 1450°C

	Density	Average	STDEV	W (a)	G	% of TD
Sample B	5.95511555			2.8258	0.4739	
Sample C	5.899433423	5.932305	0.029173	2.85549	0.4834	97.5708
sample D	5.942365614			2.90186	0.4877	

Temperature 1400°C

	Density	Average	STDEV	W (a)	G	% of TD
Sample A	5.971213545			2.87051	0.4801	
Sample B	5.874959463	5.891048	0.073455	2.89482	0.4921	96.89223
sample C	5.826970054			2.87642	0.493	

Temperature 1350°C

	Density	Average	STDEV	W (a)	G	% of TD
Sample B	5.722071033			2.76103	0.4819	
Sample C	5.719667007	5.756111	0.061053	2.89961	0.5063	94.67288
sample D	5.826596096			2.88557	0.4946	

3. Density test data sheet for two-step sintering (Technox 2000 grade) discs.

Density Measurement by using Density Measuring Kit

Two-step sintering

Density of water at 20.1°C ρ (fl) = 0.99821

Temperature

Sample 1380°C / 2-step / @ 4 hrs

	Density(g/cc)	Average	STDEV	W (a)	G	% of TD
Sample A	5.878891579			2.84	0.4824	
Sample B	5.802029707	5.839648324	0.038457	2.85864	0.492	96.04685
Sample C	5.838023686			2.8413	0.486	

Sample 1380°C / 2-step / @ 8 hrs

	Density(g/cc)	Average	STDEV	W (a)	G	% of TD
Sample A	5.967035392			3.06066	0.5122	
Sample B	5.950650103	5.922077862	0.052422	2.97121	0.4986	97.4026
Sample C	5.848548092			2.85228	0.487	

Sample 1380°C / 2-step / @ 12 hrs

	Density(g/cc)	Average	STDEV	W (a)	G	% of TD
Sample A	5.989313728			2.93234	0.4889	
Sample B	5.990018233	5.986965577	0.00469	2.83011	0.4718	98.46983
Sample C	5.981564771			2.8956	0.4834	

Sample 1380°C / 2-step / @ 16 hrs

	Density(g/cc)	Average	STDEV	W (a)	G	% of TD
Sample A	5.993193662			2.87842	0.4796	
Sample B	5.984208592	5.993804732	0.009916	2.83935	0.4738	98.58231
Sample C	6.004011941			2.92631	0.4867	

APPENDIX E

Pycnometry density measurements for different quantities of samples

Fig. E shows densities measured for the both Tosoh and Technox powders, and also for a standard of known density (Arklow flint, ρ=2.48 g/cm^3).

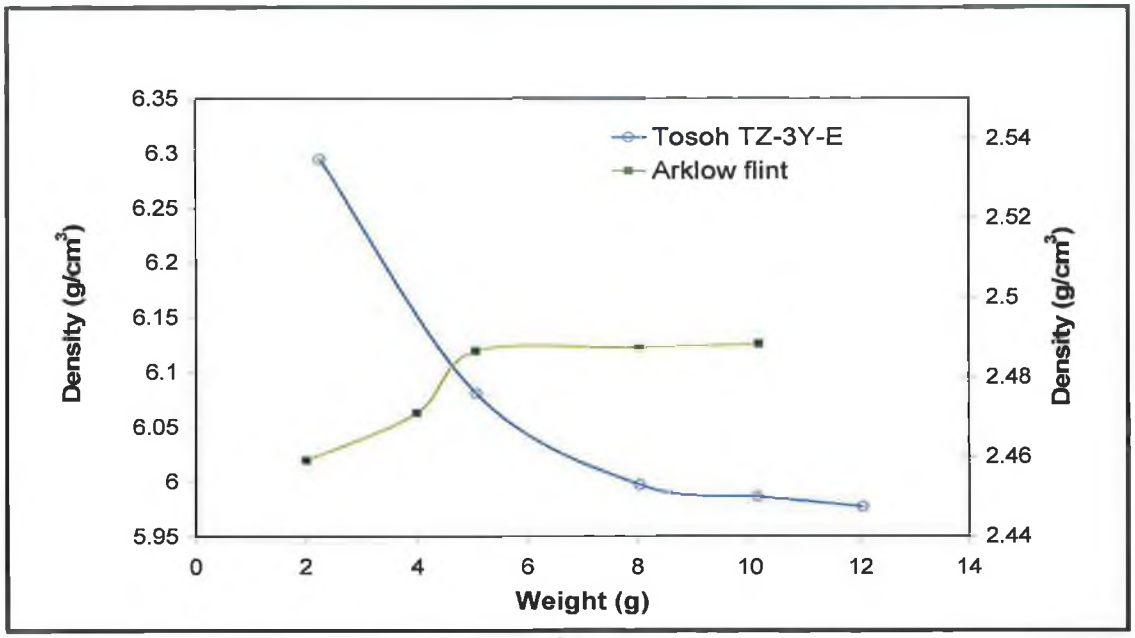

(a)

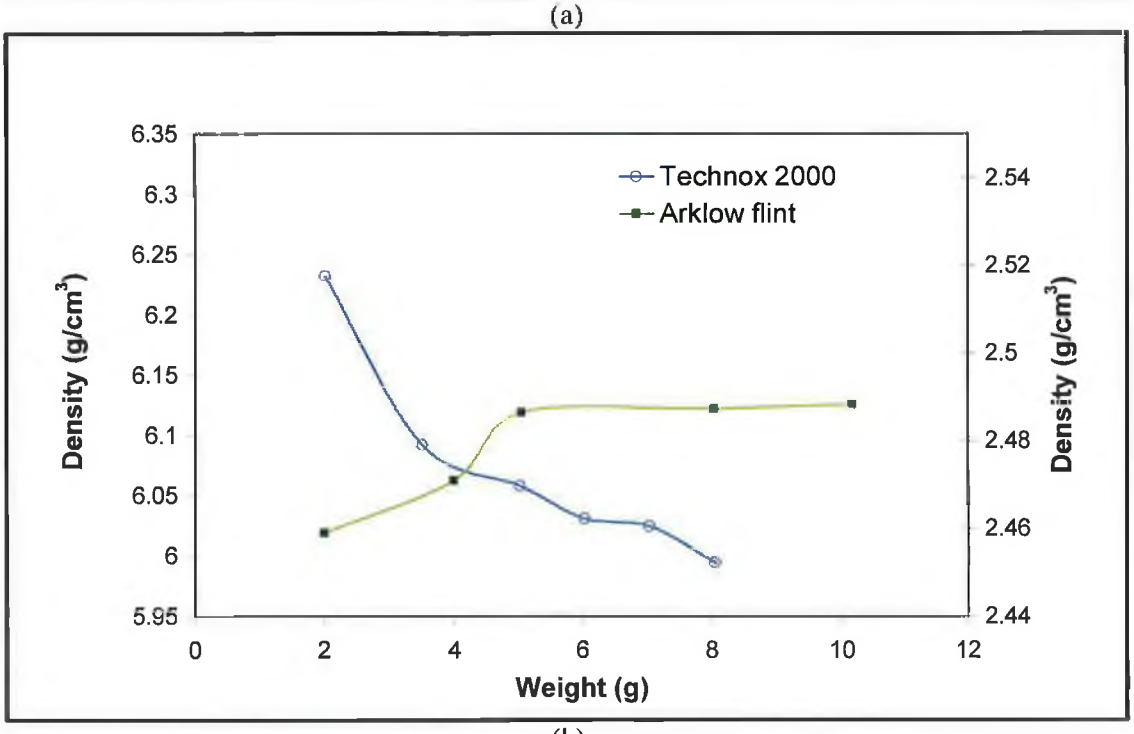

(b)

Figure E Pycnometry density measurements for different quantities of samples for (a) Tosoh powder (b) Technox (arrows in Fig. indicates the axes to which the curves correspond).

Small quantities of Arklow flint, i.e. 2 g and 4 g yielded density values of 2.46 g/cm^3 and 2.47 g/cm^3 respectively. Only when the quantity of powder was made >5 g did the density stabilise and give expected values, i.e. 2.48 g/cm^3 correct to two decimal places. A quantity of 8 g corresponded to the sample chamber being visually 2/3 full, which is the level recommended by the manufacturer.

APPENDIX F

BET surface area Calculation

For each point designated for surface area calculations, the BET[1] transformation is calculated as follows:

$$B_I = \frac{\text{Prel}_I}{(1.0 - \text{Prel}_I)(\text{Nads}_I)}$$

where

B_I = units of g/cm^3 STP

Prel_I = relative pressure

Nads_I = amount of gas adsorbed after equilibrating Ith dose (cm^3 STP)

A least-squares fit is performed on the (B_I, Prel_I) designated pairs where B is the dependent variable and Prel_I is the independent variable. The following are calculated:

- Slope (S g/cm^3 STP)
- Y-intercept (Y_{INT} g/cm^3 STP)
- Error of the slope (SERR g/cm^3 STP)
- Error of the y-intercept (YI_{ERR} g/cm^3 STP)
- Correlation coefficient (C_C)

Using the results of the above calculations, the following can be calculated:

BET Surface Area (m^2/g):

$$SA_{BET} = \frac{(CSA)(6.023 \times 10^{23})}{(22414 cm^3 STP)(10^{18} nm^2 / m^2)(S + Y_{INT})}$$

where

CSA = analysis gas molecular cross-sectional area (nm^2)

BET C value:

$$C = \frac{S + Y_{INT}}{Y_{INT}}$$

Volume of the Monolayer (cm^3/g STP):

$$V_M = [C(Y_{INT})]^{-1}$$

Error of the BET Surface Area (m^2/g):

$$BET_{ERR} = \frac{SA_{BET} \times (S_{ERR}{}^2 + YI_{ERR}{}^2)^{0.5}}{Y_{INT} + S}$$

Single Point Surface Area (m^2/g):

$$SIPT = V_a(1 - \mathrm{Pr}) \times 4.35 \times \frac{CSA}{0.162}$$

where

Pr = pressure closest to 0.3 of the relative pressure points designated for surface area calculations

Va = volume corresponding to Pr

0.162 = nitrogen molecule cross-sectional area (nm^2)

---

[1] Brunauer, S., Emmett, P.H., and Teller, E., J.; Am. Chem. Soc., 60 (1938) 309